Title
Surveying the global landscape of post-transcriptional regulation

Author
Reynaud, Kendra Keilani

Publication Date
2020

Peer reviewed|Thesis/dissertation

Surveying the global landscape of post-transcriptional regulation

By

Kendra Keilani Reynaud

A dissertation submitted in partial satisfaction of the

requirements for the degree of

Doctor of Philosophy

in

Biophysics

in the

Graduate Division

of the

University of California, Berkeley

Committee in charge:

Professor Nicholas Ingolia, Chair
Professor Gloria Brar
Professor Stephen Brohawn
Professor Britt Glaunsinger

Summer 2020

Abstract

Surveying the global landscape of post-transcriptional regulation

by

Kendra Keilani Reynaud

Doctor of Philosophy in Biophysics

University of California, Berkeley

Professor Nicholas Ingolia, Chair

At all stages of a messenger RNA's lifecycle, it is covered in RNA-binding proteins. These proteins regulate an RNA transcript's splicing and processing in the nucleus, its export from the nucleus into the cytoplasm, its localization and translation in the cytoplasm, and its eventual turnover and decay. Despite knowing the identities of roughly 700 RNA-binding proteins in budding yeast, the role in RNA regulation that many of these proteins perform remains unclear. Here we present two studies that are aimed at the functional characterization of proteins that regulate post-transcriptional gene expression. In the first study, we devised a high-throughput tethering assay for the characterization of proteins on a proteome-wide scale. This novel assay provides domain-level resolution for the functional regions of proteins and identifies their regulatory activity in a quantitative manner. In the second study, we characterized the yeast RNA-binding protein Mrn1p and found that it is a dynamic regulator of post-transcriptional regulation that functions through mRNA turnover. Mrn1p is especially important in linking cell wall biogenesis with mitochondrial homeostasis, and it regulates these two cellular compartments in a manner that is responsive to carbon source and cell stress. Together, we present two studies that provide new functional information about yeast RNA binding proteins, with broad implications for a better understanding of post-transcriptional gene expression.

Table of Contents

Dedication

To my husband, Joscelin Reynaud.

This thesis is the product of your support, patience and encouragement. Thank you for carrying so much on your shoulders so I could focus on my dream.

Chapter 1: Emerging principles of messenger RNA regulation

Throughout their lifecycle, messenger RNAs (mRNAs) are bound by proteins with varying affinities and stoichiometries. Since the discovery of the first RNA-protein interaction more than forty years ago, the mRNA interactome now comprises thousands of proteins. A recent review described these RNA-binding proteins (RBPs) as the "mRNA's clothes"; an apt description as an mRNA is essentially coated in RBPs through all stages of its life cycle [1]. These RBPs ensure that the different mRNA regions, including the 5` and 3` untranslated regions (UTRs) and the coding sequence, are subject to the correct regulation at the correct times. In the past decade or so, groundbreaking technologies have been developed that have identified thousands of proteins which bind RNA across different taxa. Many of the unique features of these proteins have been described, and the unifying principles of RNA regulation have begun to emerge. The technologies that have enabled these discoveries, as well as these emerging principles of RBP-mediated regulation, will be described below.

Experimental approaches to identifying RNA-protein interactions

In vitro identification of RNA-binding proteins

Early methods for systematically identifying RBPs were primarily performed *in vitro*. One pioneering method used immobilized RNA probes as bait. These probes were incubated with cellular extracts and subjected to downstream quantitative mass spectrometry (Q-MS) to identify the RBPs. Conversely, arrayed proteins were also used as bait and incubated with fluorescently-labeled cellular RNA. RNA-binding was then determined based on measuring the fluorescence intensity at each individual spot, similar to microarray analysis [2]. In a third *in vitro* approach, purified polyadenylated (poly(A)) cellular RNA was immobilized on oligo(dT) beads and incubated with cellular extract, then proteins were identified through Q-MS [3]. These methods combined identified hundreds of novel RNA binding proteins, and until the advent of higher-throughput methods over the next decade, they were the gold standard for RNA-protein interaction discovery.

In vivo identification of RNA-protein interactions

The recent development of methods that capture native RNA-protein interactions have revealed that RNA-binding activity is exhibited by a much larger portion of the eukaryotic proteome than we had previously appreciated. This *in vivo* method is called RNA interactome capture (RIC); it utilizes UV-crosslinking of RBPs to RNA in live cells followed by oligo(dT)

bead capture of poly(A) RNAs. Proteins are then identified by Q-MS [4]. This technique has radically enhanced our understanding of the RNA interactome. It has revealed the identities of 860 RBPs from HeLa cells and 791 RBPs from HEK293s. Both interactomes overlapped significantly in that they shared 543 RBPs and were both enriched for the gene ontology (GO) term for "RNA binding". Encouragingly, in addition to identifying novel RNA-protein interactions, this method captured the majority of well-established RNA binding domains such as the RNA recognition motif (RRM), the hnRNP K homology domain (KH), DEAD-box helicase domains, and some zinc finger domains. The capture of canonical RBPs with these domains suggests the method is a robust technique for identifying novel RNA-protein interactions [4,5].

RIC has since been applied to several additional human and mouse cell lines, budding yeast, unicellular parasites, plants, flies, worms, and fish. There now exists a unified RNA interactome for the model organisms *Homo sapiens* (1,914 RBPs), *Mus musculus* (1,393 RBPs), *Saccharomyces cerevisiae* (1,273 RBPs), *Drosophila melanogaster* (777 RBPs), *Arabidopsis thaliana* (719 RBPs) and *Caenorhabditis elegans* (593 RBPs). The authors of this study have also identified the common eukaryotic "core" RBPs through this method and found that evolutionarily-conserved RBPs tend to be more RNA-related than RBPs with cell type or organism-specific expression or activity [5].

RNA-binding domain identification

"RBDmap" is a method that builds upon the RIC workflow to identify the domains of RBPs that interact with RNA, which has been especially powerful in the characterization of unconventional RBPs. This method includes an additional protease digestion step with a specific enzyme that cleaves less frequently than trypsin, and these larger peptide fragments remain bound to the RNA. This digestion is then followed by a second round of oligo(dT) bead capture. Covalently-linked polypeptides are then cleaved by trypsin to liberate an unmodified peptide directly adjacent to the crosslink site, which can be distinguished from its neighboring peptide in that it retains its native mass. RBDmap detects the neighboring native peptide and extrapolates the protein's RNA-binding site computationally. RBDmap data strongly agree with data produced by RNA interactome methods, and have also confirmed the RNA binding activity of hundreds of unconventional RBPs, suggesting that these novel RBPs are truly part of the RNA interactome. As a proof-of-principle, this method also identified conventional RBDs such as the RRM and KH domains [6].

Interestingly, RBDmap revealed that many RNA-binding regions map to intrinsically disordered regions (IDRs), implicating them in RNA-protein interactions. This technique also mapped RBDs to globular domains with no known previous association with RNA, for example certain heat shock proteins containing the thioredoxin fold in HeLa cells. Finally, this study also found that mapped RNA-binding sites were enriched for homologous regions of different

proteins from the same family, and many were mapped to enzymatic cores or protein-protein interaction surfaces, suggesting an interaction between these activities and RNA-binding [5,6].

RBP RNA footprint identification

UV-crosslinking can also be adapted to identify the RNA targets for a specific RBP and can even determine its footprint on a target RNA with single nucleotide resolution. The original techniques CLIP (cross-linking immunoprecipitation) and CRAC (cross-linking and cDNA analysis) [7,8] were adapted into "eCLIP". The eCLIP technique employs UV-crosslinking, cell lysis, and limited digestion in order to fragment the RNA. The RBPs are then immunoprecipitated with a specific antibody against the RBPs in the study, and the immunoprecipitated material is then resolved by denaturing gel electrophoresis. The RNA is recovered and cDNA is generated through reverse transcription, and the regions bound by the RBP are identified through next generation sequencing. Since reverse transcription often stalls or mis-incorporates nucleotides at the site of the RNA-protein crosslink, this method offers single-nucleotide resolution of the RBP-binding site [9]. There is now eCLIP data for 122 RBPs, 34 of which lack classical RNA-binding domains (RBDs).

Computational approaches to identifying RNA-binding proteins

A recent computational approach identified RBPs based on searches for proteins that harbor a known RBD or other domain features consistent with RNA-related activities. This revealed 1542 RBPs in humans and presented a solid overlap with the experimentally-determined RNA interactome for humans [10]. However, this approach is prone to false positives in that those with classical RBDs that perform non-RNA binding functions or those that interact with RNA indirectly through another RBP will be falsely identified as having a role in RNA regulation [5]. A consistent property of RBPs is that they tend to interact with other RBPs, either indirectly or through bridging by an RNA. This behavior was exploited to develop "support vector machine obtained from neighboring associated RBPs", or SONAR, in order to identify novel RBPs. This method essentially evaluates each protein against protein-protein interaction data, and calculates its "RBP classification score" in order to identify proteins with a high likelihood of RNA-binding. SONAR data for the human, Drosophila and yeast datasets agree well with experimentally-determined RBPs [11]. However, this method is also subject to false-positives in that proteins that interact with RBPs aren't always RBPs themselves.

Emerging principles of RBP-mediated RNA regulation

The classical view of RBP-mediated RNA regulation dictates that RBPs modify the translation of a set of transcripts to meet the cell's ever-changing protein requirements. These RBPs bind to certain regions of the 5` and 3` UTRs, as well as within the coding sequence, and canonical RBPs contain identifiable RNA binding domains, such as the RRM, the KH domain, or the DEAD-box helicase, that recognize short stretches of RNA (approximately 2-10 nucleotides) often with low affinity [12]. RBPs can increase their affinity and specificity for particular RNAs based on the cooperative activity of multiple binding domains, for example the four RRMs of poly(A) binding protein can work in concert [13]. With the advent of new technologies, we are beginning to appreciate that the scope of RBPs in all kingdoms of life have been previously underestimated; the current estimation suggests that RBPs can comprise up to 11% of an organism's proteome [10]. The discovery and characterization of novel RBPs is now re-writing the way we consider post-transcriptional regulation and is revealing new complexity to this essential stage in gene expression [14,15].

RNA-binding proteins versus protein-binding RNAs

RNA-interactome capture has identified a large set of "enigmRBPs" that include highly-conserved RBPs with no previously-assigned role in RNA biology, such as metabolic enzymes. These enzymes participate in a wide variety of metabolic pathways including glycolysis, the tricarboxylic acid (TCA) cyle, lipid metabolism, DNA biosynthesis, and the catalyzation of different reactions [14]. Some of these enzymes, including pyruvate kinase M2 (PKM2) and enolase 1 (ENO1), had previously been shown to interact with RNA *in vitro* [16], but the advent of interactome capture allowed for the discovery of these metabolic proteins' interactions with RNA *in vivo*. Some of these RBPs even have important implications in disease contexts, for example mutations in the RNA-binding enzyme IMPDH1 (inosine 5′-monophosphate dehydrogenase 1) are associated with retinitis pigmentosa, a disease which causes severe vision impairment and degeneration of the retina [17]. Novel treatment options for diseases linked to RNA-interacting metabolic enzymes potentially lie within a better understanding of these interactions.

As our knowledge of the RNA-interactome has expanded to include proteins whose canonical functions lie outside of RNA regulation, new questions have arisen about the significance of these proteins binding RNA. The conventional understanding of RNA-protein interactions dictates that the protein is exerting some regulatory influence on the RNA. But the possibility that RNAs can also regulate the activity of their bound proteins has now become a reality [18]. There are examples of protein-regulating RNAs in the prokaryotic kingdom. For example, bacterial 6S RNA is a 200-nucleotide-long non-coding RNA that inhibits the transcription of housekeeping genes in *Escherichia coli* and *Bacillus subtilis*. This RNA adopts a

rod-shaped secondary structure, with a flexible core region that imitates an open promoter, which binds to and inhibits RNA polymerase. This mechanism has been identified in all branches of the bacterial kingdom [19]. Examples have also been found of RNAs regulating proteins in eukaryotic cells. Long double-stranded RNA (dsRNA) generated during viral replication can trigger protein kinase R (PKR) dimerization, resulting in its autophosphorylation and activation. PKR then targets and phosphorylates eIF2α, trapping it in the inactive state and inhibiting its ability to participate in translation initiation [20]. PKR activation by dsRNA provides an example of an RNA that can *activate* the activity of an enzyme. The above examples also point out the possibility for RNA to be more than a bystander or a passenger of RBP-mediated regulation, and they open the door for discovering new roles for RNA in controlling the function and activity of their bound proteins.

A few modes by which RNA could regulate proteins have recently been proposed by Castello, Hentze and Preiss. First, it is possible that the bound RNA overlaps with the active site and/or cofactor binding site of an enzyme, thus directly competing with substrates or cofactors. This mechanism would thereby block enzymatic activity of the protein. A second possibility would be that RNA binds to a region separate from the protein's active site, which could either have no effect on catalytic activity, or it could exert an allosteric effect on the enzyme's metabolic activity in either a positive or negative sense. Third, RNA binding could impact the interactions of the enzyme with another cellular component, for example linking it to the plasma membrane or another organelle. Fourth, enzymes often function as members of a homo- or hetero-oligomeric complex, such that the interaction with RNA could bridge connections between complex subunits, or conversely interfere with complex assembly. And fifth of all, there is the possibility of an assembly of a "metabolon", or a large aggregate where enzymes within a pathway are held together by weak interactions in order to perform a higher level of metabolic activity [18]. Evidence for the last possibility include the higher order complexes formed by GAPDH (Glyceraldehyde 3-phosphate dehydrogenase) with other glycolytic enzymes, which have been biochemically isolated and shown to be RNase-sensitive [21].

Understanding the functional significance of the interactions between metabolic enzymes and RNA present a new frontier in characterizing post-transcriptional regulation. Uncovering why these interactions happen, and what occurs when they are disrupted or dysregulated, promises to shift the current paradigm of post-transcriptional gene expression.

Protein disorder and RNA-binding

Intrinsically disordered regions (IDRs) and proteins lack stable three-dimensional structure and are known to participate in a wide variety of cellular processes, including signalling, enzymatic activity and gene expression [22]. RBPs are substantially enriched in IDRs and this disorder is evolutionarily conserved [23]. Sometimes the disorder of a given protein region will be conserved even if the underlying amino acid sequence is not, though conservation of sequence and structure is typically stronger in regions of the protein which have direct contact with RNA [24]. Many of the well-characterized RBPs with classical RNA-binding domains (RBDs) have IDRs, even if these regions don't necessarily interact with RNA. For example, polypyrimidine tract binding protein 1 (PTBP1) has flexible linker regions which separate its RRMs [25]. IDRs in RBPs allow for conformational plasticity that contributes to function; even in proteins with well-defined RNA-recognition motifs (RRMs), some plasticity is required for function. For example, CUG-binding protein 2 (CUGBP2) exists in distinct conformations that enable a switch between low-affinity binding, associated with dynamic RNA scanning, and high-affinity binding, associated with RNA target locking [26,27]. The requirement for RBPs to perform distinct functions underscores the importance of protein flexibility in the fine-tuning of RNA regulation.

Disordered regions can also occur *within* RNA-binding motifs, and the following is a short description of how each motif fits into IDR-mediated RNA regulation. Short linear motifs (SliMs) are composed of up to ten amino acid residues that bind RNA with low affinity, yet specificity can be accomplished by SliM repetition and post-translational modifications. Arginine and glycine repeats (RGG) are the second most common RBD in the human genome, and they function in broad-specificity RNA recognition. Arginine-serine or arginine-glycine (RS/RG)-rich sequences can mediate both specific and nonspecific interactions with RNA. They occur in a number of human proteins and are referred to as SR and SR-like proteins, including the pre-mRNA splicing factors. Lysine/arginine (K/R) patches are composed of four to eight K or R residues that form a highly-positive interface. K/R patches are abundant among non-canonical RBPs and frequently flank globular domains. Molecular recognition features (MoRFs) consist of 25 to 50 amino acid residues that have the ability to undergo dynamic disorder-to-order transition upon ligand binding. And finally, low-complexity (LC) sequences contain up to 100 amino acids composed of many repeats of the same amino acid or several amino acids. With increasing LC concentrations, proteins containing these sequences can polymerize into amyloid-like fibres and undergo a phase-transition into a hydrogel-like state. LC sequences are characteristic of proteins that are part of large RNA storage granules, which are important for RNA transport, storage, preservation and decay, as discussed below [26].

Protein disorder and the formation of ribonucleoprotein granules

Ribonucleoprotein (RNP) granules are eukaryotic membraneless organelles composed of non-translating mRNAs, along with proteins, that assemble upon bulk translation inhibition. They form RBP protein-protein interactions mediated by RNA scaffolding, for example through dimerization of RNA-bound Edc3, and via liquid-liquid phase separation (LLPS) driven by the presence of proteins with IDRs, for example Lsm4 [28]. There is also recent evidence that *trans* RNA-RNA interactions play a role in the recruitment of RNAs to stress granules in particular [29]. RNP granules provide the separation of specific components into one compartment without the necessity for crossing a membrane [30]. Studies utilizing fluorescence recovery after photobleaching (FRAP) have demonstrated that these structures are highly dynamic in that they are relatively easily accessed by external factors and can quickly dissolve [31]. Finally, RNP granules are fairly common in the nucleus and the cytoplasm and are found in all eukaryotes from yeast to humans [32].

In yeast, cytoplasmic RNP granules include P-bodies, which are more liquid-like, and stress granules, which are more solid-like [33]. P-bodies contain translationally-repressed mRNAs together with proteins involved in mRNA decay. These include the decapping complex Dcp1/Dcp2, the activators of decapping Dhh1, Pat1, Edc3, and Lsm1-7, and the 5`-3` exonuclease Xrn1 [34]. P-bodies also harbor components of the nonsense-mediated decay pathway, which rapidly degrades aberrant mRNAs that contain premature stop codons. Edc3 and Lsm4 are central for P-body assembly; they contain glutamine/asparagine (Q/N)-rich prion-like domains which promote self-aggregation [35]. Stress granules, on the other hand, contain mRNAs that are also translationally repressed yet stalled in the process of translation initiation, and they include translation initiation factors and ribosomal subunits. Stress granules harbor multiple components of the translation initiation machinery, including eIF4E, eIF4G, Pab1, Pub1, Ngr1 and Pbp1, although their composition can vary depending on the type of stress that elicited their formation [36]. Both P-bodies and stress granules are highly-dynamic and are formed in response to conditions that result in translation repression, including environmental stress. P-bodies can also be present in low numbers during normal growth [37].

P-bodies and stress granules have been shown to interact with each other, potentially through shared protein components or mRNA species, and in fact stress granules are often formed next to or overlapping with P-bodies [38]. This overlap suggests a model of a cytoplasmic mRNP cycle in which mRNAs are exchanged between polysomes, stress granules and P-bodies in order to be translated, stored, or degraded. The dysregulation of RNP granule assembly and disassembly could have detrimental consequences for the cell, and often are linked to various neurodegenerative diseases in humans [39].

A recent study provided evidence for a novel type of cytoplasmic granule in yeast and humans that specifically contains glycolytic mRNAs. They named these “core fermentation” (CoFe) granules, and claim they are condensates of highly-translated mRNAs where translation

is a prerequisite for localization to the granule. They also suggest that the formation of these CoFe granules provides a mechanism by which the cell can scale up protein production of the highly-translated glycolytic enzymes, and that the coordination of pathway regulation is more easily achieved within these granules [40]. This study may pave the way for the discovery of new types of cytoplasmic granules with functions separate from the canonical storage and decay provided by stress granules and P-bodies. What is clear from all of the preceding work on RNP granules is that they play an essential role in the lifecycle of the mRNA. A better understanding of RNP formation and the driving forces that lead to their assembly, dissolution, and unique compositions is crucial to a more complete understanding of RNA regulation in general.

The need for functional characterization of RNA-binding proteins

The work preceding our study nicely describes the extent to which diverse proteins interact with RNA in eukaryotes. However, the primary question remains regarding *why* many of these proteins interact with RNA in the first place. This highlights the need for the functional characterization of RNA-binding proteins. Here we present two studies that approach this biological question from different ends. The first study entails a focused analysis of a single RBP in yeast: the dynamic post transcriptional regulator Mrn1. The second study details the development and implementation of a proteome-wide survey for post-transcriptional regulation. Both methods contribute new information to our understanding of RBP-mediated RNA regulation, and add more color to the complex network of proteins that modulate mRNA across its lifecycle.

Chapter 2: Surveying the global landscape of post-transcriptional regulators

Abstract

A dynamic network of proteins modulates the translation of messenger RNA (mRNA) to meet the changing needs of the cell. RNA-binding proteins (RBPs) are the key elements in this network that determine whether a given mRNA is translationally activated or repressed, localized to a specific region or compartment within the cell, or degraded. Motivated by the important role RBPs play in gene expression, several groups have worked to identify hundreds of yeast RBPs and their mRNA targets, and the RNA-binding domains (RBDs) of these proteins have been revealed on a proteome-wide scale. Though these studies have provided important evidence for the physical interaction of these RBPs with their cognate mRNAs, it has proven more challenging to discover their regulatory functions. To answer the outstanding question of how RBPs regulate mRNA translation, we have adapted the tethering assay into a broad and powerful survey for regulatory activity on a proteome-wide scale. Our data provide functional information with domain-level resolution for proteins known to regulate translation, such as the initiation factor Ded1, and decay, such as the NMD factor Ebs1. We also identify regulatory effects from proteins with other primary functions in the cell, including metabolic enzymes, along with proteins whose cellular roles have yet to be characterized. RBPs are enriched among the most active regulators in our screen, yet notably the domains responsible for their regulatory functions do not include their RNA-binding regions. To gain further insight into the genetic networks governing individual regulatory proteins, we have extended our approach to identify suppressors and enhancers of regulatory activity by comprehensive CRISPRi screening. Our global functional analysis reveals missing links in translational control and allows a more comprehensive understanding of RNA biology.

Introduction

Post-transcriptional gene regulation is now recognized as a major control point for the transmission of genetically-encoded information into protein production. In order to meet the ever-changing needs of the cell, a highly-integrated network of regulators controls the translation of messenger RNA (mRNA) to generate a dynamic proteome [41]. This network is comprised of a complex interplay between cis-acting elements encoded by the mRNA, including RNA secondary structures, upstream open reading frames (uORFs) and internal ribosome entry sequences (IRESes), and trans-acting factors which interact with the mRNA, such as RNA-binding proteins (RBPs) and micro-RNAs (miRNAs). The influence of RBPs can determine whether a given mRNA is translationally activated or repressed, localized to a specific region or compartment within the cell, or degraded. In addition, RBPs can remodel RNA structure to make it accessible to other RBPs or enzymes, and can act as chaperones to prevent RNA aggregation and misfolding [10,42].

Due to the important role RBPs play in post-transcriptional regulation, many studies have been devoted to understanding the diversity of RBPs and how they identify their mRNA targets. This has resulted in the discovery of the most common RNA binding domains (RBDs) harbored by RBPs. These domains recognize 4-9 nucleotide segments in RNA that can occur in combinations or repeats, which allows for either different assemblies of RBPs to bind in tandem or the accumulation of one RBP [6,23,41]. However, computational searches for RBDs are limited in their utility for *de novo* identification of RBPs since many of these proteins lack a known or canonical RBD. Recent studies have favored using cross-linking paired with Oligo(dT) capture to identify proteins that bind RNA *in vivo*, termed “RBP interactome capture” [23]. While this approach can identify proteins without canonical RBDs, it will still exclude RBPs that are not efficiently cross- linked or expressed in the cell type or stage of growth used in the assay. Despite their limitations, RBP interactome studies have identified thousands of RBPs and their *in vivo* mRNA binding partners, including approximately 700 high-confidence RNA-protein interactions in budding yeast [14,23].

Though we now appreciate the extent to which RBPs interact with RNA, there is still much we don’t understand about their function. We know that a given RBP can have the capacity to bind a multitude of mRNAs, and that multiple RBPs can bind the same mRNA and together determine that mRNA’s fate [41,43]. Yet it can still be unclear when RBPs are forming synergistic complexes versus competing with other RBPs. In addition, many studies have reported evidence of metabolic enzymes ‘moonlighting’ as RBPs, however no systematic concept has been proposed to explain this phenomenon. This suggests some currently hidden connection between post- transcriptional regulation and metabolism which has yet to be integrated into our understanding of cell biology [14].

Here we have employed the well-described tethering assay in a high-throughput format to expand upon the network of RBPs and their cognate mRNAs as identified by previous studies

[44]. We've identified proteins which specifically activate or repress post-transcriptional regulation, and have found that many RBPs are active through their domains outside of their RNA-recognizing regions. We've demonstrated that this assay can be used to characterize completely unknown proteins as well as provide new functional insights into well-characterized RBPs. All-in-all, we've developed a novel high-throughput method for the functional characterization of post-transcriptional regulators that could be adopted to other cellular contexts including stress, development and disease, and we've expanded our comprehension of the complex regulation that happens at the post-transcriptional level.

Results

The quantitative dual-reporter tethering assay reveals reliable and reproducible functional information about mRNA regulatory proteins.

Our primary goal was to functionally assess proteins across the entire genome for a role in RNA regulation. In order to do this, we first needed to establish an assay that would allow us to reliably and reproducibly characterize proteins involved in mRNA metabolism. To this end, we devised a dual fluorescent reporter tethering assay where we could selectively modulate the expression of one fluorescent protein (e.g., YFP) by targeting its transcript with a candidate regulatory protein while using a second non-targeted fluorescent protein (e.g., RFP) as an internal control. This setup provided the distinct advantage of a high-precision quantitative readout since changes in the targeted mRNA's expression could be normalized to the expression of the non-targeted mRNA **(Figure 1A)**. In addition, by utilizing fluorescent proteins as our readout, we were able to employ flow cytometry and fluorescence-activated cell sorting (FACS) to analyze the functional effects of tethered proteins in a single-cell format. Each reporter contained either five BoxB RNA hairpins or three PP7 RNA hairpins in its 3` UTR, which have a high affinity for the LambdaN coat protein or PP7 coat protein (PCP), respectively [45]. This allowed us to precisely target query proteins to the 3` UTR of either reporter and examine the effects on the targeted reporter's expression. Regulatory effects could be separated from RNA-specific or hairpin-specific effects by swapping the RNA-hairpin pairings and validating our results across all four configurations. Additionally, the activity of all proteins assayed with our tethering constructs are reported relative to a tethered Halo protein that exhibited no regulatory activity.

To validate our ability to measure post-transcriptional changes in reporter expression, we began by targeting known mRNA regulatory proteins to our reporters. We examined the cells expressing these constructs for evidence of the tethered proteins' activity. For example, Poly(A)-binding protein, or Pab1, plays a key role in translation initiation [46], so we expected it to robustly activate reporter expression. Conversely, Pop2 is a subunit of the CCR4-NOT deadenylase complex mediating 3` mRNA degradation[47], thus we expected it to solidly repress reporter expression. By tethering each combination of regulatory protein and fluorescent reporter using BoxB and LambdaN, we found Pab1 upregulated reporter expression approximately 2.8-fold (± 0.1 standard deviation), whereas Pop2 reduced expression by approximately 5.4-fold (± 0.05) **(Figure 1B)**. When we tethered Pab1 and Pop2 with PP7 and PCP, we noted that both proteins still changed the targeted mRNA's expression in the direction we expected, although we saw more variation in activity depending on the reporter targeted **(Figure 1C)**. Pab1 still upregulated expression by 2.8-fold (± 0.3), yet Pop2 was weaker in this context as it repressed mRNA expression only about 2.3-fold (±0.2). In order to further validate tethering with PCP and PP7, we tethered Pat1, which activates decapping and recruits 5` and 3` decay machinery to

mRNA [48], to both mRNA reporters. Though we observed low variability between Pat1 replicates targeting the same reporter, we still noted there was some degree of variability across the two reporters **(Figure S1A)**. We thus used the BoxB-LambdaN system for the remainder of our experiments to ensure less noise would be introduced into our data based on experimental design.

Finally, we wanted to verify that we could use the tethering assay to reproducibly characterize the activity of unknown regulators. Sgn1 is a poorly understood RNA-binding protein that seems to be involved in regulation of translation based on co-immunoprecipitation with Pab1 and negative genetic interactions with the budding yeast eIF4G alleles [49] **(Figure 1D)**. We determined Sgn1 regulatory activity by targeting it to YFP, and discovered it is a powerful activator. It upregulated YFP expression by approximately 6.4-fold (Fig. 1E) relative to RFP, even after accounting for the increased expression in both YFP and RFP in Sgn1-expressing cells **(Figure 1E)**. Through this rigorous validation, we felt confident the dual reporter tethering assay would be a powerful tool for a high-throughput, proteome-wide survey for regulators of post-transcriptional gene expression.

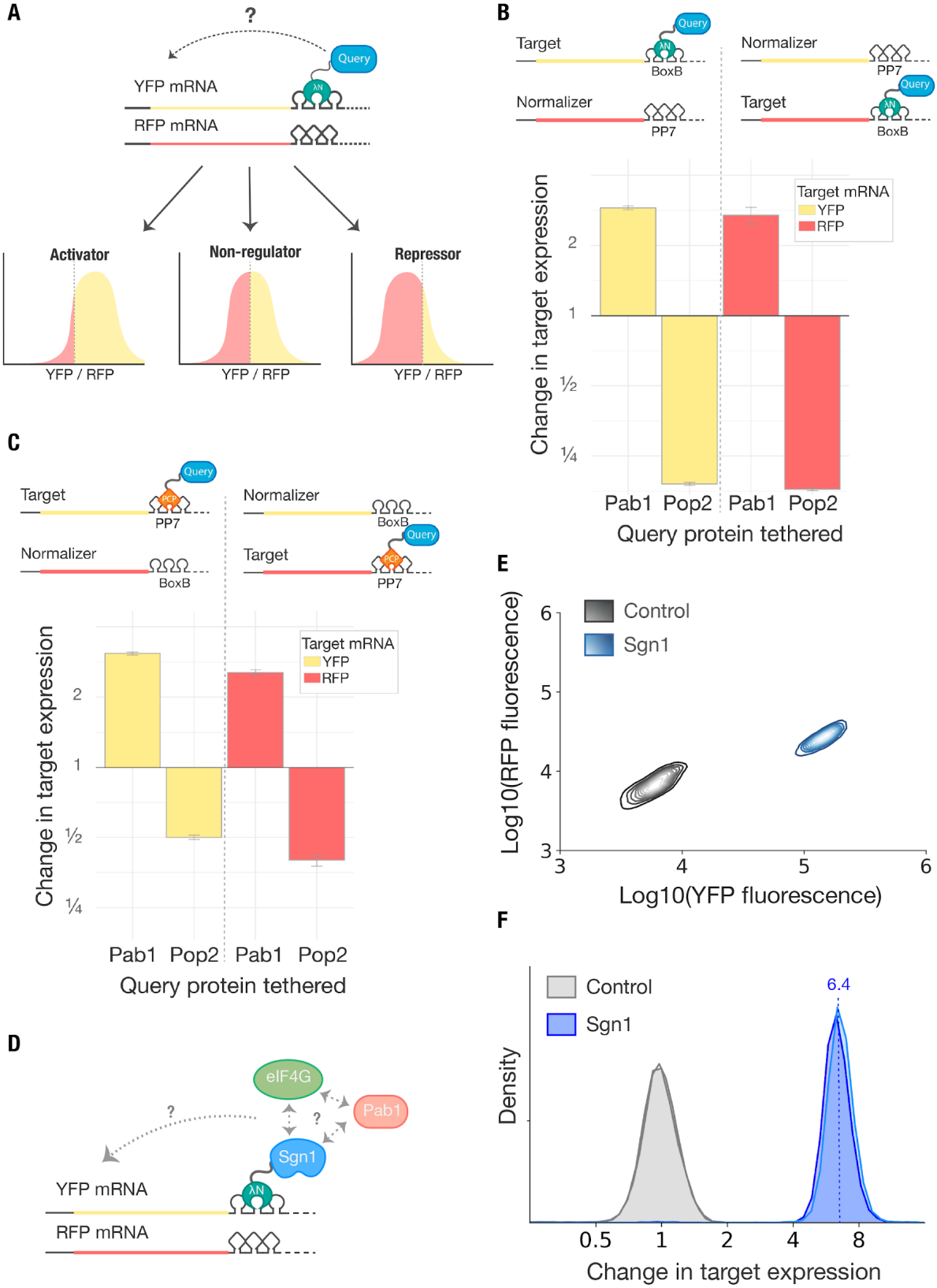
A
?
Query
λN
YFP mRNA
RFP mRNA
Activator
Non-regulator
Repressor
YFP / RFP
YFP / RFP
YFP / RFP
B
Target
Query
λN
BoxB
Normalizer
PP7
Normalizer
PP7
Target
Query
λN
BoxB
Target mRNA
YFP
RFP
Change in target expression
2
1
½
¼
Pab1 Pop2 Pab1 Pop2
Query protein tethered
C
Target
Query
PCP
PP7
Normalizer
BoxB
Normalizer
BoxB
Target
Query
PCP
PP7
Target mRNA
YFP
RFP
Change in target expression
2
1
½
¼
Pab1 Pop2 Pab1 Pop2
Query protein tethered
D
eIF4G
Pab1
?
?
Sgn1
λN
YFP mRNA
RFP mRNA
E
Control
Sgn1
Log10(RFP fluorescence)
6
5
4
3
3 4 5 6
Log10(YFP fluorescence)
F
Control
Sgn1
6.4
Density
0.5 1 2 4 8
Change in target expression

Figure 1. The dual reporter tethering assay is a powerful tool to functionally characterize post-transcriptional regulators.

(A) Schematic representation depicting phenotypic readout when the tethered query protein is a post-transcriptional activator, non-regulator, or repressor of expression.

(B) Pab1 and Pop2 tethered to either YFP or RFP using the BoxB RNA hairpins and the LambdaN viral coat protein yield reproducible phenotypes.

(C) Pab1 and Pop2 tethered to either YFP or RFP using the PP7 hairpins and the PP7 coat protein yield reproducible phenotypes.

(D) The change in YFP reporter fluorescence relative to the change in RFP reporter fluorescence is used to calculate the quantitative regulatory effect of the tethered query protein.

(E) Sgn1 is likely a post-transcriptional upregulator based on previously-published interactions with translation initiation machinery, including eIF4G and Pab1.

(F) Sgn1 is a 6.4-fold upregulator of YFP expression, normalized to RFP.

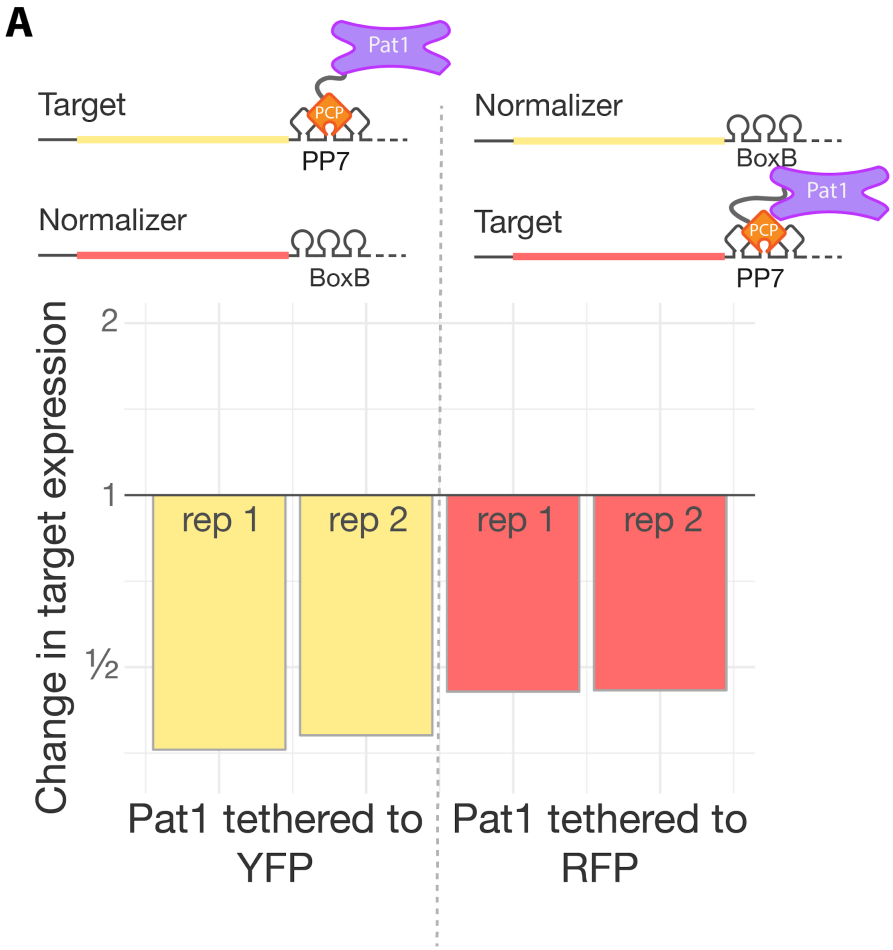

Figure S1A. Pat1 tethering with PP7 yields reproducible repression within YFP and RFP replicates, but more variability between RFP vs. YFP tethering.

The generation of a comprehensive, unbiased tethering screen library requires a preliminary selection for fragments in the correct reading frame.

The primary goal of this project was a comprehensive survey of the yeast proteome for post-transcriptional regulatory activity in an unbiased manner. We aimed to create a library of yeast DNA fragments randomly selected from the yeast genome, however the inclusion of only in-frame DNA fragments in the library presents a major technical challenge. This is because of the triplet nature of the genetic code; randomly fragmented DNA is unlikely to start and end in frame. We addressed this challenge by integrating a selectable marker into our DNA fragment expression cassette so that only in-frame fragments would grow in selective media. We generated our fragment library from yeast genomic DNA using the Nextera XT tagmentation kit by Illumina, which randomly cuts DNA and adds 5` and 3` adaptors to the free DNA ends **(Figure 2A)**. We size-selected for fragments of roughly 500 base pairs, as we wanted to assay fragments that were less than the size of a full-length protein, and then used the aforementioned adaptor regions to clone our DNA fragments into an expression vector using homologous recombination in yeast. This expression vector situated the DNA fragments such that they would be initiated and terminated by the same start and stop codon as a downstream selectable marker. This means that only fragments that start and end in frame, and are in the correct orientation, will support growth in selective media. Out-of-frame fragments are statistically likely to encode a premature stop codon, and thus will not grow in selective conditions **(Figure 2B)**. We analyzed select clones from our fragment library with sanger sequencing and found 10 out of 10 of the samples we tested encoded in-frame fragments, indicating that our strategy for selecting the correct reading frame is very efficient.

The incorporation of barcodes in high-throughput screens can increase the statistical robustness of the screen readout [50,51]. We barcoded our in-frame fragments by subcloning them into a library of vectors encoding lambdaN and BFP, and introduced unique 25 nucleotide barcodes. We aimed to assign roughly 3 unique barcodes to each fragment in order to examine whether all barcoded copies of the same fragment behaved similarly in the screen. We maintained the mean size of our fragment library at approximately 500 base pairs, indicating that the additional subcloning step did *not* preferentially select for smaller fragments **(Figure 2C)**.

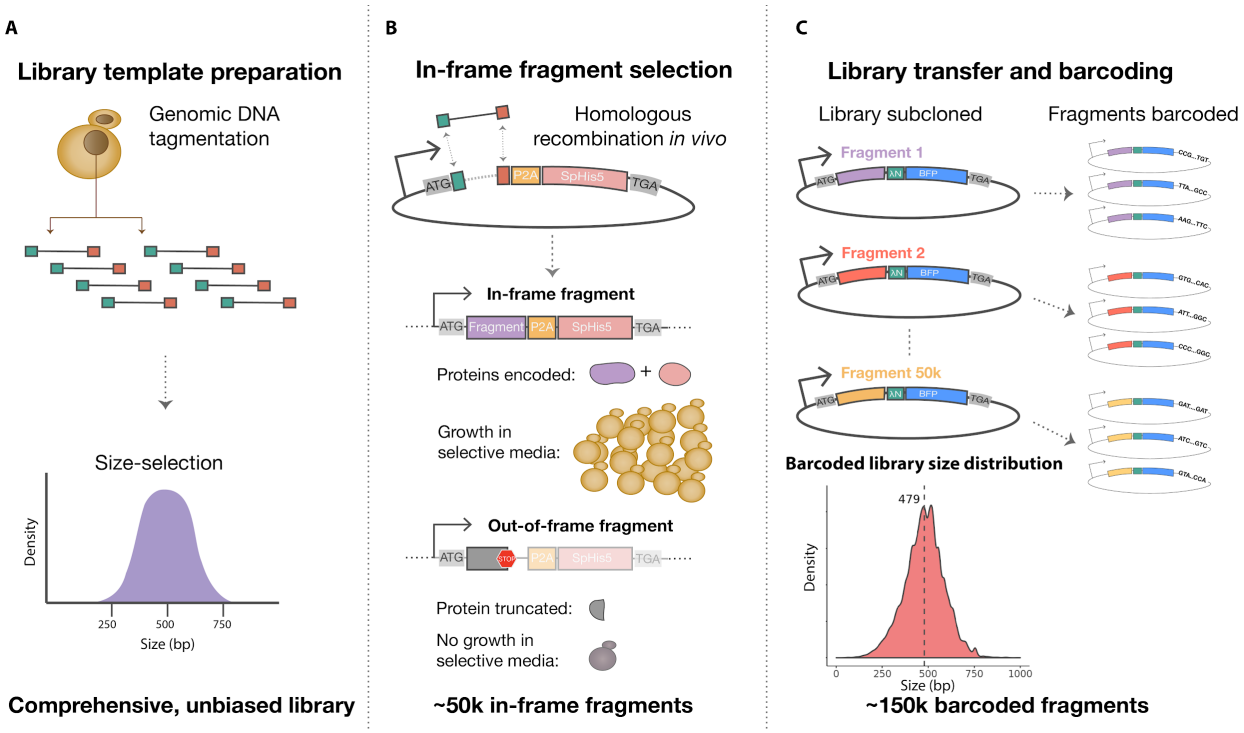

Figure 2. Selection for the correct reading frame is a major technical hurdle in unbiased fragment library generation.

(A) Genomic yeast DNA was fragmented with the Nextera XT Tagmentation kit, and size selected for an average size of 500 base pairs.

(B) Fragments were cloned via homologous recombination into a vector with a downstream SpHis5 protein. Only in-frame fragments will grow on minus-histidine synthetic media, all out of frame fragments are statistically likely to encode a stop codon and will not grow in minus-histidine medea.

(C) The in-frame fragment library was subcloned into a vector with a downstream lambdaN coat protein and a BFP. Each fragment was barcoded approximately three times with a unique 25-nucleotide barcode.

A high-throughput activity assay for characterizing tethered fragments in a single-cell format.

The tethering assay allows us to analyze the activity of tens of thousands of yeast protein fragments simultaneously in a single-cell format. We can sort cells based on their phenotypic changes in YFP versus RFP expression, which allows us to isolate and identify activators and repressors of post-transcriptional gene expression. We transformed the dual reporter strain with our barcoded tethering library and examined their phenotypes via fluorescence activated cell sorting (FACS). We drew four equal FACS gates so that an equal number of cells would be sorted into each bin, which allowed us to group cells based on their changes in YFP versus RFP expression **(Figure 2A)**. We isolated the plasmid DNA expressed in our sorted cells and amplified the barcodes from those plasmids. We then quantified each barcode using next generation sequencing.

Based on the enrichment pattern in the four bins from the sort, we could determine how strongly each fragment activated or repressed YFP expression. For example, a particular fragment of Sbp1 showed up as a strong activator in our screen in that it sorted almost entirely into the far right bin, associated with high YFP relative to RFP expression, indicating it strongly increased YFP expression. Conversely, an Ebs1 fragment showed up as a strong repressor in our screen in that it sorted almost entirely into the far left bin, indicating it strongly down-regulated YFP expression **(Figure 2B)**. We used these sort patterns to determine the "activity score" for each fragment in our screen, which is a score between -2.0 and +2.0. The more negative a fragment's score, the stronger a repressor it is; the aforementioned Ebs1 fragment had an activity score of -1.9. The closer a fragment's score is to +2.0, the stronger an activator it is, for example the above Sbp1 fragment had an activity score of +1.9. Most fragments in our library demonstrated a normal distribution in that their activity scores were close to zero, indicating weak or no activity in the screen **(Figure 2C)**. The fragments that were most enriched in either end of the activity score distribution represent the most active fragments in the screen.

Interestingly, canonical RBPs were enriched among the most active fragments in the tethering assay screen. We compared four overlapping datasets that reported RNA-protein interactions and designated the requirement that a protein must appear in more than one dataset in order to be considered truly RNA binding [3,43,52,53]. Proteins that were reported to bind RNA in one or fewer datasets were considered "non RNA-binding". We found that when we plotted the absolute activity score of all proteins in the screen vs. the non-RNA-binding and RNA-binding proteins, proteins with a high-confidence RNA interaction were likely to have a *higher* absolute activity score **(Figure 2D)**. This result increases our confidence in the tethering assay screen and demonstrates that it is an effective survey for detecting bonafide RNA-regulatory activity.

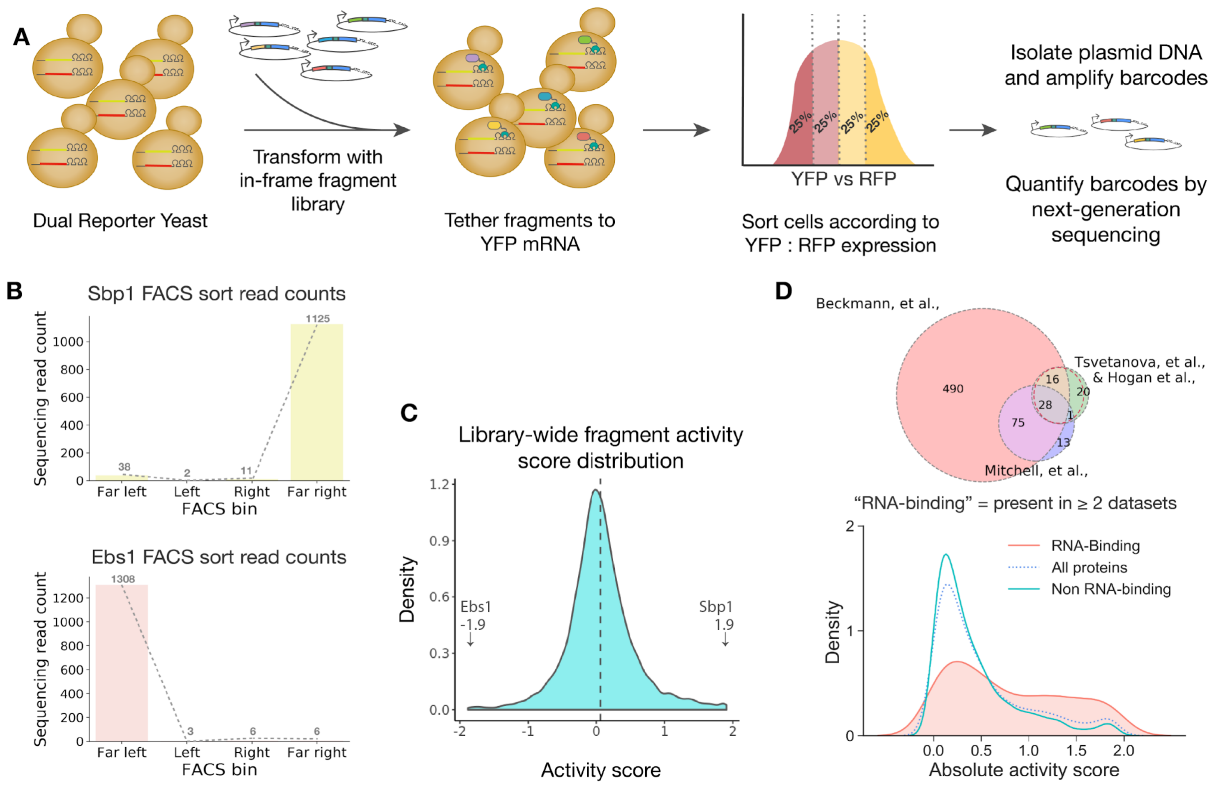

Figure 2. Identification of activators and repressors of post-transcriptional gene regulation through the high-throughput tethering assay.

(A) Our dual reporter yeast strain was transformed with the barcoded tethering library. Cells were sorted based on their phenotypic changes in YFP relative to RFP, and the fragments expressed by each cell were isolated, amplified, and quantified via next-generation sequencing.

(B) An Sbp1 fragment showed up as a strong activator in the screen and was almost entirely enriched in the far-right gate.

(C) An Ebs1 fragment showed up as a strong repressor in the screen in that it was almost entirely enriched in the far-left gate.

(D) The library-wide distribution of fragments along the activity score spectrum.

(E) Four studies were compared to find high-confidence RNA-protein interactions. Those proteins that were identified as true RNA-binding proteins were more enriched in the most active fragments in the screen.

The tethering assay is a tool that can be adapted to characterize RBPs in higher eukaryotes.

The dual fluorescent reporter tethering assay is a versatile tool that can be adapted to higher eukaryotes. We established the tethering assay in mammalian cells and demonstrated that tethering a post-transcriptional repressor to the 3` UTR of a reporter mRNA could downregulate expression, as we saw in yeast. We integrated into the HEK293 genome a cassette encoding divergently-expressed green fluorescent protein (GFP) and RFP, with PP7 and BoxB hairpins encoded in the 3` UTRs of these reporters, respectively. We then tethered the C-terminal silencing domain of TNRC6A, one of three human paralogs of GW182, to the 3` UTR of both reporters. Since GW182 is an essential component of the microRNA-induced silencing pathway in animals, we expected GW182 to be a robust repressor of reporter expression [54]. GW182 was also fused to a BFP which allowed us to gate for and only examine cells that were BFP positive as a proxy for cells expressing our GW182 tethering construct.

In cells expressing the GFP-targeting version of GW182, we noted an inverse correlation between the expression of GFP and BFP, indicating that the more cells expressed our GW182-BFP fusion protein, the more we effectively shut down GFP expression **(Figure 3A,B)**. Likewise, we saw the same effect in the cells expressing the RFP-targeting version of our GW182 tethering construct in that RFP and BFP expression were also inversely correlated **(Figure 3C,D)**. This indicates that the artificial tethering of post-transcriptional regulators to reporter mRNAs can be used for the quantitative functional characterization of mammalian proteins as well as yeast proteins. We did attempt to design a high-throughput tethering assay in mammalian cells, however the selection of in-frame human cDNA fragments was not as straight-forward as in yeast. Nonetheless, this technique will provide a powerful tool for the characterization of highly-conserved human orthologs of active proteins we discover in the yeast screen.

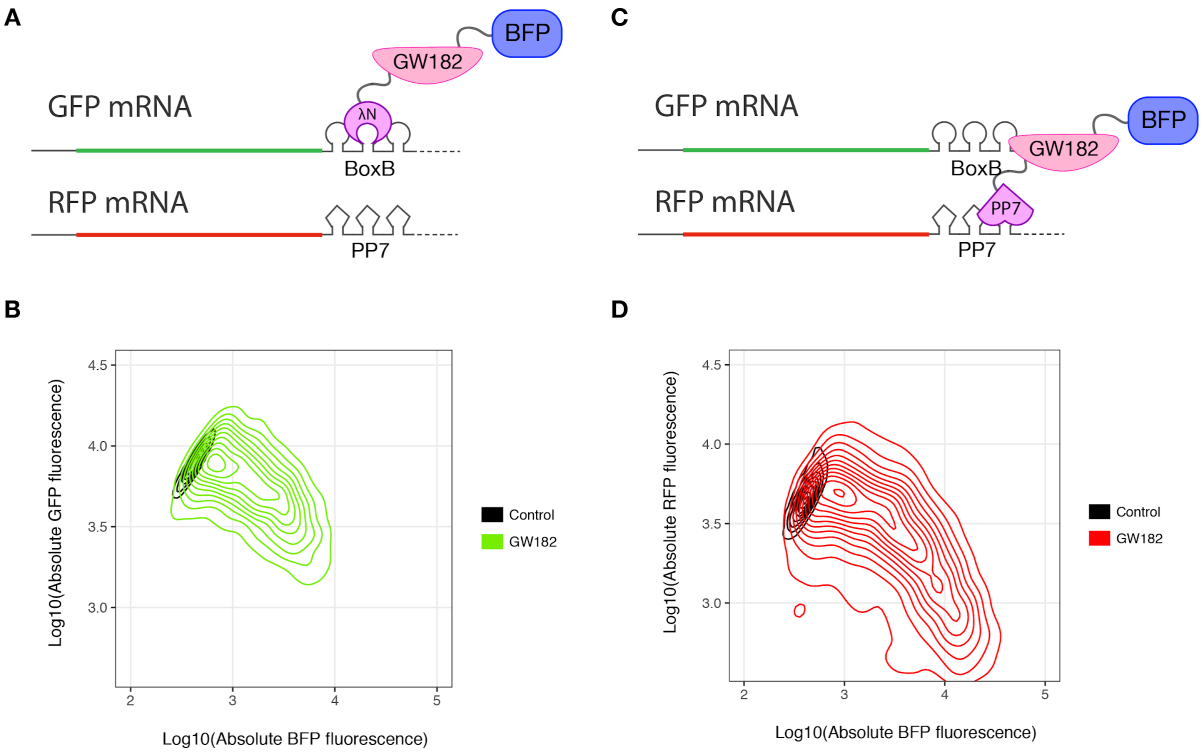

Figure 3. The dual fluorescent reporter tethering assay is a powerful tool that can be adapted to characterize RNA regulators in mammalian cells.

(A) The silencing domain of GW182 tethered to GFP via the BoxB hairpins and LambdaN coat protein.

(B) GFP expression is inversely correlated with the expression of BFP; an indicator for GW182 repression.

(C) The silencing domain of GW182 tethered to RFP via the PP7 hairpins and PP7 coat protein.

(D) RFP expression is inversely correlated with the expression of BFP; an indicator for GW182 repression.

The tethering screen reports real protein regulatory effects that can be individually recapitulated.

The tethering screen identified three "categories" of post-transcriptional regulators; first were the type of proteins we expected to see, based on their known RNA-regulatory activity like the DEAD-box RNA helicase Ded1, which is important for translation initiation of yeast transcripts [55], or Ngr1, which induces the decay of POR1 mRNA [56]. Second were proteins with characterized cellular functions outside of RNA regulation with a poorly-understood role in RNA regulation, including the small heat shock chaperone Hsp26 that has previously-identified mRNA binding activity [57]. And finally, there were the proteins of unknown function, like Her1, which may interact with ribosomes based on co-purification experiments [58].

We selected a handful of hits from the screen with a range of activity scores to test individually in the tethering assay, including a few representatives from each of the above categories **(Figure 4A)**. An important follow-up for any high-throughput screen is the individual validation of the screen results, so we wanted to ensure that we could recapitulate the activity that we observed with these hits in the screen. We identified the exact amino acid coordinates of the fragments from the screen, and cloned these fragments into a vector expressing the lambdaN coat protein. We were pleased to see that twelve out of twelve of the hits that we validated demonstrated the expected phenotype **(Figure 4B)**. In fact, when we plot the tethering screen activity score against the log2 change in the expression of the mRNA targeted in the tethering assay, we found a clear linear correlation between the two methods of measuring fragment activity **(Figure 4C)**. This indicates that the activity we are reading out in the tethering assay is an accurate representation of how these fragments behave in an individual context.

The protein fragments we characterized in the screen may have activity that varies from the full length version of the protein. We selected a handful of hits to validate the full length version of the protein alongside the screen fragments to assess how adding back the rest of the protein may influence its activity. Sbp1 is an RBP with two RRMs and an RGG-motif in the middle of the protein that recruits Pab1 [59]. The screen fragment containing only the first RRM and the RGG motif was approximately a 3-fold activator, whereas the full-length version of the protein was only a 2-fold activator **(Figure 4D)**. We hypothesize that the inclusion of the second RRM interferes with its ability to recruit Pab1 as efficiently, making it a weaker activator. Sro9 is a La-motif-containing RNA binding protein that is hypothesized to activate translation through recruitment of the closed-loop-forming translation initiation complex [60]. We found that the Sro9 fragment from the screen was roughly a 2-fold activator of expression, whereas the full length protein was an even more robust activator and increased reporter expression by nearly 4-fold **(Figure 4E)**. We also assayed both the Jsn1 screen fragment and full-length Jsn1, a poorly-characterized protein that recruits the Arp2/3 complex to mitochondria in yeast [61]. The Jsn1 screen fragment only modestly repressed YFP expression by about 25%, whereas full length Jsn1 was a slightly stronger repressor in that it repressed expression around 35% **(Figure 4F)**. And finally, we characterized Yap1801, a component of clathrin cage assembly in endocytosis [62].

We found that though the Yap1801 fragment repressed expression by around one third in the tethering screen, the full length protein was barely a repressor at all, and only downregulated expression by about 15% **(Figure 4G)**.

The variability between the activity of the fragments characterized in the screen and the full-length version of the protein can be a product of several situations. First of all, it could be that we are incompletely capturing the activity of a protein because we are missing key domains for the protein's full activity, which is likely the case for Sro9 since the full length protein is a stronger regulator than the screen fragment. Alternatively, in the screen we may be expressing a domain of a protein that has a particular function that is context-dependent, for example the RGG motif in Sbp1 and its role in Pab1 recruitment. And finally, we may be expressing a region of a protein that has a particular localization that alters the expression of the tethered mRNA, for example the Yap1801 fragment may be involved in localization to the plasma membrane where the mRNA is less actively-translated. Each of these results provides an interesting glimpse into post-transcriptional regulation and the adaptive strategies the cell has employed to differentially regulate RNA expression throughout various conditions.

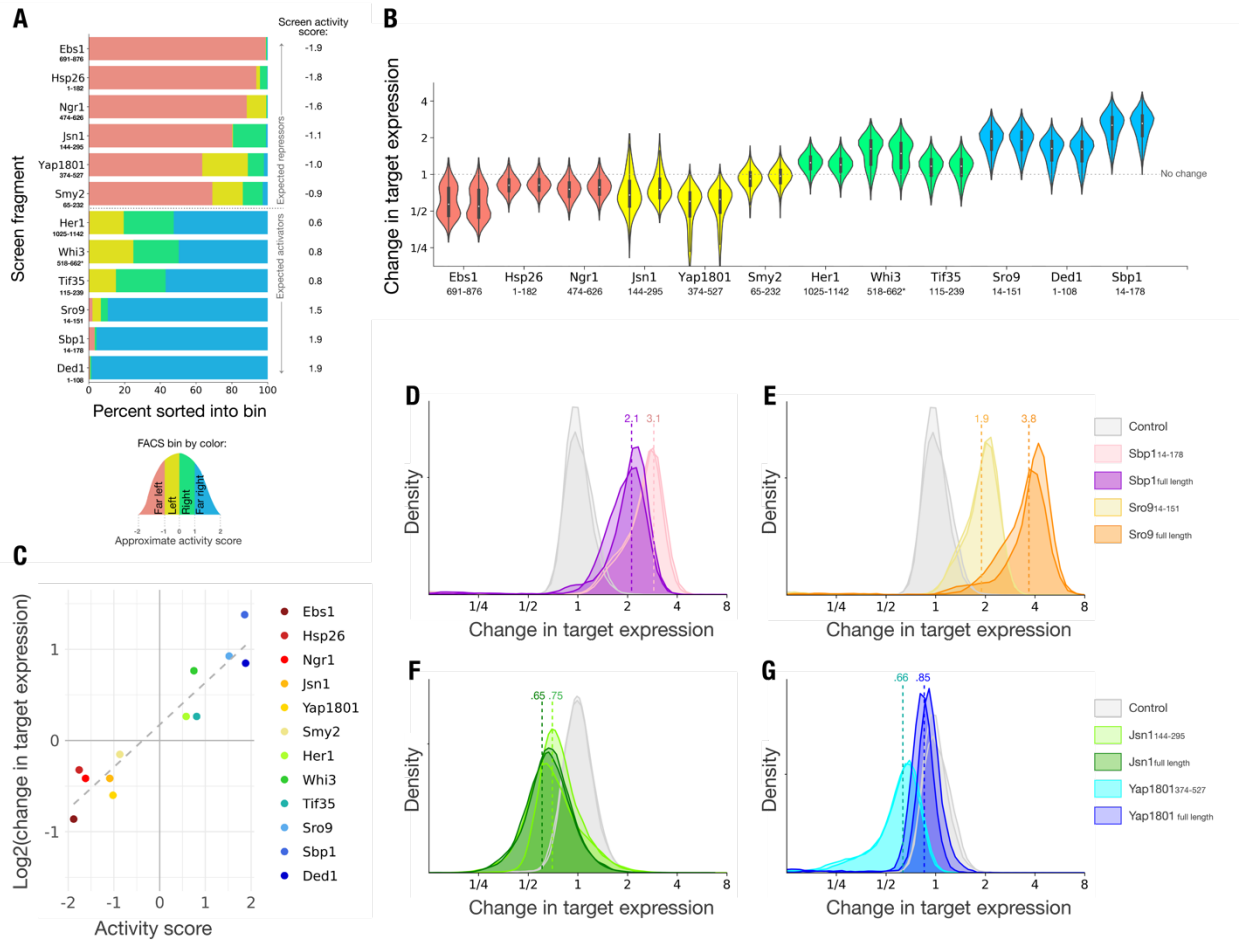

Figure 4. The tethering screen identifies real regulatory effects that can be individually recapitulated.

(A) A selection of fragments with variable screen activity based on the percentage of each fragment sorted into the bin. Inset represents activity score designation based on sort enrichment.

(B) All twelve fragments assayed recapitulated the activity they presented in the screen.

(C) The screen activity score and the change in target expression from the individual tethering assay are linearly correlated.

(D) Sbp1 fragment versus full length activity.

(E) Sro9 fragment versus full length activity.

(F) Jsn1 fragment versus full length activity.

(G) Yap1801 fragment versus full length activity.

Sro9 is a La-motif-containing post-transcriptional activator.

Sro9 is one of three La-motif-containing proteins in yeast and has been shown to associate with translating ribosomes and poly(A)-binding protein (Pab1). It is believed to stimulate translation and/or promote the stability of its bound mRNAs, and based on previous knockout studies it appears to be particularly involved in the regulation of mRNAs involved in protein synthesis [60]**.** We identified a short Sro9 N-terminal fragment in the tethering screen, Sro9(14-151), which had an activity score of 1.5, indicating it was a strong activator, and we verified that this fragment increases reporter expression in the tethering assay by around 2-fold.

In order to further characterize the rest of Sro9 in the tethering assay, we subdivided it into three domains. The first included the N-terminus of the protein up to the end of the screen fragment, Sro9(1-151), the second was an extended N-terminal fragment that includes the domain rich in asparagines, histidines, and glutamines in the middle of the protein, Sro9(1-251), and finally the third fragment spanned the remainder of the protein which includes the La-motif, Sro9(252-434) **(Figure 5A)**. We tagged these Sro9 truncations and full length Sro9 with a lambdaN coat protein for use in the tethering assay and a 3xFLAG tag to track their expression. We tethered these constructs to the 3` UTR of YFP and examined their impact on its expression. Interestingly, the inclusion of the NHQ-rich domain did not positively impact the activity of Sro9(1-251) compared to Sro9(1-151), as they were 2.1- and 2.2-fold activators of YFP expression, respectively. The La-motif containing domain, Sro9(252-434), had only a mild effect on the reporter in that it boosted expression by about 20%. Full length Sro9 was a 4-fold activator in this experiment, indicating that a protein's activity can be more powerful than the sum of its parts **(Figure 5B)**. We ensured that none of the differences in activity were due to fragment expression or stability by performing a western blot against the FLAG tag in each of these Sro9 truncations and found they were all robustly expressed **(Figure 5C)**. This discrepancy between full length activity and the activity of the Sro9 fragments could be explained by a few factors; first of all it may be that a certain conformation is only adopted by the full length protein that is required for Sro9's full function, or there may be a synergistic effect of the different domains that come together to cause it to strongly activate expression. Either way, we have identified a minimal active domain with the tethering screen in the N-terminus of Sro9 indicating the screen is an effective method for finding the functionally relevant regions of proteins.

A previous study discovered that Sro9 interacts with the 40S subunit of the ribosome and Pab1 [60]. We were curious whether the Sro9(1-151) fragment were sufficient for a stable Pab1 interaction, so we performed a co-IP experiment against the 3xFLAG tag on Sro9 and Sro9(1-151), and then blotted for Pab1 via western blot analysis. We discovered that Sro9(1-151) was sufficient to form a stable interaction with Pab1 and that it was enriched in Pab1 relative to a FLAG-tagged Halo control **(Figure 5D)**. This may indicate the C-terminal parts of Sro9 are involved in interaction with the ribosome, whereas the N-terminal region is sufficient and necessary for Pab1 interaction. Finally, we wanted to assess whether Sro9 is a translational activator, whether it promotes the stability of mRNA, or both. We performed RT-qPCR analysis

on the YFP mRNA with Sro9 tethered at its 3` UTR, and found Sro9 only increased YFP mRNA expression and/or stability by around 1.5-fold **(Figure 5E)**. Since Sro9 activates YFP expression by 4-fold, this would indicate that the majority of its function is through upregulation of translation.

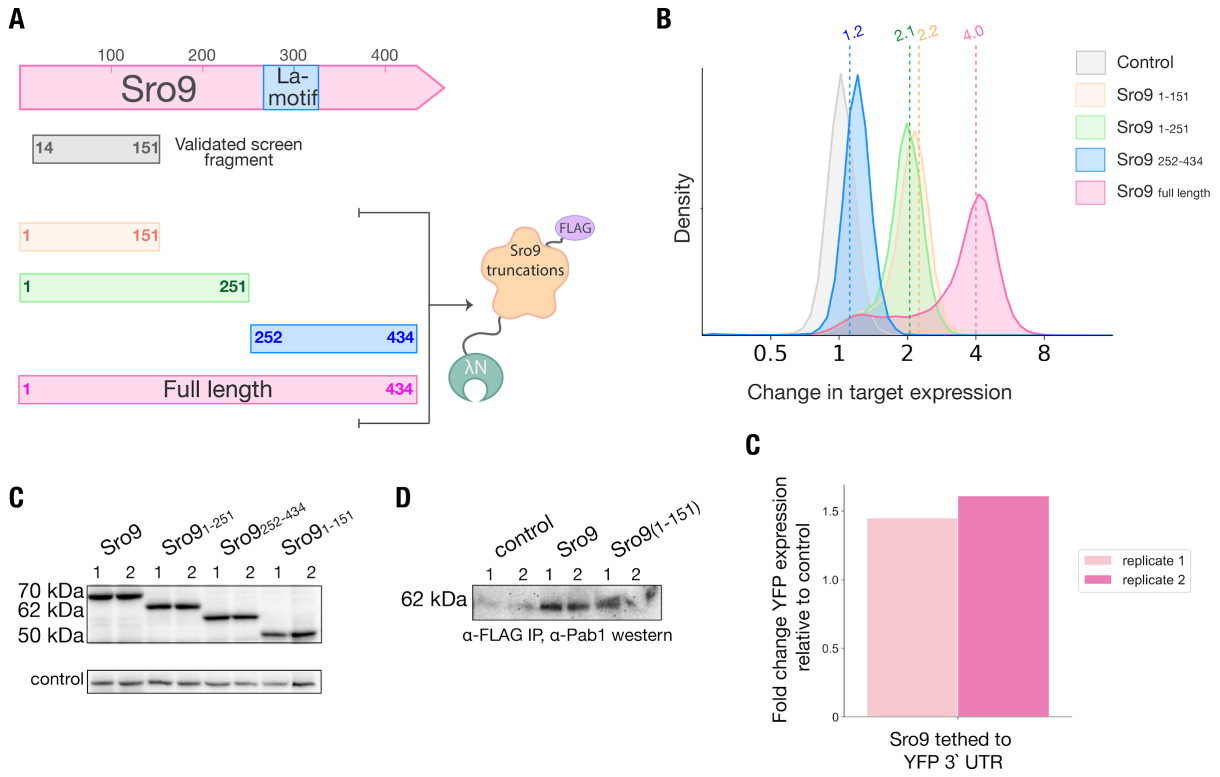

Figure 5. Sro9 is a translational activator that interacts with Pab1 via its N-terminus.

(A) Domains of Sro9 characterized in the tethering assay.

(B) Change in target mRNA expression with the Sro9 domains tethered to the 3` UTR.

(C) Western blot analysis against 3xFLAG tag indicates Sro9 domains are stably expressed in tethering assay.

(D) Co-IP against the FLAG tag and western blot against Pab1 indicates Sro9(1-151) is sufficient for Pab1 interaction.

(E) RT-qPCR analysis of YFP mRNA expression with Sro9 tethered to 3` UTR. Fold change is normalized to RFP expression and reported relative to tethering the Halo control protein.

The tethering assay reveals new functional information about the well-characterized post-transcriptional regulators, Ded1 and Ccr4.

Ccr4 is an important exonuclease in the Ccr4-Not complex that participates in mRNA deadenylation [63]. The Ccr4-Not complex is highly-conserved, and the architecture of its components have been well-described. Ccr4 contains a disordered N-terminus and a down-stream leucine-rich repeat (LRR) domain, both of which flank a region that interacts with the LRR domain. The C-terminal half of the protein contains a nuclease domain [64]. We characterized many fragments in the tethering screen that covered the N-terminal half of Ccr4, and found that most of these were distributed on the negative end of the activity score spectrum **(Figure 6A)**. Indeed, the median activity score of all of our Ccr4 fragments was -0.5, which is consistent with Ccr4's role in mRNA deadenylation. The strongest Ccr4 fragment in the screen had an activity score of -1.8 based on sorting primarily in the far-left FACS bin **(Figure 6B)**. We obtained excellent resolution of the N-terminal half of Ccr4 and found that the fragments spanning the disordered N-terminus, including the first 200 amino acids of the protein, were the strongest repressors with a median activity score of -0.9. The fragments spanning the LRR-interacting region were moderate repressors, with a median activity score of -0.6. And finally the fragments spanning the LRR region were fairly weak repressors or were non-active in the screen, with a median activity score of -0.1 **(Figure 6C)**. This indicates the disordered N-terminus is important for the negative regulatory activity by the first half of Ccr4 **(Figure 6D)**. Unfortunately, we were unable to assay the C-terminal region of Ccr4 in the tethering screen, which could be due to limitations of the input library or a selective disadvantage for cells over-expressing Ccr4's nuclease domain.

Ded1 is a highly-conserved RNA helicase of the DEAD-box family which promotes the formation of the eIF4F pre-initiation complex during translation initiation in yeast [55]. Ded1 fragments appeared amongst the strongest of the post-transcriptional activators in the tethering screen; nearly all of the Ded1 fragments were primarily distributed above 1.0 in the screen activity score spectrum **(Figure 6E)**. This is consistent with our expectation that Ded1 would promote translation initiation of the tethered mRNA reporter. The strongest Ded1 fragment was sorted almost entirely in the far right FACS bin in the screen, indicating it is a very potent post-transcriptional activator **(Figure 6F)**. We obtained excellent resolution for Ded1 activity across its disordered N-terminus, and in-fact were nearly able to read out the contribution of each amino acid in the activity of Ded1's N-terminus. A recent study from the Hinnebusch lab performed a fine-toothed-comb-level deletion analysis of residues in the Ded1 N-terminus and found that Ded1(21-57) is responsible for interacting with eIF4A, and that Ded1(59-95) is responsible for interacting with eIF4E [65]. This lines up nicely with our observation that the Ded1 fragments become moderate activators with the inclusion of residues spanning Ded1(30-60) and robust activators with the inclusion of residues spanning Ded1(60-100) **(Figure 6G)**. This apparently indicates that full Ded1 activator activity requires bridging synergistic interactions between eIF4A and eIF4E, mediated by Ded1(30-60) and Ded1(60-100), respectively. We observed that a

fragment spanning Ded1(326-490) was a modest repressor in the tethering screen in that it had an activity score of -0.6. This fragment partially includes the ATP-binding helicase domain of Ded1 [64]. It's unclear how this contributes to Ded1's mechanism of action other than suggesting that the helicase alone is insufficient to upregulate translation. We also didn't obtain any coverage of Ded1's C-terminal region, but the Hinnebusch lab study noted that it was responsible for interacting with eIF4G, suggesting that fragments spanning that region of Ded1 would also have been activators in our tethering screen [65].

With the data from the tethering screen characterizing Ded1 and Ccr4, we demonstrate that this assay is even useful in garnering new functional information about relatively well-understood post-transcriptional regulators. These data also provide a starting point for more pointed domain-level analysis of regulatory activity in that they help draw the boundaries between the distinct active domains of RNA regulatory proteins.

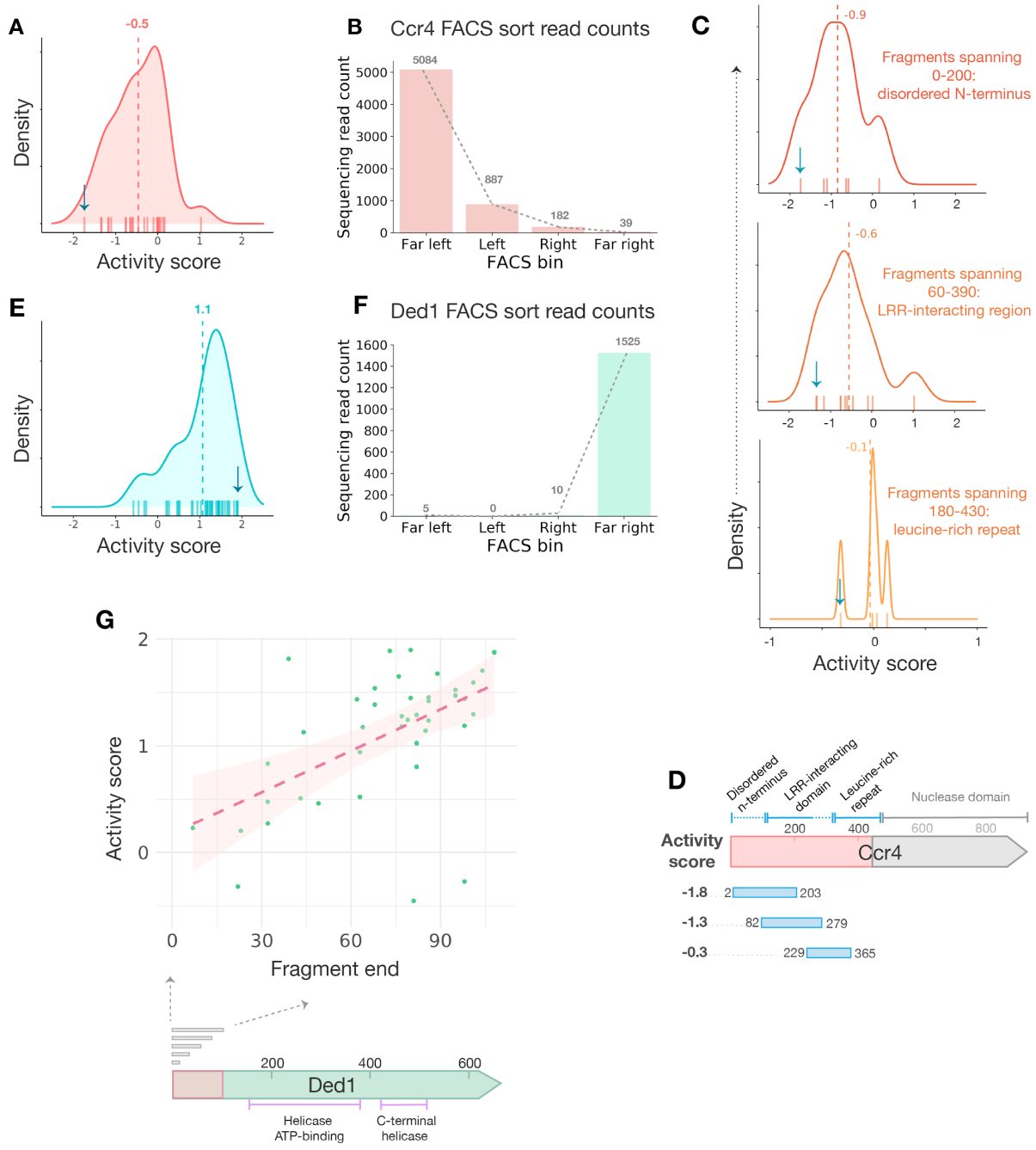

Figure 6. The tethering screen identifies active regulatory domains of Ccr4 and Ded1.

(A) Distribution of activity scores of Ccr4 fragments in tethering screen.

(B) The FACS sort read counts for the strongest Ccr4 repressive fragment from the tethering screen (blue arrow in [A]).

(C) Distribution of activity score for Ccr4 fragments broken down by the disordered N-terminal domain, Ccr4(1-200), the LRR-interacting region, Ccr4(60-390), and the LRR domain, Ccr4(180-430).

(D) Schematic representation of Ccr4 domains, with strongest repressor fragments from each domain represented (blue arrows in [C]).

(E) Distribution of activity scores of Ded1 fragments in tethering screen.

(F) The FACS sort read counts for the strongest Ded1 activator fragment from the tethering screen (blue arrow in [E]).

(G) Dot plot depicting Ded1 fragments spanning N-terminus (dots indicate the terminal residue of each fragment) versus the activity score. Schematic depiction of Ded1, the best fragment coverage overlapped with the disordered N-terminus spanning Ded1(1-110).

Tethering screen reveals strongest regulatory domains include non-RNA recognizing regions.

Prior to performing the tethering screen, we had a working hypothesis that the RNA-binding regions of RBPs were most important for cargo selection and that adjacent to the RNA-interacting regions were the domains of the protein with the true regulatory activity. For example, many RBPs contain intrinsically-disordered regions (IDRs) which allow them to act as regulatory hubs, bringing together RNA and proteins into functional nodes [66]. Sometimes these IDRs can be embedded within the RNA-recognition domain, such as the RGG/RG motif [23]. More often, however, these IDRs interact with other proteins and can sometimes adopt a more stable conformation upon ligand binding, for example in the case of the disordered N-terminus of Ded1 [55,65]. We were curious whether there were other types of domains of RNA-regulatory proteins that were enriched amongst the most active regulators that we characterized, and whether this might reveal new regulatory mechanisms for the proteins that contain these types of domains.

We performed an analysis of all of the fragments in our database that had at least 75% of a known Pfam protein family, which is a database of protein families designated by multiple sequence alignments and hidden Markov models [67]. We then took the mean activity score for each protein family, based on the fragments that contained that domain in the screen, and plotted the mean scores of families with adjusted P-values of less than 0.05 **(Figure 7A)**. This allowed us to visualize the most active domains in the screen. Amongst the repressors, the adenylosuccinate synthetase domain was the strongest, which include enzymes involved in purine biosynthesis that catalyze the first committed step of synthesis of AMP from IMP [68]. Unsurprisingly, the endo/exonuclease/phosphatase family showed up among the strong repressors; these include certain subunits of the Ccr4-Not complex, for example [67]. Amongst the strongest activators, we observed eIF3 subunits to contain the highest mean activity score, which was unsurprising since they are involved in translation initiation [69]. This list also included domains that we didn't necessarily expect to see, including for example Vacuole-related protein 17, which moves the vacuole along actin cables into the bud, showed up amongst the activators [70]. This table of domains and their mean activity scores serves as an excellent jumping off point in the exploration of aspects of RNA regulation that don't fit into our current paradigm for post-transcriptional control.

Figure 7A. Pfam protein families enriched in the active tethering screen fragments plotted by their mean activity scores.

Discussion

Here we have described a novel method for the functional characterization of post-transcriptional regulators on a proteome-wide scale. This method provides new information for many different types of proteins involved in RNA regulation. For example, we did not do follow-up experiments on certain metabolic enzymes which have been shown to interact with RNA, like PGK1 or CDC19 [14], however we did recover data from fragments of these proteins that indicate they have an impact on RNA when tethered. Many Pgk1 fragments were mostly mild activators whereas most Cdc19 fragments were strong repressors. This begins to answer outstanding questions about whether metabolic enzymes are passive passengers when bound to RNA, or whether they have a true regulatory role. Indeed, the data from this screen serves as an excellent starting point for further investigation of these metabolic enzymes, and will help shed light on their contribution to mRNA metabolism.

We present here new data on the well-characterized proteins Ccr4 and Ded1; we provide a finer-resolution understanding of their roles as a post transcriptional repressor and activator, respectively. We also have characterized Sro9 as a translational activator and have defined, by following up on the most active domain of Sro9 identified in the screen, the region of the protein that interacts with Pab1. Future experiments to complete this study will include follow up experiments on the AAA-ATPase Cdc48, best known for its role in endoplasmic reticulum-associated degradation (ERAD), as well as the poorly-understood protein Gta1. Cdc48 shows up as a strong activator in our screen and our validation experiments have verified that the N-terminus of Cdc48 strongly upregulates expression. We are now in the process of investigating whether this effect is due to localization of Cdc48 at the ER membrane, as the N-terminus of Cdc48 is known to interact with ER proteins that recruit it to the site of ERAD[71], or if this is reflecting a novel cytosolic function not yet uncovered. Gta1 is a protein of unknown function which, based on systematic analyses, appears to be involved in golgi vesicle trafficking [72]. We have found it behaves as a very strong repressor of post-transcriptional regulation both in the screen and in validation experiments, and through RNA-seq and proteomics analysis we aim to understand its repressive mechanism.

The tethering screen did entail certain limitations which narrowed the scope of the fragments we were able to characterize. High-throughput alignment of our library to the yeast genome suggests that we had at least one representative fragment from roughly 50% of yeast genes. Since the time of the generation of this library, we have improved our technique for transforming large libraries into yeast such that we are now getting 10-to-20-times better transformation efficiency. This suggests that if we were to repeat the screen today, we would be able to cover a higher percent of the yeast genome with our fragment library.

Finally the context of the screen can change the readout of regulatory activity in the tethering assay. For example, if the assay were performed under a stress context, that could tell us much about how the yeast proteome responds on the post-transcriptional level during times of

metabolic or unfolded protein stress. In addition, we know that the assay works well in mammalian cells with individual proteins tethered. Once we have established a better method for in-frame selection of a mammalian library, we could scale up this technique to assess how similar post-transcriptional regulation is with the mammalian orthologs from our yeast hits. Alternatively, we could perform the screen in a disease or developmental context to understand more about how RNA regulation contributes to or responds to these cellular states. Regardless, this method provides a new and powerful tool for answering outstanding questions about post-transcriptional gene regulation, and it establishes an excellent starting point for future mechanistic studies of the top hits we have characterized in this pilot screen.

Materials and methods

Strain construction

The dual reporter yeast strain NIY293 was transformed with plasmid pKS137 encoding tethered proteins expressed by a pPGK1 promoter, and initiated and terminated as the same start and stop codons as LambdaN::1XFLAG::BFP. The pKS137 plasmid also contains a C-terminal nuclear export signal to ensure cytoplasmic localization. The dual reporter mammalian strain mKS017 was generated in naive HEK293 cells provided by the UC Berkeley cell culture facility. These cells were nucleofected with the plasmid pKS064 encoding a divergent eF1A promoter sequence driving the expression of an eGFP::3XPP7 cassette and a turboRFP::5XBoxB cassette. This plasmid expresses the sleeping beauty transposon technology and integrates at random TATA repeats when co-nucleofected with the pSB100 vector encoding transposase. Monoclonal populations were selected by single-cell FACS sorting in with a BD Influx cell sorter.

Culturing conditions

Cultures for the tethering assay were grown to mid-exponential growth phase at OD_{600} 0.6 OD, before harvest for flow cytometry analysis with incubation in 4% paraformaldehyde. For in-frame fragment selection, BY4741 yeast populations were transformed with size-selected, tagmented yeast gDNA and linear pKS132 which encodes P2A::SpHis5 by the same start and stop codon as the DNA fragment. Cultures were then incubated at 30 °C with shaking for 96 hours in SD-His media with consistent back-dilution. NIY293 was transformed with the tethering plasmid libraries and maintained in SD-His media with 2% glucose at an optical density of OD_{600} 1.0 in the turbidostat for 48 hours.

Fluorescence measurements and Fluorescence-activated cell sorting

Expression of YFP and RFP in the tethering assay was measured using flow cytometric readout with excitation by the 488mm blue laser and 561 mm yellow-green laser, captured on the FITC and PE-TexRed channels, respectively. Fluorescence activated cell sorting was performed with a BD influx sorter by gating four equal populations based on FITC and PE-TexRed emission. Roughly two million cells were sorted into each gate. The sort was performed with two technical replicate libraries.

In-frame library generation

Plasmids harboring in-frame fragments were then harvested with the Zymo yeast miniprep kit from yeast selected in synthetic minus histidine media. The in-frame fragments were then subcloned into the tethering library vector pKS137 for use in the tethering assay with the overlapping Nextera XT forward and reverse primer sites and propagated in DH10beta cells at maximum transformation efficiency. Barcodes were assigned to each fragment on average 3 to 4 times by gibson cloning barcodes into the linearized tethering library and controlling for

transformation efficiency so that we recovered approximately 150,000 bacterial transformation colonies. This library was transformed into NIY293 through the lithium acetate method as described in [73]**.** Transformation cultures were monitored in the turbidostat. Library plasmid DNA was harvested with the Zymo yeast plasmid prep kit. RNA was harvested with the previously described phenol chloroform method [74]. All PCR reactions were performed using Q5 polymerase according to manufacturer protocols. DNA was purified using DNA clean & concentrator kits from Zymo, and when applicable AMPure XP beads were used to purify full-length DNA product. Size distributions and concentrations were measured before next generation sequencing using an Agilent TapeStation 2200. Barcode RNA was prepared with an adjacent T7 promoter sequence, and amplified through a limited cycle PCR with Illumina dual-index primers. Barcodes were assigned to yeast fragment DNA with next generation sequencing using the PacBio Single Molecule Real-Time (SMRT) technology.

Barcode quantification and sequencing analysis

Sequencing data was processed using Cutadapt to remove sequencing adapter sequences. HISAT2 was used to align sequencing reads to the yeast genome to identify fragment DNA. Trimmed barcodes were then counted and tabulated as described in [75]. Barcodes that lacked at least 32 counts in one of the sorted gates were filtered out.

Protein expression analysis via Western blotting

Total protein was isolated from mid-exponentially growing yeast through rapid capture of protein expression through 5% tricarboxylic acid treatment for ten minutes, followed by a wash in acetonitrile. The cell pellets were then dried at room temperature for 30 minutes before bead-beating in cell lysis buffer for 5 minutes at room temperature. Samples were then resuspended in SDS-loading buffer from NuPage, boiled for five minutes, and loaded on 4-12% polyacrylamide Bis-Tris gels and separated by electrophoresis in MOPS buffer. Proteins were then transferred to a nitrocellulose membrane, and were blocked for 1 hour in TBST with 5% bovine serum albumin. Primary antibodies were incubated with membranes for one hour at room-temperature, washed with TBST, and then incubated for 30 minutes at room temperature with anti-rabbit and anti-mouse HRP-linked antibodies. Membranes were developed with Pierce ECL western blotting substrate and imaged on the chemiluminescence channel on a ProteinSimple.

Chapter 3: Dynamic post-transcriptional regulation by the RBP Mrn1 links cell wall homeostasis to mitochondrial protein expression.

Abstract

Mrn1 is a *Saccharomyces cerevisiae* RNA-binding protein (RBP) with over 300 mRNA targets, including those involved in cell wall biogenesis and degradation, as well as plasma membrane and ER-encoding mRNAs [43]. MRN1 has also been shown to localize to granules under glucose starvation conditions, however why it enters granules rather than remaining cytoplasmic is still unknown [52]. Despite binding many mRNAs, this RBP's role in RNA regulation remained poorly understood prior to this study. We have performed a tethering assay and characterized Mrn1 as a repressor of post-transcriptional gene expression. The first 200 amino acids in the N-terminus of Mrn1 comprise a predicted-to-be-disordered, asparagine-rich domain that is a 3.5-fold repressor, whereas the full-length protein is a 2-fold repressor. RT-qPCR analyses have revealed that Mrn1 primarily acts by RNA turnover. We determined via growth experiments on non-fermentable media that an *Δmrn1* knockout strain recovers faster after diauxic shift than wild-type BY4741 yeast. RNA-seq studies on *Δmrn1* grown in fermentable media showed an upregulation of genes involved in ion transport and cell wall organization and biogenesis, which is consistent with the previous study identifying Mrn1 as an RBP with a role in cell wall homeostasis [43]. In non- fermentable media, *Δmrn1* shows an upregulation of genes involved in the cell's response to oxidative stress, the mitochondrial electron transport chain, and the TCA cycle. We further elucidated the gene interaction network that regulates Mrn1 activity using CRISPRi analyses of Mrn1 in fermentative and respiratory-growth conditions. We conclude, based on these analyses, that Mrn1 acts as a hub for integrating cell wall integrity and mitochondrial biosynthesis in a carbon-source responsive manner.

Introduction

Mrn1 is a yeast RNA-binding protein that likely plays an important role in RNA regulation. It binds over 300 mRNAs including those encoding cell wall organization and biogenesis proteins, and it contains four RNA-recognition motifs (RRMs), suggesting it has substantial transcript specificity. It also shares many targets with a subset of RBPs specifically enriched in cell wall regulatory mRNAs, including Khd1, Scp160, and Ssd1 [43]. In the pioneering study on Mrn1 in which Hogan *et al.* identified Mrn1's cognate RNAs, they made no foray into investigating Mrn1's function, but they did speculate it played an important role in post-transcriptional regulation. An early study found Mrn1 is also a growth suppressor of *rsc nhp6 ΔΔ* synthetic sickness and that it shuttles back and forth between the nucleus and the cytoplasm. They claimed this was evidence for Mrn1 playing a role in chromatin remodeling and mRNA processing [76]. We chose to focus more on Mrn1's role in regulating cell wall biogenesis mRNAs in the cytoplasm, but future studies could work on exploring the link between Mrn1's nuclear and cytosolic functions.

Mrn1 contains a predicted-to-be-disordered poly-N N-terminal domain. Structural disorder is typical among proteins that interact with RNA, and is also important in the assembly of phase separated bodies in the cytoplasm, including stress granules and P-bodies [77]. Mitchell *et al*. found that Mrn1 localizes to cytoplasmic granules upon glucose deprivation, and based on known P-body markers colocalizing with Mrn1, they found Mrn1-containing granules to be more "P-body like" than "stress granule-like" [52]. This localization may in part be explained by post-translational modifications. For example, Chang *et al.* found Mrn1 was among a list of RBPs that become hyper-phosphorylated upon glucose deprivation, and many of the other RBPs in this group are known to localize to stress granules upon introduction of cellular stress, including Pab1, Dhh1, and Sbp1 [78,79]. However, Mrn1 was the sole protein among this group of hyperphosphorylated RBPs whose phosphorylation was not relieved by the deletion of the kinase SNF1. This result suggests that Mrn1 plays a role in the cell's response to glucose-limiting conditions that is unique from the other Snf1-regulated RBPs.

Here we performed a series of functional and genetic analyses on Mrn1 and discovered that it is a potent post-transcriptional repressor that functions in RNA turnover through its disordered N-terminus. We also determined that Mrn1 is a novel RBP which links cell wall and mitochondrial homeostasis, and provides a mechanism by which these two physically distinct organelles within the yeast cell can ensure their translational programs are aligned.

Results

Mrn1's N-terminal domain represses post-transcriptional gene expression through RNA turnover.

As an initial step in understanding Mrn1's role in post-transcriptional regulation, we assessed its impact on mRNA expression. We utilized the well-described tethering assay to artificially tether Mrn1 to a reporter mRNA and observed the change in reporter RNA expression based on Mrn1's proximity [44]. The lambdaN viral coat protein has a low-nanomolar affinity for the BoxB RNA hairpins [45], which makes it an excellent tool to precisely target Mrn1 to the 3` UTR of a yellow fluorescent protein (YFP) reporter mRNA **(Figure 1A)**. We first validated that this tethering assay was capturing known regulatory effects by tethering the functionally-characterized protein Dhh1, a DEAD-box RNA helicase that stimulates mRNA decapping [80]. We observed that Dhh1 repressed the expression of YFP by roughly 25%. Mrn1 repressed YFP expression by roughly 30% **(Figure 1B)**. This initial experiment demonstrated that the regulatory activity of proteins tethered to the 3` UTR was reflected in the YFP expression levels, and the introduction of an untargeted red fluorescent protein (RFP) reporter **(Figure 1A)** in subsequent experiments allowed us to calculate the absolute activity of tethered proteins in a more quantitative manner. From this point on, we report regulatory effects that are first normalized to RFP and compared to a non-regulator control.

Mrn1 contains an unstructured N-terminus, based on the Globplot2 disorder prediction algorithm, followed by four predicted RNA-recognition motifs (RRMs), which led us to question which portion of the protein was responsible for its regulatory effects [81] **(Figure 1C)**. We subdivided the protein into the disordered N-terminus, Mrn1(1-200), the first two RRMs, Mrn1(201-370), and the remaining C-terminal part of the protein containing the third and fourth RRMs, Mrn1(371-612) **(Figure 1 D)**. Each of these domains of Mrn1 was tethered to a lambdaN viral coat protein for use in the tethering assay. We compared the activity of these truncations to full-length Mrn1 and found that Mrn1(1-200) is roughly a 3.5-fold repressor of mRNA expression, whereas the full length protein was approximately a 2-fold repressor of expression. It is possible that full length Mrn1 is subject to negative regulation that Mrn1(1-200) evades by missing the C-terminal regions of the protein. In contrast, Mrn1(201-370) and Mrn1(371-612) seemed to have a mild stabilizing effect on the reporter mRNA, increasing YFP expression by about 15% to 20%, respectively **(Figure 1E)**. We next removed the asparagine-rich first 28 amino acids in the N-terminus of Mrn1(1-200) to examine the impact of that region on Mrn1's activity. The change in phenotype of Mrn1(29-200) in the tethering assay was minimal, as it was still an approximate 3-fold repressor of YFP **(Figure 1F)**. This might indicate that the asparagine stretch in Mrn1's N-terminus is more important for a function not captured in the tethering assay, for example localization or turnover during a specific cellular condition.

Finally, we assessed whether the phenotype we observed with Mrn1 in the tethering assay was due to translational repression or RNA turnover. We performed reverse-transcription

quantitative PCR (RT-qPCR) with Mrn1, Mrn1(1-200), and a non-regulator Halo protein tethered to the 3` UTR of a YFP reporter mRNA. We discovered the majority of Mrn1's activity is due to RNA turnover, as the RT-qPCR data nearly recapitulated the level of repression we observed in the tethering assay **(Figure 1G)**.

We next verified that regulation via RNA turnover could be captured on an endogenous target of Mrn1 by testing whether Mrn1 repression could be exacerbated or relieved by an Mrn1-over expression (Mrn1-OE) or Mrn1 knockout *(Δmrn1)* strain, respectively. We examined the impact of manipulating Mrn1 expression levels on RAD51 mRNA, which was previously-published to interact with Mrn1 [43]. Indeed, in the Mrn1-OE strain we observed nearly a 2-fold reduction in RAD51 expression, whereas in *Δmrn1* we saw RAD51 mRNA levels increase by 2.5-fold **(Figure 1H)**. This validates that Mrn1 is indeed a post-transcriptional repressor that functions via turnover of its endogenous mRNA targets.

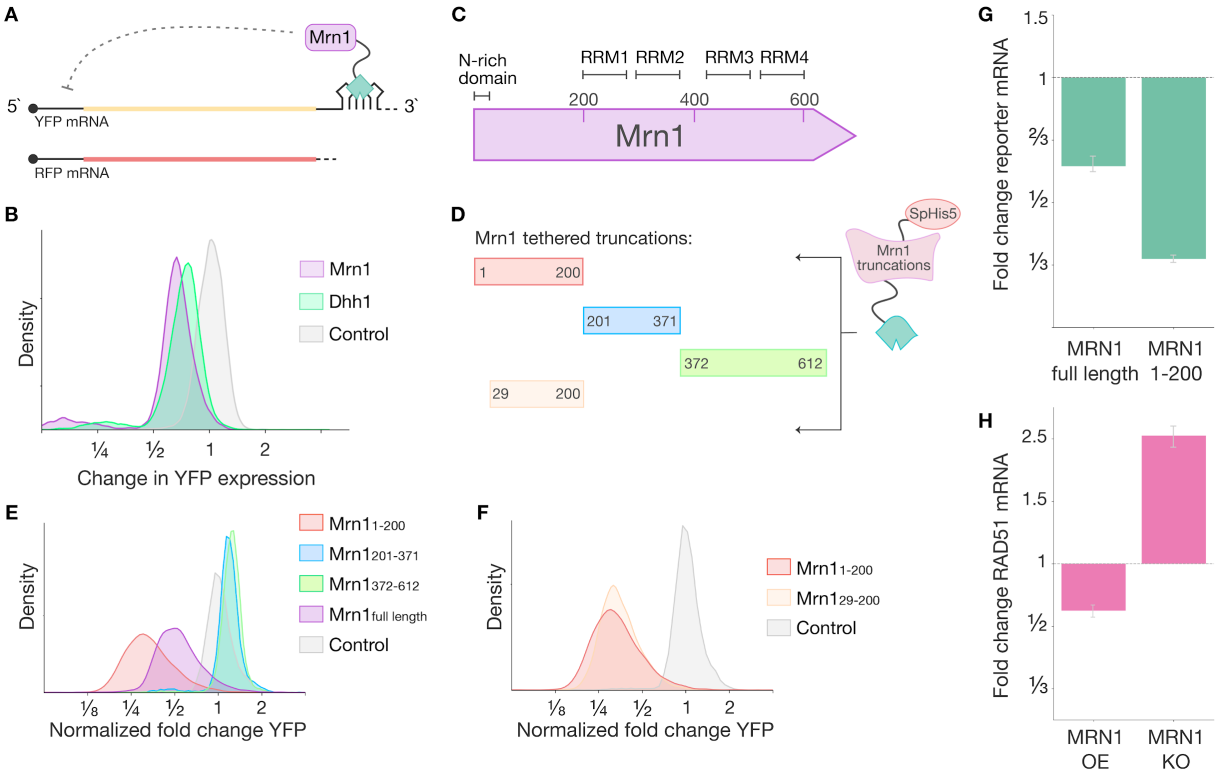

Figure 1. Mrn1 is a post-transcriptional repressor that stimulates mRNA-turnover.

(A) Schematic of the dual-reporter tethering assay used to characterize Mrn1 activity.

(B) Mrn1 and Dhh1 repress YFP expression in the tethering assay relative to a non-regulator control.

(C) Mrn1 has an N-rich N-terminal domain, followed by four RRMs.

(D) Schematic of the Mrn1 protein truncations analyzed in the tethering assay.

(E) Histogram depicting Mrn1 full length and truncation activity relative to a non-regulator control in the tethering assay.

(F) Histogram depicting Mrn1 N-terminus activity with ($Mrn1_{1\text{-}200}$) and without the N-rich region ($Mrn1_{29\text{-}200}$) in the tethering assay.

(G) RT-qPCR analysis of YFP with Mrn1 tethered to the 3` UTR reveals it primarily functions via RNA turnover.

(H) Mrn1 over-expression and gene knock-out impact endogenous Mrn1 target RAD51 expression via nearly 2-fold repression or 2.5-fold upregulation, respectively.

Mrn1 regulates cell wall biogenesis and organization.

In their seminal study on yeast RBPs, Hogan, *et al.* found that Mrn1 associates with over 300 mRNAs, and a large fraction of these encode proteins that localize to the cell wall, plasma membrane, or extracellular matrix [43]. We performed the PANTHER gene ontology (GO) term enrichment test on their list of Mrn1 targets to gain a more complete picture of the processes it regulates. This analysis revealed that, in addition to cell wall homeostasis, Mrn1 targets were also enriched in GO terms for various types of transmembrane transport, including glucose import, and cyclin-dependent kinase activity **(Figure 2A)**. The breadth of GO terms in this report as well as the Hogan, *et al.* study hint that Mrn1 participates in crosstalk within a highly-interconnected network linking various cellular processes. For example, Hogan *et al.* found a link between cell-cycle control and cell wall expansion in that Mrn1 and the RBPs Pub1 and Khd1 each associate with a set of mRNAs that encode cell wall enzymes (SUN4, DSE2, CTS1, SCW4 and EGT2) as well as CLN2, which encodes a G1 cyclin important for cell cycle control. This pattern of shared targets might indicate these RBPs help regulate cell wall expansion in a cell cycle dependent manner.

We speculate that expressing the Mrn1 RRMs independent of the other regulatory parts of the protein might compete with endogenous Mrn1 binding and block its effects, thereby interfering with the correct regulation of the bound mRNAs. Consistent with this hypothesis, we noted that the expression of Mrn1(201-370) and Mrn1(371-612) exhibited phenotypes that indicate a dysregulated cell cycle. When we examined these strains via flow cytometry, both Mrn1(201-370) and Mrn1(371-612) had upshifted forward scatter values relative to the other Mrn1 constructs or wild type, indicating a dysregulation of cell size **(Figure S2A)**. In order to assay our Mrn1-expressing strains for cell cycle defects, we stained their cellular DNA with Sytox Green dye. Both Mrn1 and Mrn1(1-200) had slightly more cells in G1 phase relative to wild type, and Mrn1(1-200) had a major reduction of cells in G2 **(Figure S2B, S2D)**. The large peak around 0 on the x-axis of this histogram may indicate that we weren't 100% efficient at getting the Sytox Green dye into these cells. Mrn1(201-370) seemed to exhibit a fairly typical distribution of cells in G1 vs. G2/M in terms of percentage of cells in each stage, however they were upshifted in the FITC channel. Finally, Mrn1(371-612) demonstrated an increase in cells in G1 phase relative to G2/M, potentially pointing at a delay in cell cycle progression after G1 phase **(Figure S2C,S2D)**.

Knowing that Mrn1 stimulates turnover of its target RNAs, we next investigated whether *Δmrn1* would exhibit an upregulation of RNAs in Mrn1-regulated pathways. We grew *Δmrn1* and wild-type triplicate cultures to exponential growth phase in standard 2% dextrose-containing media, which is a fermentable carbon source, and then harvested the cultures via rapid methanol fixation in order to perform RNA-seq. We were pleased to find that many of the RNAs that were upregulated were consistent with Mrn1's previously-identified target transcripts, including many proteins involved in cell wall homeostasis **(Figure 2B)** [43]. The PANTHER GO term enrichment test indicated that over 30 of the mRNAs upregulated in *Δmrn1* are classified under fungal-type cell wall organization (P value: 1.88E-04, FDR: 0.04). These encode proteins

involved in 1,3-beta-glucan synthesis and regulation as well as mannoproteins, GPI-anchored proteins, chitin synthases and plasma membrane proteins that regulate the cell wall **(Figure 2C)**. Though RNAs involved in cell wall organization were most numerous among those that were upregulated in *Δmrn1*, it was interesting to note that the individual RNAs showing the strongest expression changes were involved in mitochondrial organization and biosynthesis, including NCA3, OAC1, BAT1, and DIC1. Notably, the NCA3 paralog UTH1 was also upregulated. This gene encodes a mitochondrial inner-membrane protein whose deletion leads to an upregulation in 1,6-beta-glucan synthesis [82]. This implicates Uth1 as having some role in cell wall biosynthesis, and the increased expression of proteins that regulate both organelles in *Δmrn1* suggests Mrn1 provides a link between cell wall and mitochondrial homeostasis; an exciting and novel function for an RBP.

We were curious whether knocking out Mrn1 meant its endogenous targets would thus be upregulated. We compiled the list of RNAs from Hogan, *et al.* found to have a statistically significant interaction with Mrn1, and then plotted the fold change in mRNA expression observed in *Δmrn1* against the "Mrn1 mRNA binding score", which we derived from the log2 fold enrichment with Mrn1 from Hogan, *et al.* **(Figure 2D)**. We did find that the RNAs with a significant interaction with Mrn1 were more likely to have a fold change in expression greater than 1 in *Δmrn1* **(Figure 2D inset)**. However we did note this trend was not universal, and that in some cases the change in RNA expression of Mrn1 targets was quite mild. Hogan, *et al.* noted that Mrn1 had a very similar list of targets as Pub1, a poly(A)-binding protein that is important for the stability and translation of many transcripts [83]. We compared the binding scores for Pub1 and Mrn1 for all RNAs in the Hogan *et al.* study and found a strong overlap between the mRNAs that were most upregulated in *Δmrn1* and the RNAs that were more enriched in Mrn1 relative to Pub1 **(Figure 2E)**. For example, RAD51, RPI1, and BGL2 all have higher Mrn1 binding scores than Pub1 binding scores, and are also amongst the RNAs most highly-upregulated in *Δmrn1*. This might indicate Mrn1 and Pub1 compete for target RNAs, and those that are more tightly bound by Pub1 are more protected from the RNA turnover that Mrn1-binding elicits. In support of this theory, Hogan, *et al.* reported that the RNA sequence motif for Mrn1 binding very closely matched the motif for Pub1, and there's currently no evidence to indicate that these proteins physically interact. This suggests that they do not bind simultaneously, but rather trade off or compete for binding of their cognate RNA targets [43].

Finally, since Mrn1 appears to regulate the turnover of cell wall organization and biogenesis RNAs, we reasoned that subjecting an Mrn1 over-expression strain to cell wall stressors would hinder the strain's ability to recover from such stress. We constructed strains over expressing full-length or N-terminal Mrn1 along with a BFP control (Mrn1-OE, Mrn1(1-200)-OE, and BFP-OE, respectively). The cell wall integrity pathway is induced in response to prolonged elevated temperatures above 37 °C [84], therefore we stressed triplicate cultures of each strain for 20 minutes at 42 °C. We then back-diluted our cultures to 0.1 OD_{600} and monitored growth over the next 24 hours. The BFP-OE strain was the first to recover after shock and had the shortest doubling time of 2.5 hours once entering exponential growth. Both Mrn1

over-expression strains took longer to recover after heat shock, though Mrn1(1-200)-OE had a slightly faster doubling rate once it did start to recover (2.75 hours) compared to Mrn1-OE (3 hours) **(Figure 2F)**. It is possible that the slower growth rate of Mrn1(1-200)-OE relative to BFP-OE reflects a stress of over-expressing a disordered protein domain, rather than an endogenous activity of Mrn1. We also subjected our over-expression strains to treatment with 100 mM lithium acetate, which is a reagent used to disrupt the yeast cell wall in order to transform in exogenous DNA [73]. This time, Mrn1(1-200)-OE recovered from stress as rapidly as the BFP-OE strain and also doubled in 2.5 hours. However, Mrn1-OE was still slower to recover and grew at a slower rate post-stress **(Figure 2G)**.

The Mrn1-OE phenotype may be at least partially explained by an increased turnover of the aforementioned Mrn1 target RPI1, which is a transcription factor important for modulating the cell wall integrity pathway in yeast during growth at elevated temperatures or growth on ethanol [85]. In addition to mediating the turnover of an upstream factor like RPI1, which is key for the cell's response to cell wall stress, Mrn1-OE likely also leads to the increased turnover of RNAs encoding important components of the cell wall, thus hindering the cell's ability to rebuild the cell wall after stress-induced injury.

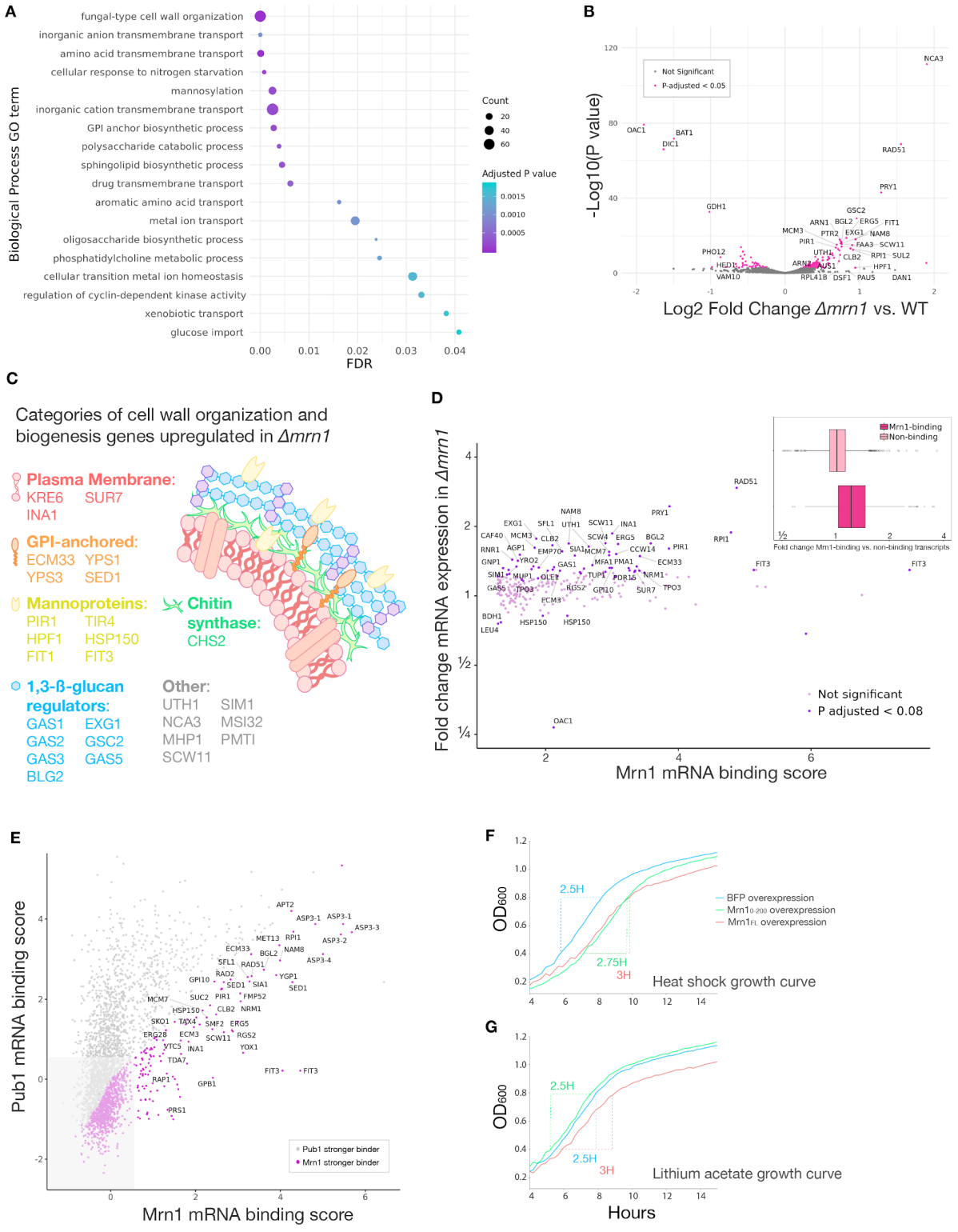

Figure 2. Mrn1 regulates cell wall homeostasis through turnover of cell wall organization and biogenesis RNAs.

(A) Panther GO term enrichment test results for mRNAs bound by Mrn1.
(B) Change in mRNA expression in *Δmrn1* during fermentative growth.
(C) Location of proteins encoded by mRNAs upregulated in *Δmrn1*.
(D) Comparison of Mrn1-binding RNA targets vs. fold change expression in *Δmrn1*.
(E) Comparison of Mrn1-binding and Pub1-binding RNAs by RBP binding score from Hogan, *et al.*
(F) Growth curve of strains over-expressing BFP, Mrn1, and Mrn1(1-200) after heat shock stress, x-axis indicates time after stress.
(G) Growth curve of strains over-expressing BFP, Mrn1, and Mrn1(1-200) after lithium acetate stress, x-axis indicates time after stress.

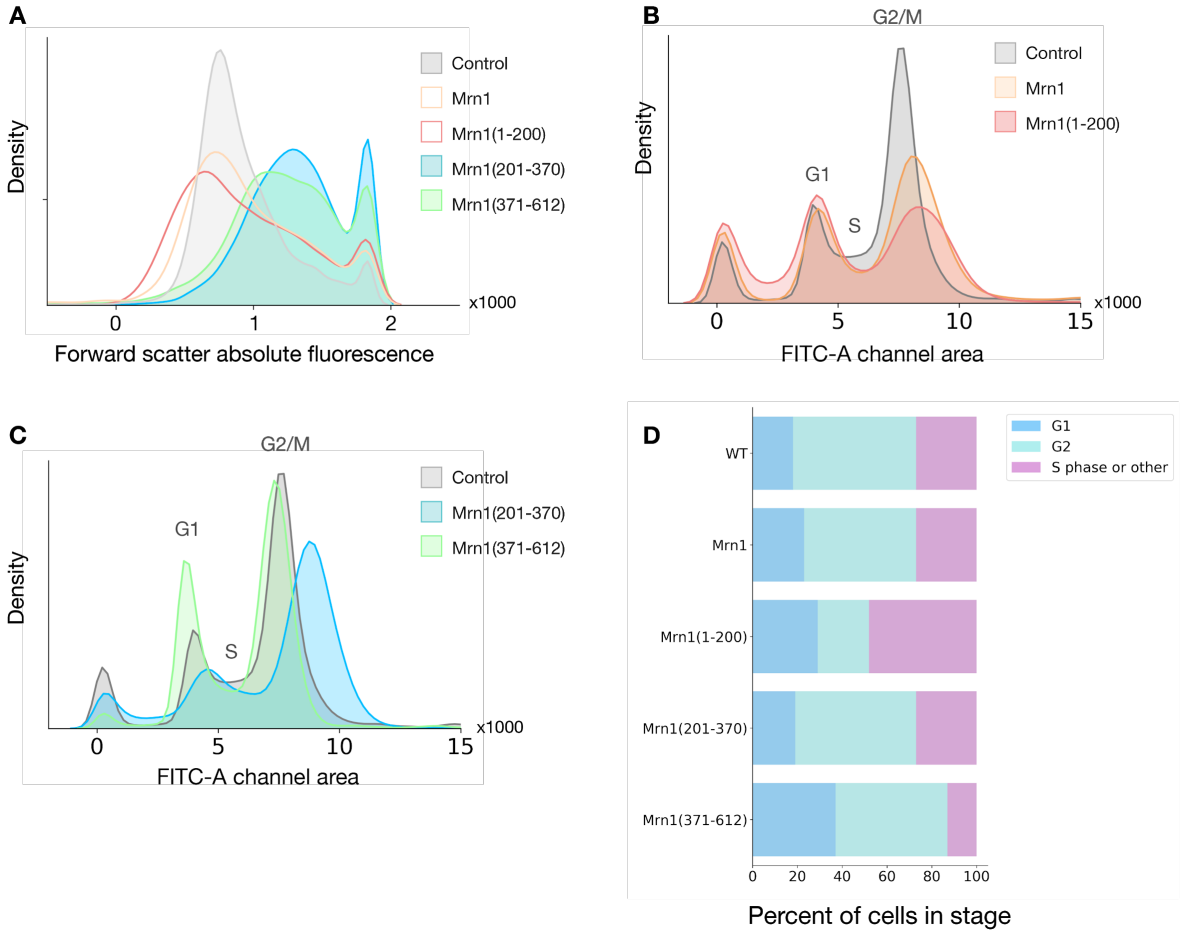

Figure S2. Mrn1 RRM-only expression interferes with normal cell cycle regulation.
(A) Forward scatter absolute fluorescence in control, Mrn1 and Mrn1-truncation expressing cells.
(B) FITC-A readout of Sytox-Green stained cells expressing a control, Mrn1, and Mrn1(1-200).
(C) FITC-A readout of Sytox-Green stained cells expressing a control, Mrn1(201-370), and Mrn1(371-612).
(D) Percentage of each strain in G1, G2, or S phase based on Sytox-Green flow cytometric readout.

Mrn1 represses expression of many mitochondrial mRNAs until diauxic shift.

When yeast cells are grown in media rich with glucose, their primary form of metabolism occurs via glycolysis, which releases ethanol into the media. Once glucose becomes limiting or depleted, they undergo what is referred to as a diauxic shift in which new growth is slowed as their metabolism switches to the aerobic utilization of ethanol [86]. This transition from fermentation to respiration involves a major restructuring of mitochondrial metabolism; this transition is initiated at the mitochondrial level before extending to the rest of the yeast cell [87]. Regarding Mrn1's activity during this switch, Mitchell, *et al.* found that upon glucose deprivation, Mrn1 switches from being broadly distributed in the cytoplasm to being localized primarily into punctae with P-body-like properties. They also found other RBPs like Pat1, Xrn1, Khd1 and Slh1, which are primarily involved in translation repression or RNA-turnover, had similar patterns of P-body localization [52]. Inspired by this observation, we began to examine Mrn1 regulation during glucose deprivation beginning with growing *Δmrn1* and WT yeast in fermentable media, and then switching these actively-growing cultures to non-fermentable media with glycerol and ethanol as the only carbon sources. Interestingly, we consistently observed that *Δmrn1* would recover faster after this shift and would enter exponential growth phase almost a full doubling-time sooner than WT cells **(Figure 3A)**. Curious to know what was occurring at the transcriptional level in these cells, we repeated the above growth experiment and harvested samples for RNA-seq 20 minutes after the shift to non-fermentable media via rapid methanol fixation. We hypothesized that by capturing cells soon after the shift to ethanol- and glycerol-containing media, we would identify the early changes in the transcriptional program that allow *Δmrn1* to undergo diauxic shift more rapidly than WT cells.

We discovered that the majority of transcripts that were upregulated in *Δmrn1* were involved in some stage of the mitochondrial response to respiration. NCA3 was still one of the most highly-upregulated transcripts, which we observed during growth in glucose as well, and in fact the upregulation of this transcript, along with other genes involved in mitochondrial respiration, during fermentation may explain why *Δmrn1* is more rapidly able to cope with the shift to respiratory growth than WT **(Figure 3B)**. NCA3 is a member of the SUN family of genes (*SIM1*, *UTH1*, *NCA3* and *SUN4)* and regulates the expression of the mitochondrial F_0-F1 ATP-synthase, which is responsible for generating ATP during cellular respiration by coupling ATP-synthesis to a proton gradient (H^+) across the mitochondrial membrane [88,89]. NCA3 was not included in the list of potential RNA targets in the Hogan, *et al.* study, so it is unclear whether the impact of Mrn1 regulation on NCA3 expression is direct or indirect. However, in order to be sure we could recapitulate the change in NCA3 expression in *Δmrn1*, we performed RT-qPCR on the NCA3 transcript in clonal populations of *Δmrn1*. We found NCA3 is upregulated approximately 2-fold during growth on glucose and 3-fold during growth on ethanol and glycerol as the carbon source, which closely matches the fold changes in expression that we observed in the RNAseq data, indicating that the effect is reliable and reproducible **(Figure 3C)**.

We performed the PANTHER GO term enrichment test on our list of RNAs upregulated

in *Δmrn1* and found the most significant terms included the tricarboxylic acid cycle, elements of the mitochondrial electron transport chain, and the glyoxylate cycle, among others **(Figure 3D)**. This would indicate that Mrn1's endogenous function includes the suppression of these genes during fermentative growth and in the early stages of diauxic shift. One possibility is that Mrn1 keeps the cell from undergoing a major restructuring of its mitochondria until it has crossed some threshold of glucose limitation to ensure the cell doesn't prematurely invest its energy towards cellular respiration until absolutely necessary.

The removal of Mrn1 regulation upon diauxic shift could occur via shut down of Mrn1 at the transcription level. To verify this, we performed RT-qPCR on the endogenous MRN1 transcript in wild type cells just prior to diauxic shift, and then in ten minute increments after the shift up to 30 minutes. We found over the 30-minute period following diauxic shift, MRN1 expression was decreased to roughly 50% of it's levels during fermentative growth **(Figure 3E)**. We tagged endogenous Mrn1 with a Halo-tag, and performed a western blot analysis against Halo-tagged Mrn1 from cultures at 0, 30 and 90 minutes post-diauxic shift. We found that the level of Mrn1 protein at 30 minutes also decreased by roughly 50%, and after 90 minutes post-shift, it had decreased to about 30% **(Figure 3G)**. This would indicate that, as soon as diauxic shift begins, the cell begins to shut down Mrn1 expression to reduce the amount of repression it can enact upon mitochondrial protein expression.

Based on the impact of Mrn1 regulation on mitochondrial protein expression, we were curious whether knocking out or over-expressing Mrn1 would impact mitochondrial morphology. We harvested cells during mid-exponential growth on fermentable media, as well as cells that had been switched from fermentation to respiratory growth for 30 minutes, and stained their mitochondria with MitoTracker Red dye. We then fixed and imaged the cells with super resolution microscopy using a ZEISS Elyra microscope **(Figure 3H)**. Compared to WT mitochondria, which were localized in small bar-shaped clusters at one end of the cell, the *Δmrn1* cells grown on glucose had much longer mitochondria that were spread throughout more of the cell. In the Mrn1-OE cells, the mitochondria were localized in small discrete punctae in a few locations in the cell. In the cells grown on ethanol and glycerol, the WT mitochondria were spread more like a fine mesh across most of the cell, whereas in *Δmrn1* they were more tightly concentrated into long thin bars with brighter points along those bars. And finally, in the Mrn1-OE cells, the mitochondria more closely-resembled those of WT, in that they were finely spread out throughout the entirety of the cells, rather than clustered into discrete shapes. This experiment will require more replicates to ensure what we are seeing in these preliminary images is biologically-relevant, however thus far this would indicate Mrn1 regulation has a significant impact on mitochondrial morphology.

Given that Mrn1 is shut down during respiratory growth, we speculated that Mrn1 would become a weaker repressor in the tethering assay under respiratory growth conditions. We grew our strains expressing the Mrn1 dual-reporter tethering constructs to mid-exponential growth phase, with glucose as the carbon source, then back-diluted them into minus histidine media with ethanol and glycerol. We then grew the cultures for 6 hours to allow changes in reporter protein

expression to occur **(Figure 3I)**. The Mrn1(371-612) tethering strain grew extremely slowly in the non-fermentable media, so it was excluded from this experiment. Full-length Mrn1 showed no change in activity as it still repressed reporter expression by about 50%, and the very weak effect of Mrn1(201-371) median activity appeared unchanged, although the broadness of its YFP histogram did increase. However, Mrn1(1-200) went from repressing reporter expression from 70% to only about 30%. This might indicate that the disordered N-terminus is especially prone to negative regulation during respiration.

We also examined strains expressing Mrn1 and its truncations for changes in cell cycle progression during respiratory growth in order to compare those data to growth on fermentation. Both WT and Mrn1 showed an increase in G1 phase cells during respiratory growth relative to fermentation. Mrn1(1-200) also showed a slight increase in G1 phase cells relative to fermentation, but this was more modest than the increase seen in WT or Mrn1 **(Figure S3A, C)**. Interestingly, Mrn1(201-370) looked almost unchanged relative to its distribution during fermentative growth and showed the same accumulation of cells in G2/M phase. In addition, these cultures took almost twice as long to double as WT and Mrn1, and considering the WT cells had shifted largely to G1 away from G2/M, this suggests Mrn1(201-370) is undergoing dysregulation of the cell cycle. Finally, the Mrn1(371-612) cultures grew extremely slowly; where the other cultures were able to double at least once within the 6 hour growth experiment on respiratory media, Mrn1(371-612) had to be grown for almost 16 hours in order to double. Almost 80% of the cells were stuck in G1 phase, per the flow cytometric readout after Sytox Green staining **(Figure S3B, C)**. If Mrn1(201-370) and Mrn1(371-612) do delay cell cycle progression by forming a dominant inhibitory mRNP complex, then under respiratory conditions when we now know Mrn1 is shut down, these complexes would be particularly detrimental to cell health.

Finally, we were curious whether other stress conditions would elicit the same decrease in Mrn1(1-200) activity as we observed during respiratory growth, so we tested the effects of media with 0.6M NaCl, which induces osmotic shock. We were surprised to see that Mrn1(1-200) actually became a *stronger* repressor in high-salt media in that it reduced reporter expression by roughly 5-fold **(Figure 3J)**. However, this is consistent with the observation that Mrn1 regulates genes involved in cell wall growth and expansion. For example, it has been shown previously that knocking out UTH1, a gene whose transcript levels increase upon Mrn1 deletion, actually generates cells with more robust cell walls that are resistant to cell wall perturbing agents like zymolyase, or calcofluor white [82]. The increased activity of Mrn1 during osmotic stress may have a similar effect as knocking out certain target transcripts and could create a more osmotic-stress-resistant cell wall.

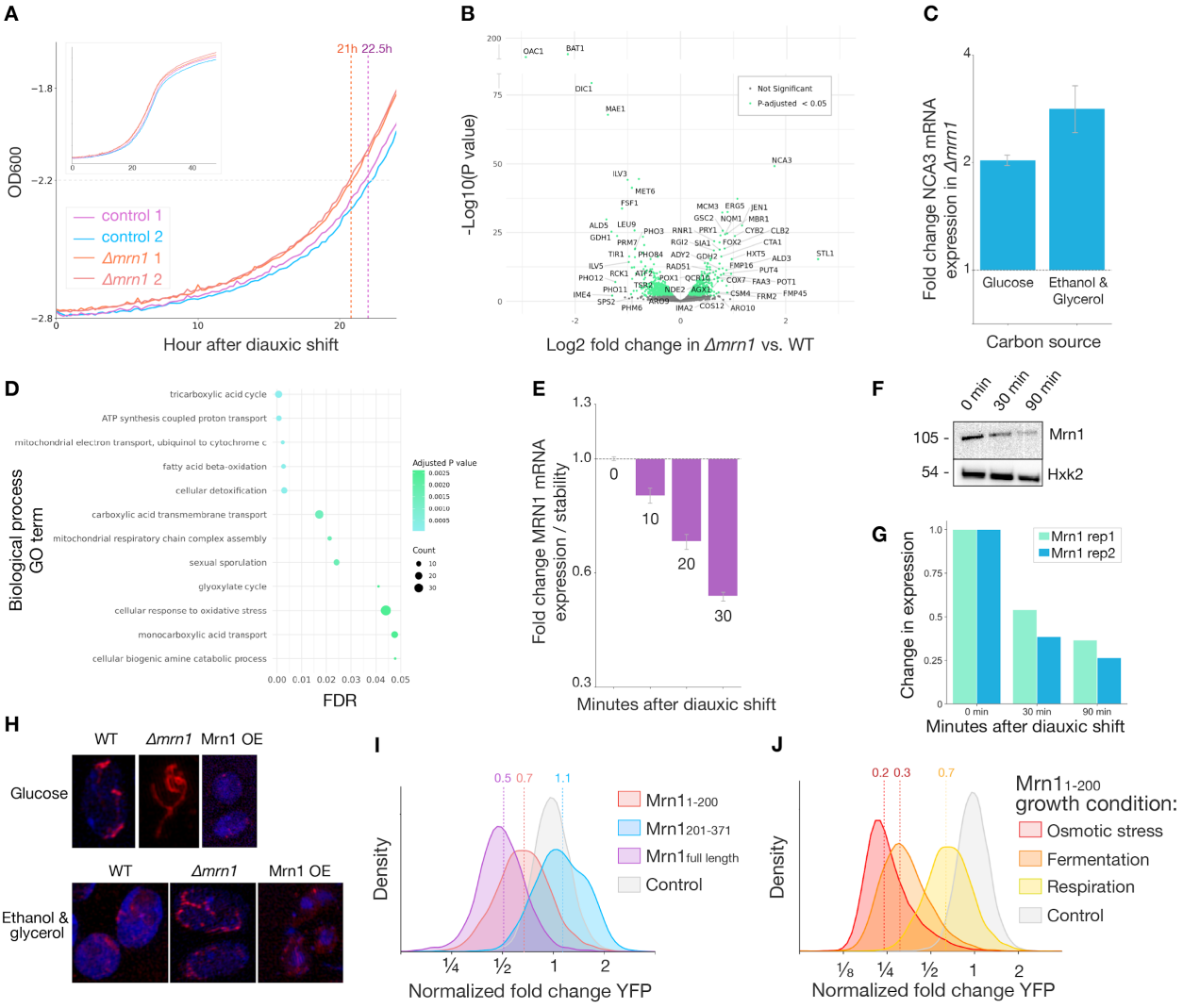

Figure 3. Mrn1 represses mitochondrial adaptation to respiration until diauxic shift occurs.

(A) *Δmrn1* adapts more quickly to diauxic shift than WT.

(B) Transcripts important for mitochondrial adaptation to respiratory growth are upregulated in *Δmrn1* during the first 20 minutes of diauxic shift.

(C) NCA3 is upregulated 2-fold during fermentation and 3-fold during respiration in *Δmrn1*.

(D) PANTHER GO term enrichment for terms upregulated in *Δmrn1* during respiratory growth.

(E) MRN1 mRNA is increasingly turned over in the first 30 minutes after diauxic shift.

(F) **α**Halo western on Halo-tagged Mrn1 protein demonstrates Mrn1 expression and stability decreases after diauxic shift.

(G) Quantification of Mrn1 levels in **α**Halo western depicted in (F), n=2.

(H) Mitochondria stained with MitoTracker Red in WT, *Δmrn1*, and MRN1-OE cells during growth on media with glucose or with ethanol and glycerol as the carbon sources.

(I) Histogram of tethering assay data with Mrn1 tethering constructs during respiratory growth.

(J) Comparison of Mrn1(1-200) activity in tethering assay during different stress conditions.

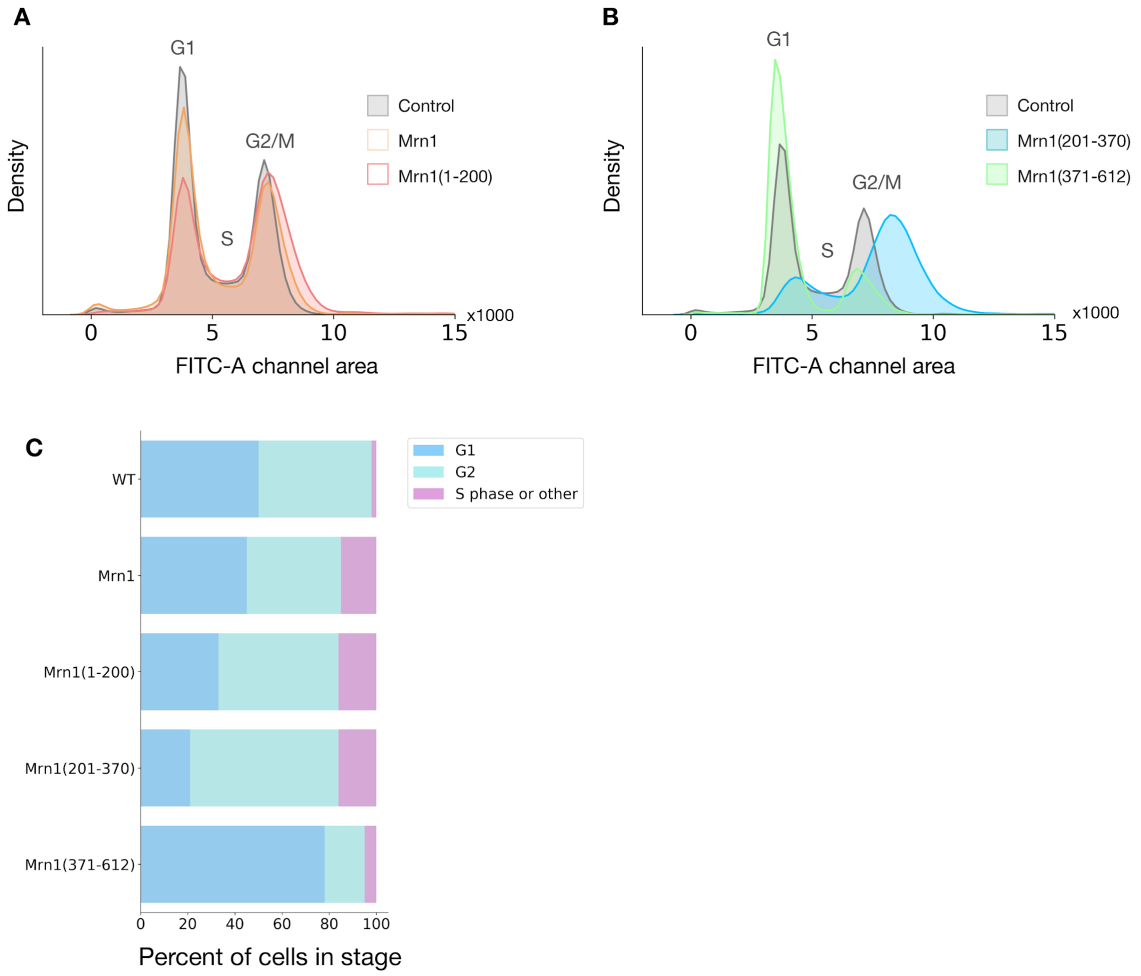

Figure S3. Mrn1 RRM-only expression interferes with normal cell cycle regulation during respiration.

(A) FITC-A readout of Sytox-Green stained cells expressing a control, Mrn1, and Mrn1(1-200) during growth on respiratory media.

(B) FITC-A readout of Sytox-Green stained cells expressing a control, Mrn1(201-370), and Mrn1(371-612) during growth on respiratory media.

(C) Percentage of each strain in G1, G2, or S phase based on Sytox-Green flow cytometric readout.

Incorporation of the tethering assay into CiBER-seq provides a novel method for screening for Mrn1 genetic interactors.

Recently, the Ingolia lab developed a novel approach for quantitative and comprehensive measurement of the cellular response to CRISPR-mediated gene perturbation. This incorporates an expressed reporter-barcode readout that is quantified via RNA-Seq in lieu of driving phenotypic changes of a fluorescent reporter protein that is read out via FACS in traditional CRISPRi [75]. In order to identify the genetic network regulating Mrn1 activity, we incorporated the tethering assay into this approach. We placed the barcoded reporter under the control of an inducible synthetic transcription factor (ZEM), and we tethered either Mrn1 or a non-regulator control to the 3` UTR of ZEM. This enabled us to capture post-transcriptional regulatory effects as knocking down Mrn1 interactors would impact the translational output of ZEM **(Figure 4A)**.

Prior to gRNA induction, Mrn1 should repress expression of ZEM 2-fold, just as it repressed expression of the fluorescent reporter in the tethering assay. Upon gRNA induction, knockdown of genes that typically inhibit Mrn1 activity or expression would result in *stronger* Mrn1 repression of ZEM and thereby reduce expression of the barcoded reporter. Likewise, knockdown of genes that typically enhance the activity or act as a co-repressor of Mrn1 should relieve its repressive effect **(Figure 4B)**. An added feature of this system is that ZEM activity is also inducible with estradiol: ZEM undergoes a conformational change upon treatment with estradiol, which allows it to enter the nucleus and activate expression of the pZ promoter[90]. This allows us to very precisely tune the amount of ZEM induction to ensure the reporter expression responds to changes in ZEM amount, and to allow all cells to achieve steady-state growth before gRNA induction. We used partial ZEM induction and found 5 nM beta-estradiol yielded intermediate reporter expression that varied based on ZEM concentration **(Figure S4A)**.

Finally we wanted to ensure this assay, like the fluorescent reporter assay, captured known regulatory effects, so we tethered Pat1, a protein that activates RNA decapping and deadenylation [91], to the 3`UTR of ZEM. The activity of Pat1 was compared to a non-regulator BFP control. Prior to induction of ZEM with estradiol, both Pat1 and the BFP control strains showed essentially zero expression of RFP mRNA by RT-qPCR. After 5 nM estradiol induction, we were able to observe that Pat1 regulation of ZEM resulted in roughly a 2-fold decrease in RFP expression relative to the BFP control **(Figure 4C)**. Since the reporter RNA encodes an RFP in this instance, we were also able to readout changes in reporter expression caused by Pat1 tethering via flow cytometry, and saw that relative to BFP, Pat1 caused a 3-fold reduction in RFP fluorescence. Finally, we incorporated a YFP reporter into the genome of our cells to use as a normalizer as we did in our previous tethering assay. This allowed us to more accurately quantify Mrn1 repression in this context, and this was useful for subsequent validation experiments as well. We tethered Mrn1(1-200) to the 3` UTR of ZEM, and found upon estradiol induction Mrn1(1-200) elicited an approximate 4-fold reduction in RFP reporter expression, normalized to stable YFP expression. These data demonstrate that the addition of the tethering assay to the CiBER-seq platform is an appropriate method for screening Mrn1's genetic interaction network.

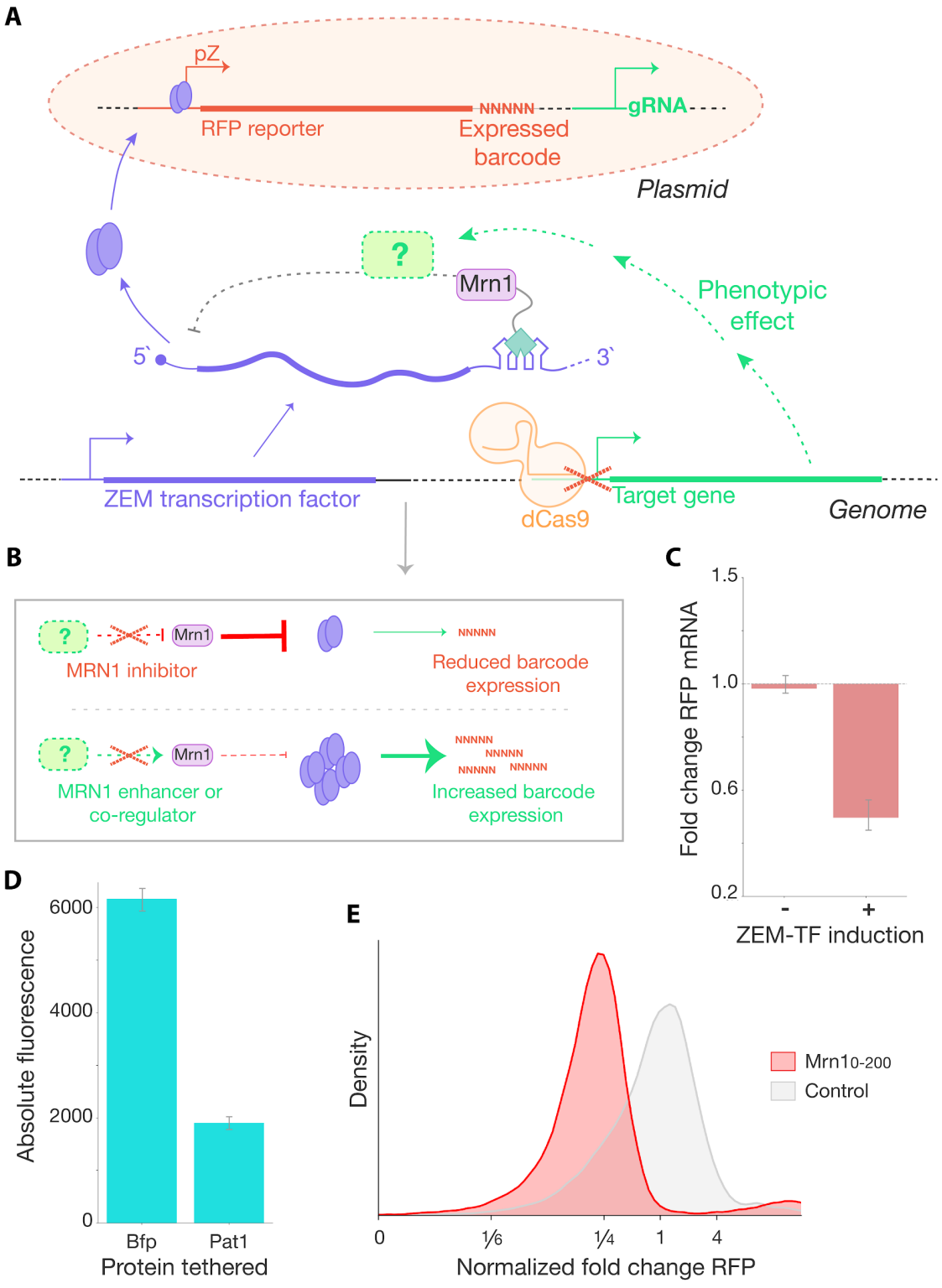

Figure 4. The tethering assay incorporated into CiBER-seq can be used to identify Mrn1's regulatory network.

(A) Schematic representation detailing tethering of Mrn1 to the 3` UTR of the ZEM transcription factor as an addition to the CiBER-seq screen design.
(B) Knockdown of Mrn1 inhibitors will result in a stronger repression of reporter-barcode expression, likewise knockdown of Mrn1 enhancers or co-regulators will result in the increased reporter-barcode expression.
(C) Pat1 tethered to ZEM represses RFP mRNA expression, through reduced ZEM expression, by approximately 2-fold, relative to a non-regulator control.
(D) Pat1 tethered to ZEM represses RFP protein expression, through reduced ZEM expression, by approximately 3-fold, relative to a non-regulator BFP control.
(E) Mrn1(1-200) represses RFP protein expression by roughly 4-fold when normalized to YFP and a non-regulator control.

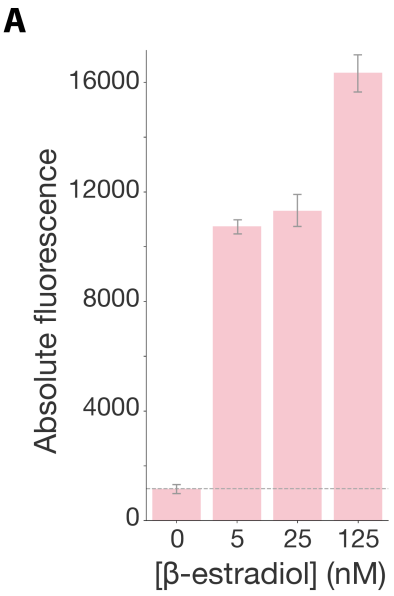

Figure S4. Beta-estradiol induction curve to identify dynamic range of ZEM-pZ expression.
(A) 5 nM beta-estradiol induction of ZEM allows for the robust yet unsaturated induction of reporter expression.

Mrn1 regulatory network indicates a feedback loop including cell wall, metabolic, mitochondrial and cell cycle inputs.

We set up a CiBER-Seq screen with Halo and Mrn1(1-200) tethering in order to identify Mrn1-specific effects. Our screen strains contained a genomically-integrated dCas9 cassette, a ZEM cassette targeted with Mrn1(1-200) or Halo via the BoxB hairpins in the 3` UTR, and a genomically-integrated YFP cassette. We did not include full length Mrn1 in this experiment for two reasons: first of all, Mrn1(1-200) elicits a stronger phenotype, thus would be a more powerful reagent for identifying genetic interactors. Secondly, the strain expressing full length Mrn1 was too slow to recover after treatment with 100 mM lithium acetate and heat shock, which was required for transformation of the barcoded library, such that it was not feasible to transform this strain with a large, high-diversity gRNA library.

The Mrn1(1-200)- and Halo-expressing screen strains were transformed with a library of 60,000 unique gRNAs, each of which were linked with three to four distinct barcodes on average. In addition to the guide-specific barcode, we added library-specific five-nucleotide indexes that pertained to either our Halo or Mrn1(1-200) strain. This allowed us to mix the Halo and Mrn1(1-200) cultures in a single experiment and deconvolve them later based on the library identifier. Thus, we inoculated two continuous-culture turbidostats with equal portions of Mrn1(1-200) and Halo and allowed them to grow for 12 hours in the presence of 5 nM beta-estradiol. The turbidostats are autonomous culturing devices that maintain steady-state growth with aeration, fresh media, and waste efflux [92]. We wanted to look for changes caused by guide induction in fermentation and for further changes arising during respiratory growth. Therefore, we harvested samples prior to guide induction, after an incubation in fermentative conditions, and after a short switch to respiratory media. We analyzed changes in barcode expression across our samples via RNAseq and used DESeq2 analysis to identify statistically-significant interactions with Mrn1 during fermentation and respiration **(Figure 5A)**.

We inferred Mrn1 negative regulators based on increases in Mrn1 activity upon knockdown. These included genes involved in cell cycle regulation, cell wall biogenesis, mitochondrial respiration, and glycolysis. *CKS1* had the strongest negative effect on barcode expression comparing post-ATc induction Mrn1(1-200) cells to pre-ATc Halo and pre-ATc Mrn1(1-200) barcode-expression levels. This means knocking down CKS1 makes Mrn1 an even stronger repressor. Cks1 is required for protein kinase activity of Cln2-Cdc28 complexes and is essential for G1/S phase and G2/M phase transitions in the cell cycle [93]. *FLO5* was the second strongest negative regulator of Mrn1 to come out of our screen. It encodes one of three genes responsible for flocculation in yeast, which is the formation of multicellular clumps by yeast which allows them to survive under stress conditions [94]. Sariki *et al*. recently published a study showing flocculation is dependent on activation by elements of the cell wall integrity (CWI) pathway, which is a key adaptive response that yeast depend on to recover from cell wall damage. Many of Mrn1's targets encode parts of the CWI pathway, including initiation by the cell wall sensor and stress transducer *WSC2*, the beta-1,3-glucanases *EXG1* and *BGL2*, the cell

wall glycoprotein *CCW14*, *HSP150*, an O-mannosylated heat shock protein that is secreted and attached to the cell wall via beta-1,3-glucan linkage, and others [84].

Another strong negative regulator of Mrn1 that came out of the screen was *ADK1*. Adk1 is involved in mitochondrial purine metabolism and is required for the ATP-dependent pre-replicative complex assembly in yeast cells [95,96]. It also forms a physical interaction with Dbf2, a Ser/Thr kinase implicated in transcription and stress response [97]. Dbf2 regulates the stability of *CLB2*, another Mrn1 RNA target that is upregulated in *Δmrn1,* which activates Cdc28 to promote the G2 to M cell cycle transition. Finally, Mrn1 is also negatively regulated by genes encoding glycolytic enzymes, including *FBA1* and *ENO2* which are both involved in glycolysis and gluconeogenesis, and *CDC19*, a pyruvate kinase that functions in formation of pyruvate, which is the input for aerobic respiration. There might be some element of feedback that is facilitated by these enzymes when the cell switches to respiratory conditions which causes Mrn1 activity to be repressed. One caveat to this interpretation is that Mrn1(1-200) and Halo are both under the control of a pPGK1 promoter, which may be subject to regulatory feedback from other glycolytic enzymes that could affect these results. For example, *PGK1* knock down caused Mrn1(1-200) to be a weaker repressor, but this is clearly due to reduction of Mrn1(1-200) expression in the screen. Altogether, these data suggest that Mrn1 is regulated by a feedback loop which incorporates elements of stress sensing at the cell wall, elements that respond to said stress within the cell's metabolic network and the mitochondria, and upstream factors that regulate cellular homeostasis and replication at the transcriptional level.

Factors whose knockdown resulted in a positive fold change in barcode expression for post-ATc Mrn1(1-200) relative to pre-ATc Halo and pre-ATc Mrn1(1-200) included several genes that could explain how Mrn1 exerts RNA turnover of its targets. These include *LSM3/4/5*, components of the heptameric Lsm1p complex involved in cytoplasmic mRNA turnover [98], of which *LSM3* had the strongest fold change and the lowest adjusted P-value. Other factors involved in mRNA degradation that were also discovered as positive regulators of Mrn1(1-200) in the screen include *XRN1*, the 5'-to-3' exonuclease, *DBP2*, the ATP-dependent RNA helicase, and *EAP1*, which competes with eIF4G to bind eIF4E and accelerate decapping [99–101]. Many of these had more modest fold changes relative to the most significant regulators discovered in the screen, which may be due to the fact that they are very general enzymes involved in RNA decay and their loss would impact the expression of the barcodes in the Halo-expressing cells to a large degree as well. The PANTHER overrepresentation GO term test for significant hits in both the positive and the negative direction for Mrn1(1-200) found translation termination and cytoplasmic translation to be the top two most significant terms, as well as terms involving ribosome biogenesis, processing, and export from the nucleus. The enrichment of these terms may actually be reflective of a general effect of interfering with translation by knocking down translation elongation machinery, ribosome components or proteins involved in ribosome biogenesis **(Figure 2B)**.

We also performed DESeq2 analysis on the RNAseq dataset for Mrn1(1-200) in respiratory growth to identify Mrn1 genetic interactions that were distinct from fermentation. We

used the post-ATc induction counts as the "pre-condition" in our DESeq2 matrix in order to identify changes that were significantly larger or smaller when shifting Mrn1(1-200) to respiratory media relative to shifting Halo to respiratory media **(Figure 5C)**. This resulted in some of the most down-regulated terms from the fermentative dataset showing up as positive regulators of Mrn1, however this measurement includes cells whose barcodes were already significantly repressed in fermentation, thus were less relatively repressed in the switch to respiratory media. This aspect of the experimental design made it more difficult to identify true positive regulators of Mrn1 in respiratory media, we therefore focused on genes whose knockdown caused an increase in Mrn1(1-200) activity. These genes included the vacuolar protein sorting proteins *VPS45* as well as *VPS35*, which is required for retrograde transport [102], *PUF3*, the mitochondrial outer membrane protein that promotes the decay of specific mRNAs [103], and finally *LSM3*, which acted as an enhancer of Mrn1 activity during fermentation, yet may be involved in the turnover of MRN1 RNA in respiratory conditions. We identified fewer interactors in respiratory conditions in that only 50 gene knock downs had an adjusted P value of less than 0.05 (compared to over 200 in fermentative conditions). Fewer Mrn1 genetic interactions during respiration may reflect the repression of Mrn1 during respiratory growth. That being said, we selected a handful of gRNAs to validate from the respiratory dataset along with gRNAs from the fermentation dataset.

In order to ensure that the genes identified in the CiBER-Seq screen were bonafide Mrn1 genetic interactors, we selected a handful of gRNAs to validate individually, including CKS1, FLO5, ADK1, LSM3, VPS35, VPS45, PUF3. Our validation experiment entailed the same setup as the CiBER-Seq screen, including gRNA induction with ATc and switching to respiratory media, except instead of examining changes in barcode RNA expression we measured changes in the expression of the RFP reporter via flow cytometry. All activity for the Mrn1(1-200) strain was reported based on changes in reporter expression from pre-to post-gRNA induction relative to the changes in the Halo-expressing control **(Figure S5A)**. For example, samples expressing Mrn1 where RFP was repressed *more* upon guide induction than Halo were validated as negative regulators of Mrn1 (*ADK1* and *FLO5* robustly, and *CKS1* weakly). Samples expressing Mrn1 where RFP was repressed *less* upon guide induction than Halo were validated as Mrn1 inducers (*LSM3* robustly, *VPS35* and *PUF3* weakly). *CKS1* was a much weaker regulator of Mrn1 than we expected based on the CiBER-Seq screen. It may be that there is a certain contribution from cell cycle regulation that we were unable to capture with this validation experiment. It is clear from these data that *ADK1* and *FLO5* both lead to the negative regulation of Mrn1, and *LSM3* induces Mrn1 activity **(Figure 5D, 5E)**.

The tethering assay for our gRNAs under respiratory conditions (*LSM3, VPS35, VPS45,* and *PUF3*) was less-conclusive. Only *LSM3* exhibited the expected effect in that knocking it down made Mrn1 over twice as strong a repressor. *VPS35, VPS45* and *PUF3* all appeared to be mild activators of Mrn1 in that knocking them down made Mrn1 a weaker repressor, however we expected them to behave as negative regulators of Mrn1 **(Figure 5F, 5G)**. It may be that flow cytometry, which reads out changes in protein expression, is not sensitive enough to capture

modest changes in Mrn1 activity, especially in respiratory growth conditions where protein translation is generally repressed [86]. In CiBER-seq we are reading out changes in barcode RNA expression, which presumably allows for the detection of mild-to-moderate phenotypic changes. That being said, it was nice to have clear validation from this assay that Lsm3 is a co-repressor of Mrn1 during fermentative growth. We plan to further confirm this phenotype by inducing LSM3 gRNA expression in a dCas9-containing dual reporter strain to verify we can also observe the above changes in Mrn1 activity in the tethering assay.

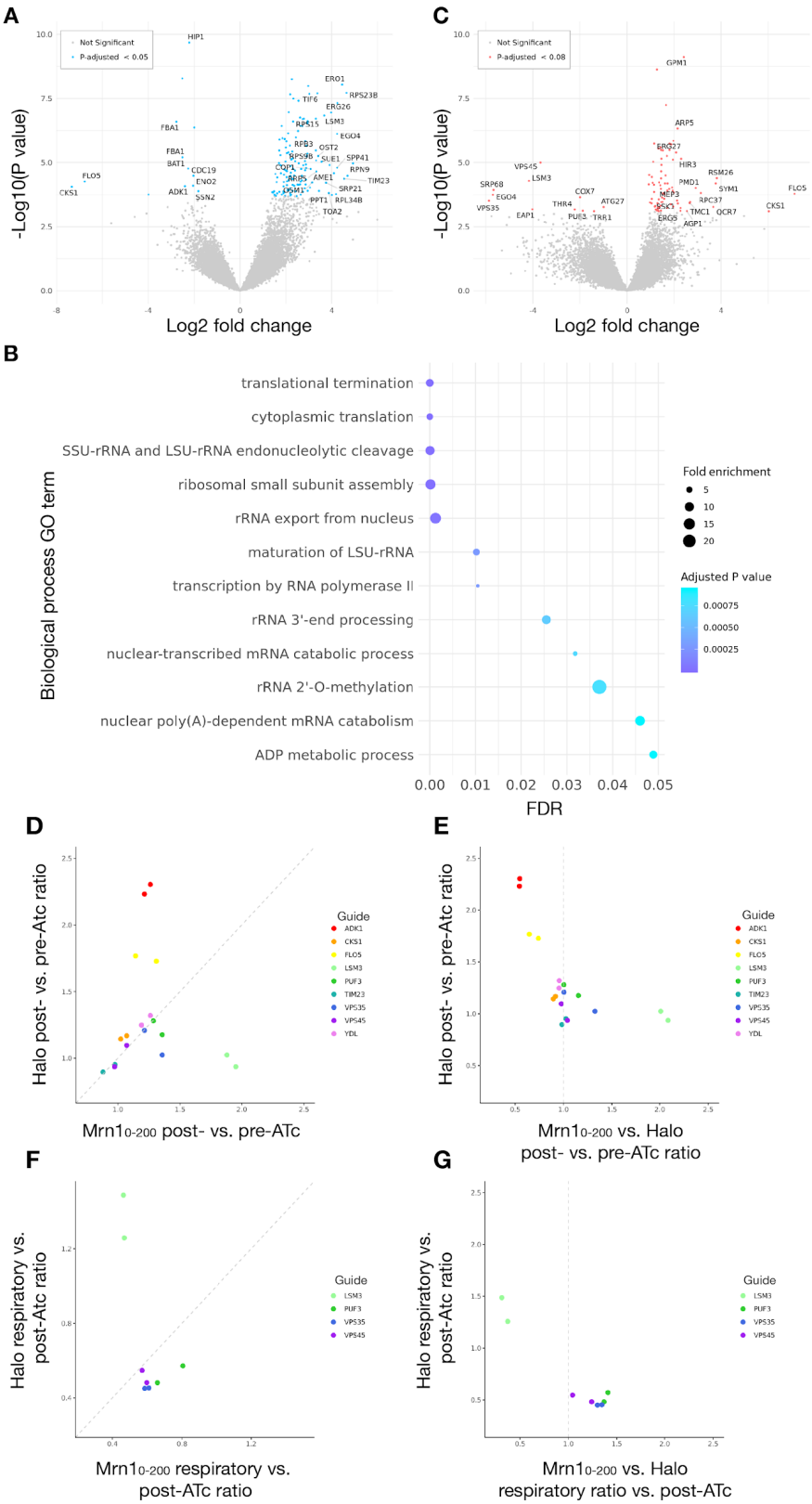

Figure 5. CiBER-Seq reveals MRN1 regulatory network integrates the cell wall integrity pathway with cell cycle regulation, glucose metabolism, and mitochondrial protein expression. (A) Log2 fold change barcode reporter expression based on gRNA gene knockdown during fermentative growth. (B) Panther GO term overrepresentation test for significant terms in ATc-induced fermentative Mrn1-expressing cells. (C) Log2 fold change barcode reporter expression based on gRNA gene knockdown during respiratory growth. (D, E) Validation of gRNA phenotypes from fermentative dataset using flow cytometry readout. (F,G) validation of gRNA phenotypes from respiratory dataset using flow cytometry readout.

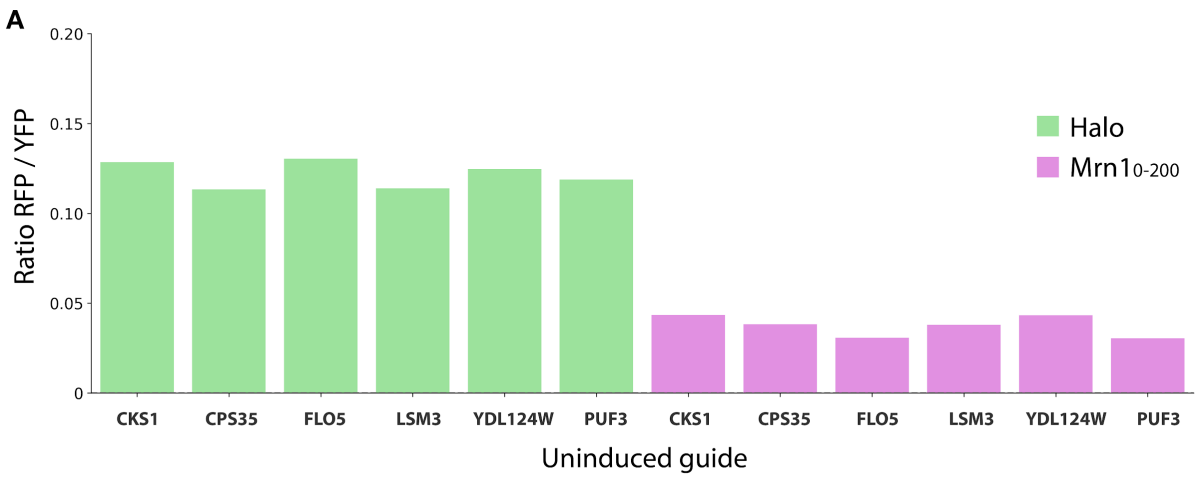

Figure S5A. Ratio of RFP to YFP expression in pre-guide induction in Halo- vs. Mrn1(1-200)-expressing cells.

Mrn1 interacts with mitochondrial membrane proteins, cell wall regulatory proteins, and cytoplasmic stress granule components.

In order to round out our mechanistic analysis of Mrn1 and learn more about its localization, we investigated Mrn1's protein-protein interactions in normal and low glucose conditions. We tagged the endogenous Mrn1 gene with a tandem SBP and Halo tag, including a TEV-cleavable sequence in between. The benefit of using the Halo tag for immunoprecipitation (IP) is that it forms a covalent bond with its corresponding resin, which allows for harsh purification conditions to remove non-specific protein interactions. The SBP tag provides a second, orthogonal affinity tag with the additional benefit of tracking the efficiency of protein elution from the Halo resin after TEV protease cleavage. As a control strain, we integrated an mCherry cassette with a C-terminal SBP-TEV-Halo tag into the HIS3 locus in the S288C genome. All protein-protein interactions that were captured in the Mrn1 strain were compared to mCherry in order to identify specifically-enriched Mrn1 interactors **(Figure 6A)**.

We grew one culture in rich media with 2% glucose, and the other was washed and transferred to low-glucose for 2 hours before harvesting. Each culture was harvested with flash-freezing in order to preserve protein-protein interactions. We lysed the cells with cryogrinding and then cross-linked the lysate by thawing in the presence of 20 mM EDC, which is a chemical cross-linking reagent that forms a stable covalent bond between carboxyl groups and primary amines. We then captured our Halo-tagged complexes and performed a series of stringent washes using the Halo Promega Magna-beads. We eluted our samples from the Halo beads with TEV protease and removed TEV from our eluate with a nickel column purification step. Finally, we trypsin-digested our samples and performed Tandem Mass Tag (TMT)-labeling of our digests before pooling them together and carrying out LC-MS analysis.

We verified our IP strategy with multiple replicate cultures of each strain **(Figure 6B)**, however TMT-labeling kits and LC-MS analysis can be cost-prohibitive. Thus, we submitted only one replicate of each strain in each condition, with the thought that the most promising protein-protein interactions could be validated individually. We compared the normalized peptide abundance between Mrn1 and the mCherry control in fermentative conditions (2% glucose) **(Figure 6C)**, and separately compared Mrn1 and mCherry under respiratory conditions (0.2% glucose) **(Figure 6D)**. We were thus able to distinguish proteins that were enriched or dis-enriched in the Mrn1 samples based on the ratio of Mrn1 enrichment versus mCherry enrichment. We also noted significant overlap between the Mrn1 enrichment of proteins in fermentative versus respiratory conditions **(Figure 6E)**, with a few notable exceptions. For example, both Pck1 and Om45 were significantly enriched in Mrn1's protein-protein interactions during respiration, yet showed no substantial enrichment during fermentative growth. Both PCK1 and OM45 are upregulated during glucose-deplete conditions, which may partially explain why they are only strong Mrn1 interactors in our respiratory samples [104].

Mrn1 interactors are involved in a wide range of biological processes, including gluconeogenesis and glycolysis, translation termination and initiation, redox homeostasis, the

unfolded protein response and ribosome biogenesis, based on the biological process GO terms enriched in both Mrn1 treatments **(Figure 6F)**. The enriched terms in the cellular component test suggest an explanation for these interactions. For instance, Mrn1 is enriched in component terms classified in the small ribosomal subunit, the polysome, the translation preinitiation complex, and cytoplasmic stress granules **(Figure S6A)**. Interestingly, there is significant overlap between the terms that are enriched in stress granules and these other terms involved in translation **(Table 1)**. It is likely, given Mrn1's role in RNA turnover, that rather than interacting with these translation regulators during active translation, these interactions are more a product of co-localization to stress granules during glucose deprivation.

Table 1. Mrn1 is enriched in cellular compartment GO terms pertaining to cytoplasmic stress granules, translation pre-initiation, and the polysome.

Cellular component GO Term	**Proteins enriched**
Cytoplasmic stress granule	TIF11, ARC1, RPG1, PAB1, HSP26, TIF4631, YHB1, SES1, PBP1, HCR1, SBP1, HRP1, TMA19, TIF3, CYS4, BHM1, TIF2, FUN12, SUP35, MRN1, GIS2
Translation preinitiation	TIF11, RPG1, HCR1, SUI3, FUN12
Polysome	GIS2, SSA1, SSA2, TSA1, PBP1, BFR1, EGD1, SSE1

The Mrn1 interactome is also enriched in proteins that localize to the intermembrane space of the mitochondria **(Table 2)**. Comparing the top twenty Mrn1 protein-protein interactions that are most highly-enriched during respiration versus fermentation, almost all of these proteins localize to the mitochondria, including proteins that regulate, bind to or are a structural component of the F_1F_0-ATP synthase (STF1, STF2, ATP1) **(Figure 6SB)**. This may indicate Mrn1's mitochondrial interactions are especially pertinent to its regulation during respiration. There are several possible explanations for how these interactions occur. It seems unlikely that Mrn1 gets imported into the mitochondrial matrix, where it could interact with mitochondrial inner membrane proteins. This seems highly unlikely given the TargetP 2.0 mitochondrial targeting sequence (MTS) predictor found a 99.9% chance that Mrn1's amino acid sequence *does not* include an MTS[105].

A second possibility is that Mrn1 is on-site for mitochondrial protein associated degradation, or mitoTAD. This involves the recruitment of Ubx2, which also functions in endoplasmic reticulum associated degradation, to the translocase of the outer membrane (TOM) complex to recruit Cdc48 for removal of arrested proteins from the TOM channel. Ubx2 binds to the outer members of the TOM complex: Tom20, Tom22 and Tom40 [106]. The arrested precursor proteins can often span the TOM channel and the TIM23 translocase, which promotes

the formation of the TOM-TIM23 supercomplex [107]. Depletion of *TIM23* or *SSC1*, which are essential components of the Translocase of the Inner mitochondrial membrane complex (TIM23), both had positive regulatory effects on Mrn1 per the CiBER-Seq dataset. In addition, Mrn1 was over 2-times more likely than our mCherry control to interact with Tom22, and it was also enriched in interactions with other components of the TIM23 complex as well as Ssc1 **(Figure 6G)**. Mrn1 may be recruited to the mitochondrial surface through some mechanism of the TOM and TIM23 complex during mitoTAD, although it is unclear what function it would perform once there. It is also clear that it does not interact with the ER, as it was actually 3-fold *dis*enriched in interactions with ER proteins, so any Mrn1 role in a global response to misfolded proteins is more likely to be mitochondria-related.

Table 2. Mrn1 is enriched in cellular compartment GO terms pertaining to the inner mitochondrial membrane space and the cell wall.

Cellular component GO Term	**Genes enriched**
Mitochondrial inner membrane space	COX4, CPR1, MIX17, HSP60, TRX1, TIM9, CYT1, MIA40, POR1, ADK1, RIB3, TIM8, TIM10, TIM13, ATP2, GPM1, QCR6, ACO1, SOD1, COX12
Fungal cell wall[1]	**PIR1**, CTR1, GAS1, CDC3, SSA2, CWP1, PIR3, TDH2, GAS5, CIS3, PHO3, EXG1, SSA1, TDH1, **ECM33**, PST1, CRH2, BGL2 ,TDH3, PIR5, **FBA1**, HSP150

One final hypothesis is that Mrn1 plays a role in mitochondria associated ribosome quality control (mitoRQC). This pathway is not yet well characterized, but it involves recognition of stalled 60S ribosomes with nascent chains co-translationally inserted into the TOM complex. The ubiquitinated nascent chains are targeted to Cdc48 for degradation, whereas non-ubiquitinated nascent chains are imported and degraded by mitochondrial AAA-proteases [108]. Mrn1 could be on-site in this context to help facilitate the turnover of aberrant mRNAs. However it is difficult to distinguish a role in mitoTAD vs. mitoRQC, as many of Mrn1's protein-protein interactions could indicate a role in either process. In fact, none of our data clarify for certain Mrn1's role in mitochondrial protein expression, but it *is* clear based on its protein-protein interactions, and on the impact of *Δmrn1* on mitochondrial RNA expression and morphology, that Mrn1 contributes to mitochondrial homeostasis.

One final thing we noted regarding Mrn1 was that there were a list of genes that we refer to as Mrn1 "superbinders", in that Mrn1 binds their mRNA, their RNA expression levels are

[1] **Bold** genes encode fungal cell wall proteins that also localize to or have a regulatory effect on the mitochondria.

upregulated (with the exception of HSP150) in *Δmrn1* in fermentative and respiratory conditions, *and* Mrn1 interacts with the proteins encoded by these genes **(Figure 6H)**. Of the six superbinders, five encode cell wall proteins. Ecm33 is a GPI-anchored mannoprotein key for efficient glucose uptake. Deletion of Ecm33 leads to the upregulation of the cell wall integrity pathway through SLT2 and activation of the high-osmolarity glycerol pathway through HOG1 [109]. Hsp150 and Pir1 are both proteins attached to the cell wall via 1,3-beta-glucan linkage, and are induced by oxidative stress and the cell wall integrity pathway, respectively [110]. Finally, Bgl2 and Gas5 are a 1,3-beta-glucanase and 1,3-beta-glucosyltransferase, respectively [111]. Mrn1's interactions with these superbinders may point to a negative feedback mechanism in which Mrn1 responds to glucose availability as signalled through Ecm33, oxidative stress as signalled by HSP150, or cell wall stress as signalled by Pir1. A phosphorylated version of Ecm33 appears in highly-purified mitochondria [112], which may have some connection to Mrn1 localization to the mitochondria.

Finally, Mrn1's protein sequence contains two sites for post-translational modifications: lysine 111 is a ubiquitination site, and serine 437 is a phosphorylation site [57]. These residues may present mechanisms that tune the localization of Mrn1 depending on the cell's needs. For example, it may localize it to the cell periphery where it regulates cell wall organization and biogenesis, it may localize to the mitochondria where it engages in regulation of mitochondrial protein expression, or it may localize to cytoplasmic granules during stress where it interacts with stalled translation machinery.

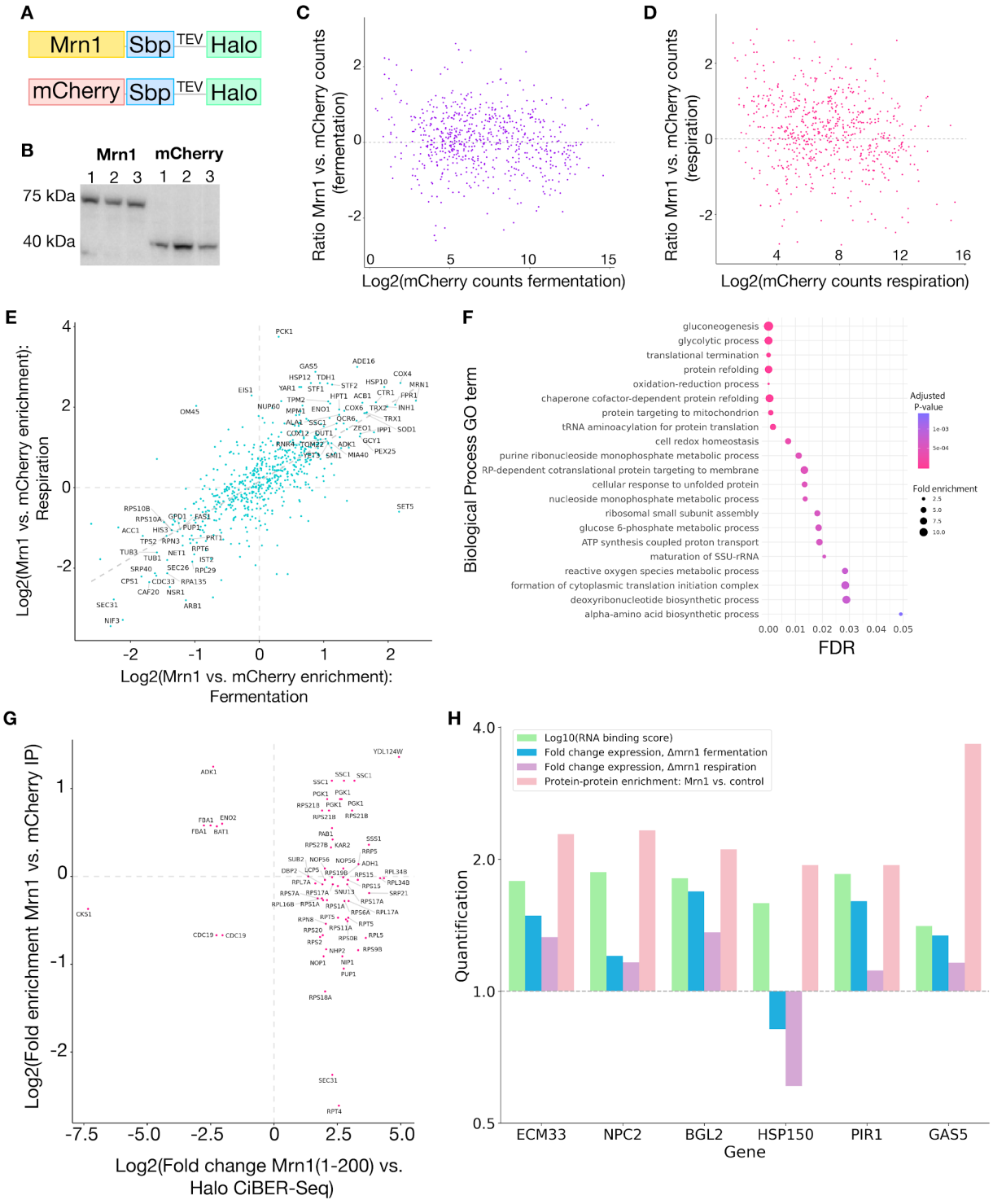

Figure 6. Mrn1 protein-protein interactions implicate regulation of mitochondria and cell wall proteins.

(A) Tagging of endogenous Mrn1, plus genomically-integrated mCherry, with SBP and Halo tags.

(B) Anti-SBP tag western after Halo-IP, TEV-protease cleavage, and elution. n=3 for each strain,

triplicate cultures were normalized by OD_{600} before IP-western.
(C) Ratio of Mrn1 vs. mCherry enrichment vs. Log2 mCherry normalized peptide counts, fermentative growth.
(D) Ratio of Mrn1 vs. mCherry enrichment vs. Log2 mCherry normalized peptide counts, respiratory growth.
(E) Mrn1 protein-protein interactions in fermentative and respiratory growth correlate well across samples with a few key exceptions.
(F) PANTHER GO term enrichment for biological processes enriched in Mrn1 vs. mCherry.
(G) Overlap between Mrn1 protein-protein interactions and genetic interactions identified via CiBER-Seq analysis.
(H) Mrn1 superbinders primarily encode cell wall regulatory proteins.

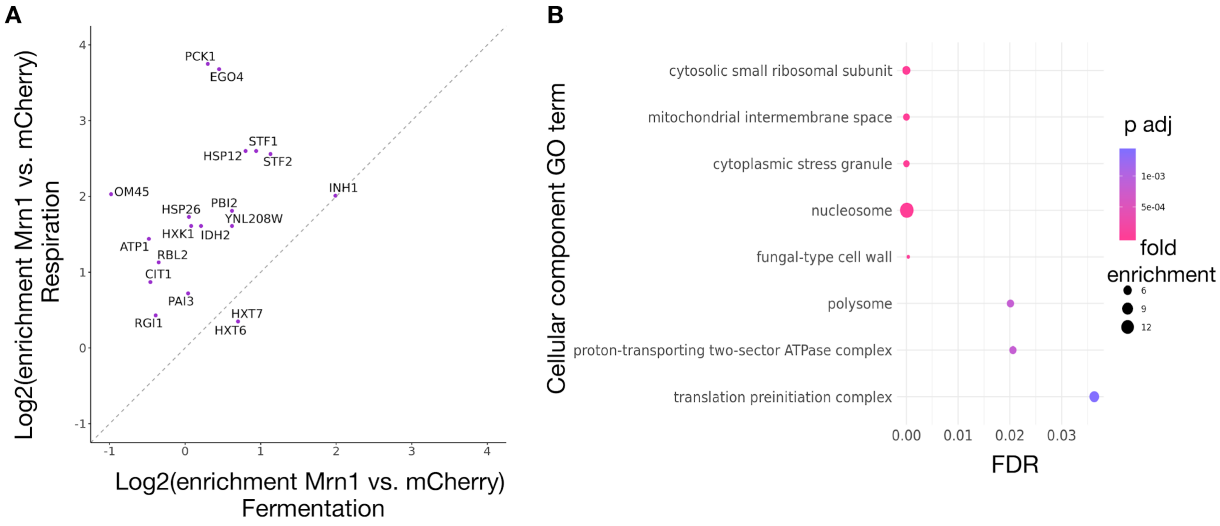

Figure S6.
(A) Top twenty most-enriched Mrn1 protein-protein interactions in respiratory growth indicate an increase in interaction with the F_1-F_0 ATP synthase components.
(B) PANTHER GO term enrichment analysis for cellular components indicate novel Mrn1 localization to cytoplasmic stress granules, the cell periphery, and the mitochondria.

Discussion

Through exploring the function and regulation of Mrn1, we have demonstrated here that yeast cell wall biogenesis and mitochondrial protein expression are more tightly-linked than previously appreciated. Mitochondria are often referred to as the "powerhouses" of the cell since one of their primary functions is providing cellular energy in the form of ATP via oxidative phosphorylation and the TCA cycle [113]. Much of the cell's energy budget is in turn devoted to cell wall biogenesis, which comprises 80 to 90% glucan polymers and composes around 30% of the cell's dry weight [84]. Thus, it is logical that the availability of extracellular carbohydrates would be communicated to the mitochondria so that they could adjust their energy production accordingly. Through this study, we have described a novel function for an RBP in the mediation of this communication.

Proper regulation of mitochondria has important implications for the cell outside of cell wall biogenesis; despite providing an energetic benefit to the cell in the form of ATP, mitochondria also provide the drawback of generating free radicals as byproducts of the electron transport chain. These free radicals cause oxidative damage to mitochondrial enzymes, DNA and RNA, which plays a major role in age-related degenerative diseases in higher eukaryotes [114]. Thus, the expansion of mitochondria that we observed in *Δmrn1* in fermentative conditions suggests improper Mrn1 regulation of the mitochondrial would be deleterious to the cell in the long term.

Future studies could clarify Mrn1's function by exploring its subcellular localization. Mitchell *et al.* performed microscopy on GFP-tagged Mrn1, and found that during fermentative growth it is spread diffusely throughout the cytoplasm [52]. However, we found through our proteomics experiment that Mrn1 forms consistent and specific interactions with proteins that reside in both the mitochondrial and plasma membrane, indicating it either shuttles back and forth between these two organelles during fermentative growth, or that there are different species of Mrn1 that localize to either compartment. The impact of post-translational modification of Mrn1's amino acid sequence at sites K111 and S437 could be explored relative to its interaction with the mitochondria or plasma membrane, as it is possible these residues may contribute to Mrn1's specific localization. Likewise, we could explore whether knocking out Mrn1's disordered N-terminal domain impacts its localization into stress granules, as it is likely that this "prion-like" domain is necessary in order to enter such cytoplasmic aggregates [39].

We also found evidence in our proteomics experiment that Mrn1 interacts with certain histone proteins, indicating an occasional nuclear localization. Indeed, Mrn1 has been previously shown to shuttle back and forth between the nucleus and that the temperature sensitive knockdown of Mex67 trapped Mrn1 in the nucleus, indicating that the Mex67-Mtr2 nuclear pore complex is required for Mrn1 exit into the cytoplasm [76]. Mrn1 was also enriched in nuclear poly(A)-dependent mRNA catabolism per the PANTHER GO test for biological process terms in our CiBER-Seq dataset. This raises questions about what role Mrn1 may play in nuclear mRNA metabolism, and whether it is distinct from the role it plays in cytoplasmic mRNA metabolism.

Despite aspects of Mrn1's mechanism and regulation remaining unclear, we have demonstrated that Mrn1 helps maintain the balance between cell wall expansion and prudent cellular energy expenditure during fermentative growth. By elucidating Mrn1's dynamic role in cell wall and mitochondrial protein expression, we've identified a novel function for an RNA-binding protein that impacts yeast cell growth and longevity.

Materials and methods

Strain construction

The dual reporter strain NIY293 was constructed by integrating pNTI282, encoding pPGK1::YFP::BoxB, into BY4741 at URA3 and pNTI473, encoding pPGK1::mCherry::PP7, into BY4742 at URA3 and mating the two strains together. *Δmrn1* was constructed by integrating a Kanamycin selection cassette into the endogenous MRN1 locus of BY4741, integration was confirmed via colony PCR. Mrn1-OE, Mrn1(1-200)-OE and BFP-OE strains were constructed by cloning an over-expression cassette of each gene driven by pPGK1 expression into the EasyClone pCfB2189 vector, and integrating the linearized vectors into the XI-2 locus in BY4741. NIY416 expresses a constitutively-expressed, genetically integrated copy of dCas9. We integrated the Kan-selectable vector pKS181 which expresses the ZEM synthetic transcription factor with BoxB hairpins in the 3` UTR and a copy of eCitrine into the XII-2 locus of NIY416. We then integrated Halo and Mrn1(1-200)::LambdaN::3XFLAG fusions into the XII-5 locus using the hygromycin-selectable pCfB2337 EasyClone vector. Plasmids for use in the tethering assay were constructed by cloning Dhh1, Mrn1 full length, Mrn1(1-200), Mrn1(29-200), Mrn1(201-371), Mrn1(372-612), and Halo into the pKS137 vector which generates a LambdaN::1XFLAG::BFP fusion protein. Guide RNA validation plasmids were generated by cloning gRNA oligos into pKS111 which encodes a gRNA scaffold driven by a pRPR1 promoter and a pGAL1:: mCherry inducible expression cassette.

Culturing conditions

Growth phenotype assessment via growth curve analysis was performed in triplicate cultures as follows: an overnight inoculum was prepared from a single clone from an agarose plate colony. The following morning, cultures were back-diluted to an OD600 of 0.1 in rich media with 2% glucose. At mid-exponential growth phase, or OD_{600} 0.6, cultures were either back-diluted back into rich media as a control, or washed once in sterile water and resuspended in respiratory growth media containing 2% ethanol and 2% glycerol as the carbon source, or in rich media containing 0.6M NaCl. Growth was then monitored in a Tecan SPARK multimode plate reader at 30 °C with shaking for up to 36 hours following back-dilution. For lithium acetate and heat shock analyses, Mrn1(1-200)-OE, full length Mrn1-OE, and BFP-OE cultures were exposed to either 100 mM LiAc at room temperature for 20 minutes or stressed at 42 °C for 20 minutes, then resuspended in rich medium and grown in the TECAN plate reader at 30 °C for 24 hours with shaking. Triplicate cultures for flow cytometry were grown to mid-exponential growth phase in selective media and harvested at OD_{600} 0.6 by a 30 minute incubation in 4% paraformaldehyde.

Yeast populations were transformed with plasmid libraries and maintained in SD-His media with 2% glucose at an optical density of OD_{600} 1.0 with 5 nM beta-estradiol to induce ZEM activation. When growth rate reached a steady state, pre-induction samples were collected before induction

with 250 ng / ml anhydrous tetracycline. Six doublings, or roughly 9 hours later, post-induction samples were collected, and then the cells were washed in sterile water then resuspended in SD-His with 2% ethanol and 2% glycerol and grown an additional three hours, roughly one doubling. Samples were then collected after this incubation in non-fermentable media and prepared for high-throughput sequencing.

Fluorescence measurement

Expression of YFP and RFP in the tethering assay was measured using flow cytometric readout with excitation by the 488mm blue laser and 561 mm yellow-green laser, captured on the FITC and PE-TexRed channels, respectively.

RNA quantification

Total RNA was harvested from triplicate cultures of each strain using the phenol chloroform method, as described in Nilsen, TW, 2013 [74]. Quantification of YFP reporter RNA expression in the tethering assay was performed via RT-qPCR analysis by comparing YFP Ct values to normalizer RFP Ct values, and experimental protein Ct values were compared to a tethered Halo control Ct values. RAD51 and NCA3 mRNA changes in *Δmrn1* and Mrn1-OE were calculated by comparing RAD51 or NCA3 expression to the housekeeping gene UBC6, and compared to wild-type BY4741. rRNA depletion was performed using the yeast Illumina yeast Ribo-zero rRNA removal kit. cDNA was generated with Protoscript II reverse transcriptase from NEB, and end cleanup and adapter ligation was performed via the NEBnext Ultra II RNA Library Prep Kit with Illumina indexes. RNA sequences were quantified using single end sequencing technology with the Illumina HiSeq4000 sequencing platform.

Barcode sequencing

All PCR reactions were performed using Q5 polymerase according to manufacturer protocols. DNA was purified using DNA clean & concentrator kits from Zymo, and when applicable AMPure XP beads were used to purify full-length DNA product. Size distributions and concentrations were measured before next generation sequencing using an Agilent TapeStation 2200.

Sequencing data analysis

Sequencing data was processed using Cutadapt to remove sequencing adapter sequences and deconvolve multiplexed libraries based on embedded nucleotide indices. Trimmed barcodes were then counted and tabulated as described in [75]. Barcodes that lacked at least 32 counts in the pre-induction samples in one of the replicates were filtered out. The remaining barcodes were analyzed using DESeq2 analysis by comparing pre-induction Halo and Mrn1, and post-induction Halo as the pre-condition in our matrix to find significant genetic interactions in the post-induction Mrn1 sample. Post-induction Mrn1 and Halo, and post-shift to respiratory conditions

Halo were used as the pre-condition to identify significant interactions in post-respiratory Mrn1 [115].

Protein expression analysis via Western blotting

Total protein was isolated from mid-exponentially growing yeast through rapid capture of protein expression through 5% tricarboxylic acid treatment for ten minutes, followed by a wash in acetonitrile. The cell pellets were then dried at room temperature for 30 minutes before bead-beating in cell lysis buffer for 5 minutes at room temperature. Samples were then resuspended in SDS-loading buffer from NuPage, boiled for five minutes, and loaded on 4-12% polyacrylamide Bis-Tris gels and separated by electrophoresis in MOPS buffer. Proteins were then transferred to a nitrocellulose membrane, and were blocked for 1 hour in TBST with 5% bovine serum albumin. Primary antibodies were incubated with membranes for one hour at room-temperature, washed with TBST, and then incubated for 30 minutes at room temperature with anti-rabbit and anti-mouse HRP-linked antibodies. Membranes were developed with Pierce ECL western blotting substrate and imaged on the chemiluminescence channel on a ProteinSimple.

Proteomic analysis

Purifications were performed in biological triplicate for troubleshooting experiments and in single replicates for submission for LC-MS. Samples were collected from exponentially-growing cells through centrifugation, washing with ice cold buffer, and resuspension in lysis buffer before flash-freezing in liquid nitrogen. Cells were lysed with cryogrinding by 6 cycles at 30 hertz for three minutes, the supernatant was clarified, and protein-protein interactions were cross-linked with 20 mM EDC chemical crosslinking reagent. The crosslinked lysate was then incubated with Halo Magna beads for 3 hours at 4 °C. Samples were eluted from the Halo beads with TEV protease digestion and total eluates were prepared according to protocols from the UC Davis proteomics facility. Briefly, this entailed protein precipitation with TCA, 0.01M HCl 90% acetone washes three times, and aire dried adn resuspended in 100 mM ammonium bicarbonate. Samples were alkylated with 500 mM iodoacetimide and incubated in the dark for 30 minutes at 60 °C. Proteins were digested in 100 mM ammonium bicarbonate and 4 ul of 0.5 µg/µl Trypsin. Tryptic digests were quenched with 50% formic acid, buffer-exchanged into 100 mM TEAB buffer, and the protein samples were labeled with four of the ten-plex labels from the Tandem-Mass Tag labeling kit by Thermo Fisher. Samples were speed-vacuumed to remove the supernatant and dessicate the proteins. Mass spectrometry analysis was performed at the UC Davis Proteomics Core Facility.

Microscopy

Mitochondria were stained using mitoTracker Red staining reagent. This entailed capturing cells during exponential growth, and incubating live cells with 100 nM mitoTracker Red reagent at room temperature with nutation for 30 minutes. Cells were washed twice with synthetic complete media, fixed in 4% paraformaldehyde for 15 minutes, and washed once with synthetic complete

media. Cells were immobilized on microscope slides with Prolong Gold antifade reagent with DAPI and incubated in the dark at room temperature for 24 hours. The mitochondria were then visualized using super resolution confocal microscopy with Elyra on the rhodamine filter set.

Chapter 4: Conclusions and future directions

Through application of the dual-reporter tethering assay in a high-throughput screen, and in an individual protein characterization format, we have identified novel elements of RBP-mediated RNA regulation. First of all, we've identified new examples of IDR function in RNA-regulatory activity. We have shown that the disordered N-terminus of Mrn1 is the primary driver of its function as a repressor. We also showed that the disordered N-terminus of Ccr4 was included in the most powerful repressive Ccr4 fragments identified in the screen. And finally, we demonstrated through the screen and in validation experiments that the disordered N-terminus of Ded1 is a powerful upregulator of mRNA expression. These results suggest that IDRs in RBPs provide more than just the flexibility to adopt different physical conformations, but are in fact essential elements in the regulatory activities of these proteins. We have also delineated distinct roles for the domains of RBPs in target selection versus regulatory activity. For instance, the lack of enrichment of classical RBDs in the most active domains in our screen, with the exception of the DEAD box helicase domain, suggests that the elements of these proteins responsible for their regulatory functions include regions outside of their RNA-interfacing domains. However, the RBDmap study did demonstrate that RNA interaction sites could map to proteins' enzymatic cores, thus at this point we cannot exclude the possibility that the active regulatory domains we've identified *do not* interact with RNA [5,6].

Finally, with the tethering screen we have developed a powerful method for determining the functional relevance of the thousands of RNA binding proteins that have been identified over the last decade. Comparisons between our dataset and the RBP interactome capture studies can begin to answer questions about what these proteins are doing once bound to RNA. An added bonus of our assay is that we have circumvented the requirement for a protein to directly interact with RNA by artificially tethering them to an RNA with the viral coat proteins. This means we are able to capture proteins that are important in RNA regulation that might otherwise be overlooked in interactome studies. All-in-all, with our method we can continue dissecting the complex and multifaceted network of RNA regulation that occurs throughout the lifecycle of a cell. This study promises to contribute to a new era of discovery in the exploration of post-transcriptional gene expression.

Outstanding questions about principles of RNA regulation that could be addressed with the tethering assay

How do physical features of the RNA reporter impact its "translatability"?

In the tethering assay, we used a codon-optimized fluorescent reporter mRNA with a short, unstructured 5` UTR, which resulted in its robust and constitutive expression. Altering features within this transcript could shed light on how different properties of an RNA impact its translation. For example, we could lengthen the 5` UTR and/or add elements that generate secondary structure, we could change the sequence context of the AUG start codon, or we could include upstream open reading frames in order to explore how these different features impact translation initiation. We could also examine the impact of altering the 3` UTR length and composition. And finally, we could alter the codon optimality of the reporter coding sequence and examine the effect on a specific RBP's regulatory function. The tethering assay could thus be used to more accurately define features encoded within the RNA itself that impact its translation.

How important is RNA sequence to the activity of an RBP?

One question that arose during the investigation of Mrn1's regulatory network with the tethering assay was how much of its regulatory network we were missing by using a non-endogenous Mrn1 target as our reporter. Presumably by artificially tethering Mrn1 to an RNA rather than it selecting its own targets through its four RRMs, we were unable to capture certain interactions that it forms or activities that it performs once bound to an endogenous target. This also begs the question of whether the correct RNA binding site is sufficient for full RBP activity. For example, if we were to include the Mrn1 binding site in a non-target RNA, would that be sufficient to induce Mrn1-associated turnover of this target, or are there other features of the RNA that are also required in order to turn Mrn1 into a strong repressor?

How is translation impacted by different subcellular locations?

The reporter mRNA could be tethered to different subcellular compartments and the impact of this localization could be read out in a quantitative manner. For example, it has been shown that even mRNAs that encode cytosolic proteins are translationally upregulated when in the proximity of the ER-membrane [116]. We could build off of this observation and tether the reporter mRNA to an ER-, plasma- or mitochondrial-membrane-bound protein and gain a quantitative measurement of translation in these different regions.

Are certain regulators identified in the tethering screen active based on their localization?

Adding on to the theme of the previous section, we identified several fragments in the tethering screen that we hypothesize are active based on their localization. For example, an N-terminal fragment of the protein Prb1 was identified as an activator in the screen, and we showed

through the validation experiment that this fragment upregulated reporter activity by around 2-fold. However, the full length protein was a modest repressor (the data are not included in validation experiments because the raw data files were lost). Prb1 encodes a vacuolar protease involved in protein degradation [117], so it is strange that the N-terminal fragment was an activator in the screen. However it is possible we have identified a signal-sequence that localizes it to the vacuole, or some other related location, where translation is upregulated. Thus, the incorporation of fluorescent-tags into the tethering assay could allow us to visualize the localization of select fragments or full-length proteins and gain a better understanding of how they are impacting the reporter's regulation.

Can the tethering assay characterize synchronized activity between two RBPs?

Hogan *et al.* found that subsets of RBPs bind a similar set of functionally-related mRNAs. They suggested that sometimes these binding events could be competitive or mutually-exclusive, however they could also indicate cooperation between two or more bound RBPS [43]. With this in mind, it would be interesting to utilise the tethering assay to target two RBPs to the same transcript simultaneously and observe the impact of that dual-localization. This might help identify specific inhibitors or co-regulators of RBPs of interest, and it could help in the characterization of the protein-protein interaction sites between dual-tethered proteins through mutation analysis.

Concluding remarks

Through the high-throughput tethering screen, the validation experiments with individual proteins, and through the incorporation of the tethering assay into CiBER-Seq, we have demonstrated that it is a highly-versatile functional assay for the characterization of RNA-regulatory proteins. There are many potential applications for this assay, and in addition to the work we have done here, it will be an invaluable tool in the deeper exploration of post-transcriptional regulation in the future.

Acknowledgements and thanks

To Nicholas Ingolia, thank you for being an incredibly patient and positive mentor, and for supporting me through my transition into working motherhood. I always leave our meetings feeling uplifted and inspired.

To my committee members, Dr. Gloria Brar, Dr. Stephen Brohawn, and Dr. Britt Glaunsinger. Thank you for shepherding me through this stage in my scientific career.

To my labmates in the Ingolia lab, thank you for being a source of plasmids, humor and encouragement, especially when the scientific "going" got tough.

To my mother and my sister, Nitsa and Kira Swain, thank you for being my emotional support system and making sure I always feel loved and appreciated.

To my baby, Aurélien Kokua Reynaud, thank you for giving new meaning to my life.

To my "baby mama science friends", Ella Hartenian, Jessica Tucker and Ina Hollerer, thank you for showing me that science and motherhood *do* go together!

To Lady Gaga, thank you for dropping a bangin' dance album as soon as I started writing. Chromatica is the soundtrack to my thesis.

References

1. Singh G, Pratt G, Yeo GW, Moore MJ. The Clothes Make the mRNA: Past and Present Trends in mRNP Fashion. Annu Rev Biochem. 2015;84: 325–354.

2. Butter F, Scheibe M, Mörl M, Mann M. Unbiased RNA–protein interaction screen by quantitative proteomics. Proc Natl Acad Sci U S A. 2009;106: 10626–10631.

3. Tsvetanova NG, Klass DM, Salzman J, Brown PO. Proteome-wide search reveals unexpected RNA-binding proteins in Saccharomyces cerevisiae. PLoS One. 2010;5. doi:10.1371/journal.pone.0012671

4. Castello A, Horos R, Strein C, Fischer B, Eichelbaum K, Steinmetz LM, et al. System-wide identification of RNA-binding proteins by interactome capture. Nat Protoc. 2013;8: 491–500.

5. Hentze MW, Castello A, Schwarzl T, Preiss T. A brave new world of RNA-binding proteins. Nat Rev Mol Cell Biol. 2018;19: 327–341.

6. Castello A, Fischer B, Frese CK, Horos R, Alleaume A-M, Foehr S, et al. Comprehensive Identification of RNA-Binding Domains in Human Cells. Mol Cell. 2016;63: 696–710.

7. Ule J, Jensen K, Mele A, Darnell RB. CLIP: A method for identifying protein–RNA interaction sites in living cells. Methods. 2005;37: 376–386.

8. Granneman S, Kudla G, Petfalski E, Tollervey D. Identification of protein binding sites on U3 snoRNA and pre-rRNA by UV cross-linking and high-throughput analysis of cDNAs. Proceedings of the National Academy of Sciences. 2009;106: 9613–9618.

9. Van Nostrand EL, Pratt GA, Shishkin AA, Gelboin-Burkhart C, Fang MY, Sundararaman B, et al. Robust transcriptome-wide discovery of RNA-binding protein binding sites with enhanced CLIP (eCLIP). Nat Methods. 2016;13: 508–514.

10. Gerstberger S, Hafner M, Tuschl T. A census of human RNA-binding proteins. Nat Rev Genet. 2014;15: 829–845.

11. Brannan KW, Jin W, Huelga SC, Banks CAS, Gilmore JM, Florens L, et al. SONAR Discovers RNA-Binding Proteins from Analysis of Large-Scale Protein-Protein Interactomes. Mol Cell. 2016;64: 282–293.

12. Beckmann BM, Castello A, Medenbach J. The expanding universe of ribonucleoproteins: of novel RNA-binding proteins and unconventional interactions. Pflugers Arch. 2016;468: 1029–1040.

13. Lunde BM, Moore C, Varani G. RNA-binding proteins: modular design for efficient function. Nat Rev Mol Cell Biol. 2007;8: 479–490.

14. Beckmann BM, Horos R, Fischer B, Castello A, Eichelbaum K, Alleaume A-M, et al. The

RNA-binding proteomes from yeast to man harbour conserved enigmRBPs. Nat Commun. 2015;6: 10127.

15. Hennig J, Sattler M. Deciphering the protein-RNA recognition code: Combining large-scale quantitative methods with structural biology. Bioessays. 2015;37: 899–908.

16. Cieśla J. Metabolic enzymes that bind RNA: yet another level of cellular regulatory network? Acta Biochim Pol. 2006;53: 11–32.

17. Hedstrom L. IMP dehydrogenase-linked retinitis pigmentosa. Nucleosides Nucleotides Nucleic Acids. 2008;27: 839–849.

18. Castello A, Hentze MW, Preiss T. Metabolic Enzymes Enjoying New Partnerships as RNA-Binding Proteins. Trends Endocrinol Metab. 2015;26: 746–757.

19. Barrick JE, Sudarsan N, Weinberg Z, Ruzzo WL, Breaker RR. 6S RNA is a widespread regulator of eubacterial RNA polymerase that resembles an open promoter. RNA. 2005;11: 774–784.

20. Dabo S, Meurs EF. dsRNA-dependent protein kinase PKR and its role in stress, signaling and HCV infection. Viruses. 2012;4: 2598–2635.

21. Mazurek S, Hugo F, Failing K, Eigenbrodt E. Studies on associations of glycolytic and glutaminolytic enzymes in MCF-7 cells: role of P36. J Cell Physiol. 1996;167: 238–250.

22. Basu S, Söderquist F, Wallner B. Proteus: a random forest classifier to predict disorder-to-order transitioning binding regions in intrinsically disordered proteins. J Comput Aided Mol Des. 2017;31: 453–466.

23. Castello A, Fischer B, Eichelbaum K, Horos R, Beckmann BM, Strein C, et al. Insights into RNA biology from an atlas of mammalian mRNA-binding proteins. Cell. 2012;149: 1393–1406.

24. Varadi M, Zsolyomi F, Guharoy M, Tompa P. Functional Advantages of Conserved Intrinsic Disorder in RNA-Binding Proteins. PLoS One. 2015;10: e0139731.

25. Oberstrass FC, Auweter SD, Erat M, Hargous Y, Henning A, Wenter P, et al. Structure of PTB bound to RNA: specific binding and implications for splicing regulation. Science. 2005;309: 2054–2057.

26. Balcerak A, Trebinska-Stryjewska A, Konopinski R, Wakula M, Grzybowska EA. RNA-protein interactions: disorder, moonlighting and junk contribute to eukaryotic complexity. Open Biol. 2019;9: 190096.

27. Diarra dit Konté N, Krepl M, Damberger FF, Ripin N, Duss O, Šponer J, et al. Aromatic side-chain conformational switch on the surface of the RNA Recognition Motif enables RNA discrimination. Nat Commun. 2017;8: 654.

28. Decker CJ, Teixeira D, Parker R. Edc3p and a glutamine/asparagine-rich domain of Lsm4p function in processing body assembly in Saccharomyces cerevisiae. J Cell Biol. 2007;179: 437–449.

29. Van Treeck B, Protter DSW, Matheny T, Khong A, Link CD, Parker R. RNA self-assembly contributes to stress granule formation and defining the stress granule transcriptome. Proc Natl Acad Sci U S A. 2018;115: 2734–2739.

30. Lin Y, Protter DSW, Rosen MK, Parker R. Formation and Maturation of Phase-Separated Liquid Droplets by RNA-Binding Proteins. Mol Cell. 2015;60: 208–219.

31. Shiina N. Liquid- and solid-like RNA granules form through specific scaffold proteins and combine into biphasic granules. J Biol Chem. 2019;294: 3532–3548.

32. Guo L, Shorter J. It's Raining Liquids: RNA Tunes Viscoelasticity and Dynamics of Membraneless Organelles. Mol Cell. 2015;60: 189–192.

33. Kroschwald S, Maharana S, Mateju D, Malinovska L, Nüske E, Poser I, et al. Promiscuous interactions and protein disaggregases determine the material state of stress-inducible RNP granules. Elife. 2015;4: e06807.

34. Ling SHM, Qamra R, Song H. Structural and functional insights into eukaryotic mRNA decapping. Wiley Interdiscip Rev RNA. 2011;2: 193–208.

35. Protter DSW, Rao BS, Van Treeck B, Lin Y, Mizoue L, Rosen MK, et al. Intrinsically Disordered Regions Can Contribute Promiscuous Interactions to RNP Granule Assembly. Cell Rep. 2018;22: 1401–1412.

36. Brengues M, Parker R. Accumulation of polyadenylated mRNA, Pab1p, eIF4E, and eIF4G with P-bodies in Saccharomyces cerevisiae. Mol Biol Cell. 2007;18: 2592–2602.

37. Kedersha N, Stoecklin G, Ayodele M, Yacono P, Lykke-Andersen J, Fritzler MJ, et al. Stress granules and processing bodies are dynamically linked sites of mRNP remodeling. J Cell Biol. 2005;169: 871–884.

38. Buchan JR, Muhlrad D, Parker R. P bodies promote stress granule assembly in Saccharomyces cerevisiae. J Cell Biol. 2008;183: 441–455.

39. Shattuck JE, Paul KR, Cascarina SM, Ross ED. The prion-like protein kinase Sky1 is required for efficient stress granule disassembly. Nat Commun. 2019;10: 3614.

40. Morales-Polanco F, Bates C, Lui J, Casson J, Solari CA, Pizzinga M, et al. Core Fermentation (CoFe) granules focus coordinated glycolytic mRNA localization and translation to fuel glucose fermentation. bioRxiv. 2020. p. 741231. doi:10.1101/741231

41. Gebauer F, Preiss T, Hentze MW. From cis-regulatory elements to complex RNPs and back. Cold Spring Harb Perspect Biol. 2012;4: a012245.

42. Ott M. Cell biology: Choreography of protein synthesis. Nature. 2016. pp. 472–473.

43. Hogan DJ, Riordan DP, Gerber AP, Herschlag D, Brown PO. Diverse RNA-binding proteins interact with functionally related sets of RNAs, suggesting an extensive regulatory system. PLoS Biol. 2008;6: e255.

44. Coller JM, Gray NK, Wickens MP. mRNA stabilization by poly(A) binding protein is independent of poly(A) and requires translation. Genes Dev. 1998;12: 3226–3235.

45. Keryer-Bibens C, Barreau C, Osborne HB. Tethering of proteins to RNAs by bacteriophage proteins. Biol Cell. 2008;100: 125–138.

46. Kessler SH, Sachs AB. RNA recognition motif 2 of yeast Pab1p is required for its functional interaction with eukaryotic translation initiation factor 4G. Mol Cell Biol. 1998;18: 51–57.

47. Tucker M, Staples RR, Valencia-Sanchez MA, Muhlrad D, Parker R. Ccr4p is the catalytic subunit of a Ccr4p/Pop2p/Notp mRNA deadenylase complex in Saccharomyces cerevisiae. EMBO J. 2002;21: 1427–1436.

48. Lobel JH, Tibble RW, Gross JD. Pat1 activates late steps in mRNA decay by multiple mechanisms. Proc Natl Acad Sci U S A. 2019;116: 23512–23517.

49. Winstall E, Sadowski M, Kuhn U, Wahle E, Sachs AB. The Saccharomyces cerevisiae RNA-binding protein Rbp29 functions in cytoplasmic mRNA metabolism. J Biol Chem. 2000;275: 21817–21826.

50. Michlits G, Hubmann M, Wu S-H, Vainorius G, Budusan E, Zhuk S, et al. CRISPR-UMI: single-cell lineage tracing of pooled CRISPR–Cas9 screens. Nat Methods. 2017;14: 1191–1197.

51. Schmierer B, Botla SK, Zhang J, Turunen M, Kivioja T, Taipale J. CRISPR/Cas9 screening using unique molecular identifiers. Mol Syst Biol. 2017;13: 945.

52. Mitchell SF, Jain S, She M, Parker R. Global analysis of yeast mRNPs. Nat Struct Mol Biol. 2013;20: 127–133.

53. Beckmann BM. RNA interactome capture in yeast. Methods. 2017;118-119: 82–92.

54. Lazzaretti D, Tournier I, Izaurralde E. The C-terminal domains of human TNRC6A, TNRC6B, and TNRC6C silence bound transcripts independently of Argonaute proteins. RNA. 2009;15: 1059–1066.

55. Gupta N, Lorsch JR, Hinnebusch AG. Yeast Ded1 promotes 48S translation pre-initiation complex assembly in an mRNA-specific and eIF4F-dependent manner. Elife. 2018;7. doi:10.7554/eLife.38892

56. Chang L-C, Lee F-JS. The RNA helicase Dhh1p cooperates with Rbp1p to promote porin

mRNA decay via its non-conserved C-terminal domain. Nucleic Acids Res. 2012;40: 1331–1344.

57. Swaney DL, Beltrao P, Starita L, Guo A, Rush J, Fields S, et al. Global analysis of phosphorylation and ubiquitylation cross-talk in protein degradation. Nat Methods. 2013;10: 676–682.

58. Fleischer TC, Weaver CM, McAfee KJ, Jennings JL, Link AJ. Systematic identification and functional screens of uncharacterized proteins associated with eukaryotic ribosomal complexes. Genes Dev. 2006;20: 1294–1307.

59. Brandariz-Núñez A, Zeng F, Lam QN, Jin H. Sbp1 modulates the translation of Pab1 mRNA in a poly(A)- and RGG-dependent manner. RNA. 2018;24: 43–55.

60. Kershaw CJ, Costello JL, Castelli LM, Talavera D, Rowe W, Sims PFG, et al. The yeast La related protein Slf1p is a key activator of translation during the oxidative stress response. PLoS Genet. 2015;11: e1004903.

61. Fehrenbacher KL, Boldogh IR, Pon LA. A role for Jsn1p in recruiting the Arp2/3 complex to mitochondria in budding yeast. Mol Biol Cell. 2005;16: 5094–5102.

62. Wendland B, Emr SD. Pan1p, yeast eps15, functions as a multivalent adaptor that coordinates protein-protein interactions essential for endocytosis. J Cell Biol. 1998;141: 71–84.

63. Webster MW, Chen Y-H, Stowell JAW, Alhusaini N, Sweet T, Graveley BR, et al. mRNA Deadenylation Is Coupled to Translation Rates by the Differential Activities of Ccr4-Not Nucleases. Mol Cell. 2018;70: 1089–1100.e8.

64. Xu K, Bai Y, Zhang A, Zhang Q, Bartlam MG. Insights into the structure and architecture of the CCR4-NOT complex. Front Genet. 2014;5: 137.

65. Gulay S, Gupta N, Lorsch JR, Hinnebusch AG. Distinct interactions of eIF4A and eIF4E with RNA helicase Ded1 stimulate translation in vivo. Elife. 2020;9. doi:10.7554/eLife.58243

66. Calabretta S, Richard S. Emerging Roles of Disordered Sequences in RNA-Binding Proteins. Trends Biochem Sci. 2015;40: 662–672.

67. El-Gebali S, Mistry J, Bateman A, Eddy SR, Luciani A, Potter SC, et al. The Pfam protein families database in 2019. Nucleic Acids Res. 2019;47: D427–D432.

68. Honzatko RB, Stayton MM, Fromm HJ. Adenylosuccinate synthetase: recent developments. Adv Enzymol Relat Areas Mol Biol. 1999;73: 57–102, ix–x.

69. Aitken CE, Beznosková P, Vlčkova V, Chiu W-L, Zhou F, Valášek LS, et al. Eukaryotic translation initiation factor 3 plays distinct roles at the mRNA entry and exit channels of the ribosomal preinitiation complex. Elife. 2016;5. doi:10.7554/eLife.20934

70. Peng Y, Weisman LS. The cyclin-dependent kinase Cdk1 directly regulates vacuole inheritance. Dev Cell. 2008;15: 478–485.

71. Stolz A, Schweizer RS, Schäfer A, Wolf DH. Dfm1 forms distinct complexes with Cdc48 and the ER ubiquitin ligases and is required for ERAD. Traffic. 2010;11: 1363–1369.

72. Mattiazzi Usaj M, Sahin N, Friesen H, Pons C, Usaj M, Masinas MPD, et al. Systematic genetics and single-cell imaging reveal widespread morphological pleiotropy and cell-to-cell variability. Mol Syst Biol. 2020;16: 30.

73. Kawai S, Hashimoto W, Murata K. Transformation of Saccharomyces cerevisiae and other fungi: methods and possible underlying mechanism. Bioeng Bugs. 2010;1: 395–403.

74. Nilsen TW. The fundamentals of RNA purification. Cold Spring Harb Protoc. 2013;2013: 618–624.

75. Muller R, Meacham ZA, Ferguson L, Ingolia NT. CiBER-seq dissects genetic networks by quantitative CRISPRi profiling of expression phenotypes. bioRxiv. 2020. p. 2020.03.29.015057. doi:10.1101/2020.03.29.015057

76. Düring L, Thorsen M, Petersen DSN, Køster B, Jensen TH, Holmberg S. MRN1 implicates chromatin remodeling complexes and architectural factors in mRNA maturation. PLoS One. 2012;7: e44373.

77. Zagrovic B, Bartonek L, Polyansky AA. RNA-protein interactions in an unstructured context. FEBS Lett. 2018;592: 2901–2916.

78. Chang Y, Huh W-K. Ksp1-dependent phosphorylation of eIF4G modulates post-transcriptional regulation of specific mRNAs under glucose deprivation conditions. Nucleic Acids Res. 2018;46: 3047–3060.

79. Swisher KD, Parker R. Localization to, and effects of Pbp1, Pbp4, Lsm12, Dhh1, and Pab1 on stress granules in Saccharomyces cerevisiae. PLoS One. 2010;5: e10006.

80. Coller JM, Tucker M, Sheth U, Valencia-Sanchez MA, Parker R. The DEAD box helicase, Dhh1p, functions in mRNA decapping and interacts with both the decapping and deadenylase complexes. RNA. 2001;7: 1717–1727.

81. Linding R, Russell RB, Neduva V, Gibson TJ. GlobPlot: Exploring protein sequences for globularity and disorder. Nucleic Acids Res. 2003;31: 3701–3708.

82. Ritch JJ, Davidson SM, Sheehan JJ, Austriaco N. The Saccharomyces SUN gene, UTH1, is involved in cell wall biogenesis. FEMS Yeast Res. 2010;10: 168–176.

83. Santiveri CM, Mirassou Y, Rico-Lastres P, Martínez-Lumbreras S, Pérez-Cañadillas JM. Pub1p C-terminal RRM domain interacts with Tif4631p through a conserved region neighbouring the Pab1p binding site. PLoS One. 2011;6: e24481.

84. Levin DE. Cell wall integrity signaling in Saccharomyces cerevisiae. Microbiol Mol Biol Rev. 2005;69: 262–291.

85. Puria R, Mannan MA-U, Chopra-Dewasthaly R, Ganesan K. Critical role of RPI1 in the stress tolerance of yeast during ethanolic fermentation. FEMS Yeast Res. 2009;9: 1161–1171.

86. Galdieri L, Mehrotra S, Yu S, Vancura A. Transcriptional regulation in yeast during diauxic shift and stationary phase. OMICS. 2010;14: 629–638.

87. Di Bartolomeo F, Malina C, Campbell K, Mormino M, Fuchs J, Vorontsov E, et al. Absolute yeast mitochondrial proteome quantification reveals trade-off between biosynthesis and energy generation during diauxic shift. Proc Natl Acad Sci U S A. 2020;117: 7524–7535.

88. Pélissier P, Camougrand N, Velours G, Guérin M. NCA3, a nuclear gene involved in the mitochondrial expression of subunits 6 and 8 of the Fo-F1 ATP synthase of S. cerevisiae. Curr Genet. 1995;27: 409–416.

89. Kuznetsov E, Kučerová H, Váchová L, Palková Z. SUN family proteins Sun4p, Uth1p and Sim1p are secreted from Saccharomyces cerevisiae and produced dependently on oxygen level. PLoS One. 2013;8: e73882.

90. Aranda-Díaz A, Mace K, Zuleta I, Harrigan P, El-Samad H. Robust Synthetic Circuits for Two-Dimensional Control of Gene Expression in Yeast. ACS Synth Biol. 2017;6: 545–554.

91. Lobel JH, Gross JD. Pat1 increases the range of decay factors and RNA bound by the Lsm1-7 complex. RNA. 2020. doi:10.1261/rna.075812.120

92. McGeachy AM, Meacham ZA, Ingolia NT. An Accessible Continuous-Culture Turbidostat for Pooled Analysis of Complex Libraries. ACS Synth Biol. 2019;8: 844–856.

93. Reynard GJ, Reynolds W, Verma R, Deshaies RJ. Cks1 is required for G(1) cyclin-cyclin-dependent kinase activity in budding yeast. Mol Cell Biol. 2000;20: 5858–5864.

94. Sariki SK, Kumawat R, Singh V, Tomar RS. Flocculation of Saccharomyces cerevisiae is dependent on activation of Slt2 and Rlm1 regulated by the cell wall integrity pathway. Mol Microbiol. 2019;112: 1350–1369.

95. Cheng X, Xu Z, Wang J, Zhai Y, Lu Y, Liang C. ATP-dependent pre-replicative complex assembly is facilitated by Adk1p in budding yeast. J Biol Chem. 2010;285: 29974–29980.

96. Konrad M. Analysis and in Vivo Disruption of the Gene Coding for Adenylate Kinase (ADK1) in the Yeast Saccharomyces cerevisiae". Plan Perspect. 1988;19468: 19474.

97. Mah AS, Elia AEH, Devgan G, Ptacek J, Schutkowski M, Snyder M, et al. Substrate specificity analysis of protein kinase complex Dbf2-Mob1 by peptide library and proteome array screening. BMC Biochem. 2005;6: 22.

98. Wu D, Muhlrad D, Bowler MW, Jiang S, Liu Z, Parker R, et al. Lsm2 and Lsm3 bridge the interaction of the Lsm1-7 complex with Pat1 for decapping activation. Cell Res. 2014;24: 233–246.

99. Larimer FW, Stevens A. Disruption of the gene XRN1, coding for a 5'----3' exoribonuclease, restricts yeast cell growth. Gene. 1990;95: 85–90.

100. Rendl LM, Bieman MA, Vari HK, Smibert CA. The eIF4E-binding protein Eap1p functions in Vts1p-mediated transcript decay. PLoS One. 2012;7: e47121.

101. Xing Z, Ma WK, Tran EJ. The DDX5/Dbp2 subfamily of DEAD-box RNA helicases. Wiley Interdiscip Rev RNA. 2019;10: e1519.

102. Seaman MN, McCaffery JM, Emr SD. A membrane coat complex essential for endosome-to-Golgi retrograde transport in yeast. J Cell Biol. 1998;142: 665–681.

103. Olivas W, Parker R. The Puf3 protein is a transcript-specific regulator of mRNA degradation in yeast. EMBO J. 2000;19: 6602–6611.

104. DeRisi JL, Iyer VR, Brown PO. Exploring the metabolic and genetic control of gene expression on a genomic scale. Science. 1997;278: 680–686.

105. Almagro Armenteros JJ, Salvatore M, Emanuelsson O, Winther O, von Heijne G, Elofsson A, et al. Detecting sequence signals in targeting peptides using deep learning. Life Sci Alliance. 2019;2. doi:10.26508/lsa.201900429

106. Mårtensson CU, Priesnitz C, Song J, Ellenrieder L, Doan KN, Boos F, et al. Mitochondrial protein translocation-associated degradation. Nature. 2019;569: 679–683.

107. Wenz L-S, Ellenrieder L, Qiu J, Bohnert M, Zufall N, van der Laan M, et al. Sam37 is crucial for formation of the mitochondrial TOM-SAM supercomplex, thereby promoting β-barrel biogenesis. J Cell Biol. 2015;210: 1047–1054.

108. Zheng J, Li L, Jiang H. Molecular pathways of mitochondrial outer membrane protein degradation. Biochem Soc Trans. 2019;47: 1437–1447.

109. Zhang J, Astorga MA, Gardner JM, Walker ME, Grbin PR, Jiranek V. Disruption of the cell wall integrity gene ECM33 results in improved fermentation by wine yeast. Metab Eng. 2018;45: 255–264.

110. Moukadiri I, Zueco J. Evidence for the attachment of Hsp150/Pir2 to the cell wall of Saccharomyces cerevisiae through disulfide bridges. FEMS Yeast Res. 2001;1: 241–245.

111. Lesage G, Bussey H. Cell wall assembly in Saccharomyces cerevisiae. Microbiol Mol Biol Rev. 2006;70: 317–343.

112. Reinders J, Wagner K, Zahedi RP, Stojanovski D, Eyrich B, van der Laan M, et al. Profiling phosphoproteins of yeast mitochondria reveals a role of phosphorylation in

assembly of the ATP synthase. Mol Cell Proteomics. 2007;6: 1896–1906.

113. Malina C, Larsson C, Nielsen J. Yeast mitochondria: an overview of mitochondrial biology and the potential of mitochondrial systems biology. FEMS Yeast Res. 2018;18. doi:10.1093/femsyr/foy040

114. Cadenas E, Davies KJA. Mitochondrial free radical generation, oxidative stress, and aging11This article is dedicated to the memory of our dear friend, colleague, and mentor Lars Ernster (1920–1998), in gratitude for all he gave to us. Free Radical Biology and Medicine. 2000;29: 222–230.

115. Love MI, Huber W, Anders S. Moderated estimation of fold change and dispersion for RNA-seq data with DESeq2. Genome Biol. 2014;15: 550.

116. Voigt F, Zhang H, Cui XA, Triebold D, Liu AX, Eglinger J, et al. Single-Molecule Quantification of Translation-Dependent Association of mRNAs with the Endoplasmic Reticulum. Cell Rep. 2017;21: 3740–3753.

117. Kerstens W, Van Dijck P. A Cinderella story: how the vacuolar proteases Pep4 and Prb1 do more than cleaning up the cell's mass degradation processes. Microb Cell Fact. 2018;5: 438–443.